UNIVERSITY OF OKLAHOMA

GRADUATE COLLEGE

PHOTOTHERMAL AND IMMUNOLOGICAL EFFECTS OF IMMUNOLOGICALLY MODIFIED GRAPHENE NANOSYSTEMS FOR CANCER TREATMENT

A THESIS

SUBMITTED TO THE GRADUATE FACULTY

in partial fulfillment of the requirements for the

Degree of

MASTER OF SCIENCE

By

COLINE FURRER

Norman, Oklahoma

2022

Downloaded from SHAREOK. Persistent Handle URL: https://hdl.handle.net/11244/335967

PHOTOTHERMAL AND IMMUNOLOGICAL EFFECTS OF IMMUNOLOGICALLY MODIFIED GRAPHENE NANOSYSTEMS FOR CANCER TREATMENT

A THESIS APPROVED FOR THE

STEPHENSON SCHOOL OF BIOMEDICAL ENGINEERING

BY THE COMMITTEE CONSISTING OF

Dr. Wei R. Chen, Chair

Dr. John Clegg

Dr. Stefan Wilhelm

© Copyright by COLINE FURRER 2022

All Rights Reserved.

Acknowledgment

Words cannot express my gratitude to my Principal Investigator and Chair of my thesis committee, Dr. Wei R. Chen. I could not have undertaken this journey without his invaluable guidance and feedback from day one. He provided me with challenging research directions and the opportunity to explore multiple engaging aspects of the research in the lab, which offered me a wealth of learning opportunities. Dr. Chen gave me the freedom to design my own project and inspired me to pursue research, through his unconditional support, guidance, and mentorship. Dr. Chen also provided me with the inestimable opportunity to attend an international conference (SPIE Photonics West in San Francisco), where I had the chance to present my work to fellow scientists, professionals, and experienced researchers. I greatly appreciate the diligent work he accomplishes with the wonderful team he managed to build.

This endeavor would not have been possible without the committee members, Dr. John Clegg, and Dr. Stefan Wilhelm.

I am also extremely grateful for the generous support from the National Cancer Institute (R01CA205348), and the Oklahoma Center for the Advancement of Science and Technology (HR16-085 and HF20-019), which financed my research.

I would like to express my deepest gratitude to Dr. Ashley Hoover who has been a great source of inspiration for this work as well as for all the people who had the chance to work with her in the lab. I would like to thank Dr. Hoover for sharing her knowledge with me, teaching me helpful skills, and for all the time she spent discussing amazing scientific subjects with me. I wish her all the best on her adventure outside academia.

I am also deeply grateful to Dr. Lin Wang who was of great help on this thesis work. I want to sincerely thank her for her expertise, the time, and the patience she granted me all through these 18 months. I look forward to working with her again on other challenging projects.

Thanks should also go to Jane Roche, Cédric Delattre, and Fabrice Audonnet, three inspiring Professors at the Clermont-Auvergne INP, France, for having supported me in this 18-month dual degree. This exchange program would be nothing without their dedication, patience, and guidance.

Sincere thanks to Trisha Valerio, a Ph.D. student in the Chen lab, for the work she helped me accomplish, and for her continuous support during my journey at OU. I am excited to work with her in the future.

I had the pleasure of working with all the people in the lab daily. My thanks go to all the team members.

I am also thankful to Kéren Fraissard, my fellow exchange graduate student from France, my dear friend, roommate, and colleague. Without her, I would have never dared to apply for the exchange program at OU and work on this dual degree.

Lastly, I am extremely grateful to my parents, my sister, and my brother. Their belief in me and their emotional support have kept my spirits and motivation high during this process. I am grateful to them for everything they have done for me, for being one of my most important sources of happiness, motivation, and support.

Without all their unconditional support, none of this work would have been possible.

Table of contents

1 **Introduction** 1

2 **Cancer biology** 2

2.1 General information on cancer 2

2.2 Cancer metastasis 3

2.3 Tumor microenvironment 4

2.4 Cancer immunology 6

3 **Cancer therapy** 10

3.1 Surgery, radiation therapy and chemotherapy 10

3.2 Phototherapy 11

3.3 Immunotherapy 12

3.4 Laser immunotherapy 17

3.5 Purpose of the work 26

4 **Study of the photothermal and immunological effects of immunologically modified graphene nanosystems** 26

4.1 *Materials and Methods* 26

4.1.1 Materials 26

4.1.2 Preparation of GO/CS and GO/GC nanoparticles 27

4.1.3 Characterization of GO/CS and GO/GC nanoparticles 27

4.1.4 Thermal study on near-infrared irradiated nanoparticle-enhanced tissue-mimicking materials 28

4.1.5 Tumor and immune cells culture conditions 30

4.1.6 *In vitro* cytotoxicity assay on treated tumor cells 30

4.1.7 *In vitro* immune stimulation and measurement of cytokines release via ELISA 32

4.1.8 *In vitro* immune stimulation and analysis of surface markers by flow cytometry……..33

4.2 *Results*..... 34

4.2.1 Synthesis and characterization of GO/CS and GO/GC nanoparticles..... 34

4.2.2 Thermal effect of near-infrared irradiated nanoparticle-enhanced phantoms of tumors...…….37

4.2.3 *In vitro* tumor cell toxicity induced by nanoparticles-based PTT..... 42

4.2.4 *In vitro* immune stimulation and nanoparticles potential as immunostimulating agents…….45

4.2.5 *In vitro* immune stimulation and analysis of surface markers by flow cytometry...……49

4.3 *Discussion*..... 51

5 **Conclusion and future work** 54

6 **References**..... 56

List of tables

Table 1. Comparison of the main characteristics of healthy cells and cancer cells [21]..... 3

List of figures

Figure 1. The proliferation of healthy cells vs cancer cells. 2

Figure 2. Metastatic cancer: the tumor spreads through the body. Example of breast cancer metastases in the brain at advanced-stage breast cancer. 4

Figure 3. The tumor microenvironment at a glance [31]. 5

Figure 4. Cancer immunoediting. 8

Figure 5. T cell-mediated tumor cell killing. 9

Figure 6. The multiple immune escape strategies of tumors. 13

Figure 7. T cell checkpoint molecules are used by tumors to suppress anti-tumor T cell activity. 14

Figure 8. Checkpoint blockade immunotherapy. 15

Figure 9. Hallmarks of cancer. 17

Figure 10. Components of the nano-ablative photo-immunotherapies for cancer treatments [70]. 17

Figure 11. LIT induces a systemic, anti-tumor immunity for the treatment of metastatic cancers. 18

Figure 12. Chemical structures of the molecules studied in this thesis work: **(A)** the chitosan molecule [102], **(B)** the N-dihydrogalactochitosan (glycated chitosan) molecule [121], and **(C)** the graphene oxide molecule [133]. 21

Figure 13. Nanotechnology-based photoimmunotherapy for cancer treatment. 25

Figure 14. Schematic of the phantom set-up for the thermal study. **(A)** Temperature measurement at different depths of the tumor-bearing tissue-mimicking materials. The thermocouple T3 is placed in the center of the GO-enhanced spherical gel. The distance between 2 probes is 0.7 cm. **(B)** Temperature measurement at different depths of the tumor-mimicking spherical phantom. The distance between 2 probes is 0.3 cm. 29

Figure 15. Timeline of the cell toxicity assay for **(A)** non-irradiated cells and **(B)** laser-irradiated cells. 32

Figure 16. Characterization of graphene oxide (GO), chitosan (CS), glycated chitosan (GC), CS-functionalized GO (GO/CS) and GC-functionalized GO (GO/GC) nanoparticles (NPs). **(A)** pH of GO (1 mg/ml), CS (10 mg/ml), and GC (10 mg/ml) solutions; **(B)** Size measurement (colloidal size distribution) of free GO and 1/4, 1/10, 1/20 ratio of GO/CS, and GO/GC NPs in Milli-Q water; **(C)** Zeta potentials (surface charge) of free GO and 1/4, 1/10, 1/20 ratio of GO/CS and GO/GC NPs in Milli-Q water. The concentrations of the solutions

are the following: 1/4 NPs: 0.05 mg/ml GO, 0.2 mg/ml CS and GC. 1/10 NPs: 0.05 mg/ml GO, 0.5 mg/ml CS and GC. 1/20 NPs: 0.05 mg/ml GO, 1 mg/ml CS and GC. Data are presented as mean ± SD (n=3). 36
Figure 17. In -depth temperature measurement of laser irradiated tissue-mimicking materials (TMM). **(A)** Schematic of the set-up for the measurement of the temperature changes at different depths of the tumor-bearing tissue-mimicking materials. The temperature was measured using a four-channel thermometer connected to four type T thermocouples placed at different heights of the TMM (T1-T4 on the schematic), including one being placed inside the dye-enhanced spherical gel (T3). **(B)** Temperature changes at different depths of the GO-enhanced TMM that was irradiated at 980 nm for 10 minutes. The thermocouple T3 measures the temperature changes at the center and the middle of the GO-enhanced spherical gel. 38
Figure 18. Thermal study on spherical dye-enhanced tumor phantoms. **(A)** TMMs with GO-enhanced spherical gels irradiated at 805 nm for 10 min; **(B)** TMMs with GO-enhanced spherical gels irradiated at 980 nm for 10 min; **(C)** GO/CS- and GO/GC-enhanced TMMs compared with GO-enhanced TMMs; **(D)** 50% GO- and 50% ICG- enhanced TMMs thermal effects comparison. 5%: 2.5 μg/ml GO, 10%: 5 μg/ml GO, 30%: 15 μg/ml GO, 50%: 25 μg/ml GO, 80%: 40 μg/ml GO, 10% GO/GC and 10% GO/CS: 5 μg/ml GO and 100 μg/ml CS and GC. GO and ICG are at the same concentrations in the phantoms, thus 50% ICG: 25 μg/ml ICG. The power density is 2 W/cm^2 at 805 nm and 980 nm. (n=3). 40
Figure 19. Temperature changes at different depths of GO-enhanced spherical phantom of tumors irradiated for 10 min with near-infrared lasers. The power density is 2 W/cm^2 at 805 nm and 980 nm. (n=3). The distance between 2 probes is 0.3 cm., 10%: 5 μg/ml GO, 50%: 25 μg/ml GO..... 42
Figure 20. In vitro cytotoxicity assay. **(A)** Relative cell viability of pancreatic Panc02-H7 cells incubated with free GO, free CS, GO/CS, free GC, and GO/GC (2.5 μg/ml GO and 50 μg/ml CS and GC) for 24h without laser irradiation and with laser irradiation (980 nm, 10 min, 0.7 W/cm^2). **(B)** Relative cell viability of melanoma B16-F10 cells incubated with free GO, free CS, GO/CS, free GC, and GO/GC (2.5 μg/ml GO and 50 μg/ml CS and GC) for 24h without laser irradiation and with laser irradiation (980 nm, 10 min, 0.5 W/cm^2). 45
Figure 21. (A) Levels of IL-6 secreted by BMDMs incubated with the indicated NPs (2.5 μg/ml GO and 50 μg/ml CS and GC). **(B)** TNF-alpha secreted by BMDMs incubated with the indicated NPs (2.5 μg/ml GO and 50 μg/ml CS and GC). **(C)** IL-6 secreted by BMDMs incubated with the indicated concentrations of GO. **(D)** TNF-alpha secreted by BMDMs

incubated with the indicated concentrations of GO. **(E)** IL-6 secreted by BMDMs incubated with the indicated concentrations of GC. **(F)** TNF-alpha secreted by BMDMs incubated with indicated concentrations of GC. Data are presented as mean ± SD (n=3). 47
Figure 22. Cytokines secretion by dendritic cells 2.4 (DCs 2.4) and bone marrow-derived macrophages (BMDMs) exposed to indicated concentrations of graphene oxide (GO). **(A)** Cytokine IL-6 secreted by DCs 2.4 after 24 h incubation with GO. **(B)** Cytokine IL-6 secreted by BMDMs after 24 h incubation with GO. **(C)** Cytokine TNF-alpha secreted by DCs 2.4 after 24 h incubation with GO. **(D)** Cytokine TNF-alpha secreted by BMDMs after 24 h incubation with GO. Data are presented as mean ± SD (n=4). 49
Figure 23. In vitro immune stimulation and analysis of surface markers by flow cytometry. **(A)** Gating strategy applied to the flow cytometry data for future analysis. **(B)** Effects of GC on the viability of activated BMDMs. **(C)** Expression of the BMDMs activation markers. ... 51

Abstract

Graphene oxide (GO) has been shown as a potential nanoadjuvant for biomedical applications. Particularly, the capability of GO in loading different therapeutic agents and in absorbing light of a broad wavelength range make GO an ideal nanoplatform for drug delivery and selective phototherapy. Chitosan (CS) is a naturally occurring compound with strong immunological stimulating effects. N-dihydrogalactochitosan, also referred to as glycated chitosan (GC), is an innovative and effective immunostimulant/adjuvant that further enhances the immunostimulatory and surfactant properties of CS. In this study, both CS and GC were used to functionalize GO to improve its biocompatibility and improve its immune-stimulating effect for cancer treatment. This work was designed to determine the main properties of GO/CS and GO/GC nanoparticles (NPs), when used in near-infrared photothermal therapy (PTT) for laser-initiated immunotherapy for cancer treatment. GO/CS and GO/GC NPs were synthesized by self-assembling in an aqueous solution *via* electrostatic interactions. GC allows for better dispersion and stabilization of NPs than CS. Compared with GO, GO/CS and GO/GC had bigger sizes and positive surface charges. GO showed high thermal conversion ability when irradiated with a near-infrared laser. *In vitro* studies were conducted to determine the effects of GO/CS + PTT and GO/GC + PTT on target pancreatic and melanoma tumor cells. Free GO was toxic to the cells whereas GO/CS and GO/GC showed limited cytotoxicity. The combination of NPs with PTT caused significant tumor cell death due to the GO-enhanced laser light absorption. Dendritic cells and macrophages were stimulated *in vitro* to investigate the potential of the NPs as immune-stimulating agents in inducing the secretion of the pro-inflammatory cytokines IL-6 and TNF-alpha. The responses of the immune cells to GC and GO were evaluated by phenotyping the surface markers by flow cytometry. Overall, GO/CS and GO/GC showed promising properties as stable, safe, and effective photothermal agents and immunostimulants for nano-ablative immunotherapy for cancer. Future *in vitro* and *in vivo* studies will be conducted to further understand the effects of GO/CS and GO/GC as nanostimulants/adjuvants for cancer treatment and vaccination. This and future work will lay the foundation for future clinical applications of these novel nanosystems.

Keywords: graphene oxide (GO); chitosan (CS); N-dihydrogalactochitosan (glycated chitosan, GC); immunostimulant; laser immunotherapy (LIT); thermal effect; cell death.

1 Introduction

Cancer is a major public health issue with a global impact across the world [1]. According to the World Health Organization (WHO), cancer is the second leading cause of death [2] and an important barrier to the increase of life expectancy in every country [3]. The burden of cancer incidence, *i.e.*, the rate of new cancers, and mortality are quickly growing worldwide, reflecting the global aging and growth of the population [4]. Numerous organizations provide updates and data on the global cancer burden, such as the most diagnosed cancers and main causes of cancer death by sex over the world [1]. For males, prostate cancer is the most frequently diagnosed cancer, followed by lung, colorectal, and liver cancers [5]. The most diagnosed cancers in females are breast and cervical cancers.

Cancer is the second cause of death in the United States [6]. According to cancer incidence and mortality statistics reported by the National Cancer Institute (NCI) [7], the most common type of cancer is breast cancer, with 284,200 new cases in the United States in 2021[8]. The next most common cancers are prostate and lung cancers [9]. Lung, breast, and prostate cancers lead to most patients' deaths. Pancreatic cancer is very deadly because even a single localized tumor can lead to a high mortality rate for the patients [9].

Cancer treatment is based on the stage of the cancer. Treatments aim to cure cancer or to stop the disease from spreading further. The patient's treatment plan may change over time[10]. Historically, cancer treatments have been constantly evolving. It started with surgery, chemotherapy, and radiation therapy. Now strategies are moving on to the most promising cutting-edge therapies, such as immunotherapy, gene therapy, and nanomedicine. These innovative therapies progressively arrive in clinical practice and on the market, presenting numerous promises and challenges. However, history shows that the fight against cancer is not an easy task, particularly because of tumor metastasis. Approximately 90% of cancer deaths are caused by metastatic cancer [11, 12]. Many types of cancers can resist conventional therapies, and different combinations of drugs and therapies (e.g., surgery together with radiotherapy and chemotherapy) are usually the only way to destroy tumor cells [13]. Current treatments present safety concerns and limited efficacy because cancer patients suffer from a weakened immune system, anemia, nausea, fatigue, etc.[14]. There are a few treatment modalities for advanced-stage cancers [15, 16, 17] and much more studies are needed to improve existing therapies and explore new ones. Nevertheless, these new ways of treatment are bringing hope for many cancer patients.

2 Cancer biology

To apprehend the challenges at stake in cancer therapy, it is important to understand the biology of cancer, as well as the growing strategies of tumors and metastasis.

2.1 General information on cancer

Cancer is a disease involving abnormal cells that divide and proliferate without control[18] because the body's immune system cannot recognize and destroy the cancer cells. **Figure 1** shows that the proliferation of healthy cells is under control and is modulated, while cancer cells proliferate uncontrollably and escape the patient's immune cells surveillance[19]. Thus, cancer cells lead to the formation of tumors.

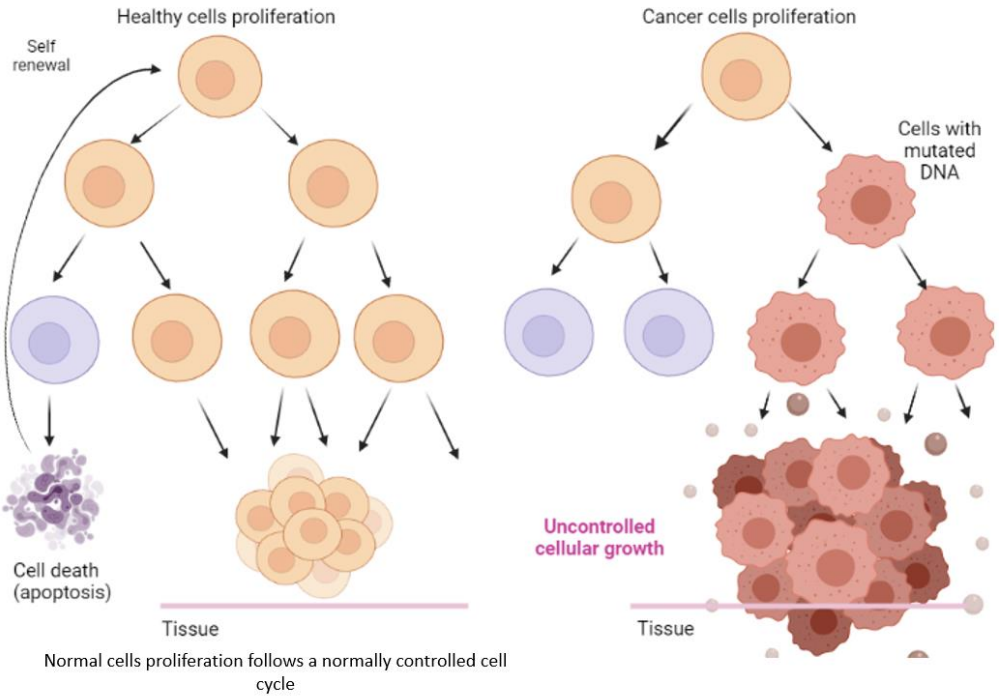

Figure 1. *The proliferation of healthy cells vs cancer cells.*

Created with BioRender.com

Cancer cells have different characteristics from healthy cells, as described in **Table 1**. Under the microscope, healthy cells look uniform, with similar sizes and orderly organization, while cancer cells look less orderly, with varying sizes and without apparent arrangement [20].

***Table 1**. Comparison of the main characteristics of healthy cells and cancer cells* [21].

Healthy cells	Cancer cells
Standard cell size and shape	Variable cell size and shape
Small and uniformly shaped nuclei	Large and variable-shaped nuclei
Differentiated cell structures and organelles	Loss and alteration of normal specialized structures
Relatively large cytoplasmic volume	Relatively small cytoplasmic volume
Normal presentation of surface markers	Abnormal expression of surface markers (overexpression or low expression of certain markers)
Cells arranged into clearly demarcated tissue	Disorganized arrangement of cells and
Controlled number of dividing cells	Uncontrolled and many dividing cells

Doctors can determine the type of cancer based on how the cells look under a microscope. Some cancers are categorized according to which type of normal cells and tissues they look like most, *i.e.*, the organs or tissue they come from. For example, cancers looking like glandular tissues are called *adenocarcinomas*. Other cancers which resemble certain immune system cells are called *lymphomas*, and those that look like bone or fat tissue are *osteosarcomas* and *liposarcomas*, respectively [22]. While identifying the cell type or tissue a cancer looks like, doctors also decide how closely they look like the healthy cells or tissues. This is the grade of cancer [23]. Cancers that look more like healthy tissues are called *low grade*, and those that do not look much like healthy tissues are *high grade* cancers. High-grade cancer tends to grow and spread faster than low-grade cancer. Patients with high-grade cancers tend to have a poorer prognosis [24, 25].

2.2 Cancer metastasis

When cancer is at an advanced stage, tumor cells spread in the body, and new tumors can appear at different distant places. Metastases are caused by the formation of one or more secondary tumors generated from a primary tumor because cancer cells have spread from the place where they first formed to another part of the body [18]. Indeed, cancer cells first break away from the original (primary) tumor, then invade nearby tissues by spreading through the bloodstream and/or lymphatic system, and form new tumors in distant sites. Cancer is then

metastasized. The new, metastatic tumor is the same type of cancer as the primary tumor [26]. For example, if breast cancer spreads to the brain, the cancer cells in the brain are breast cancer cells, not brain cancer cells [27], as shown in **Figure 2**.

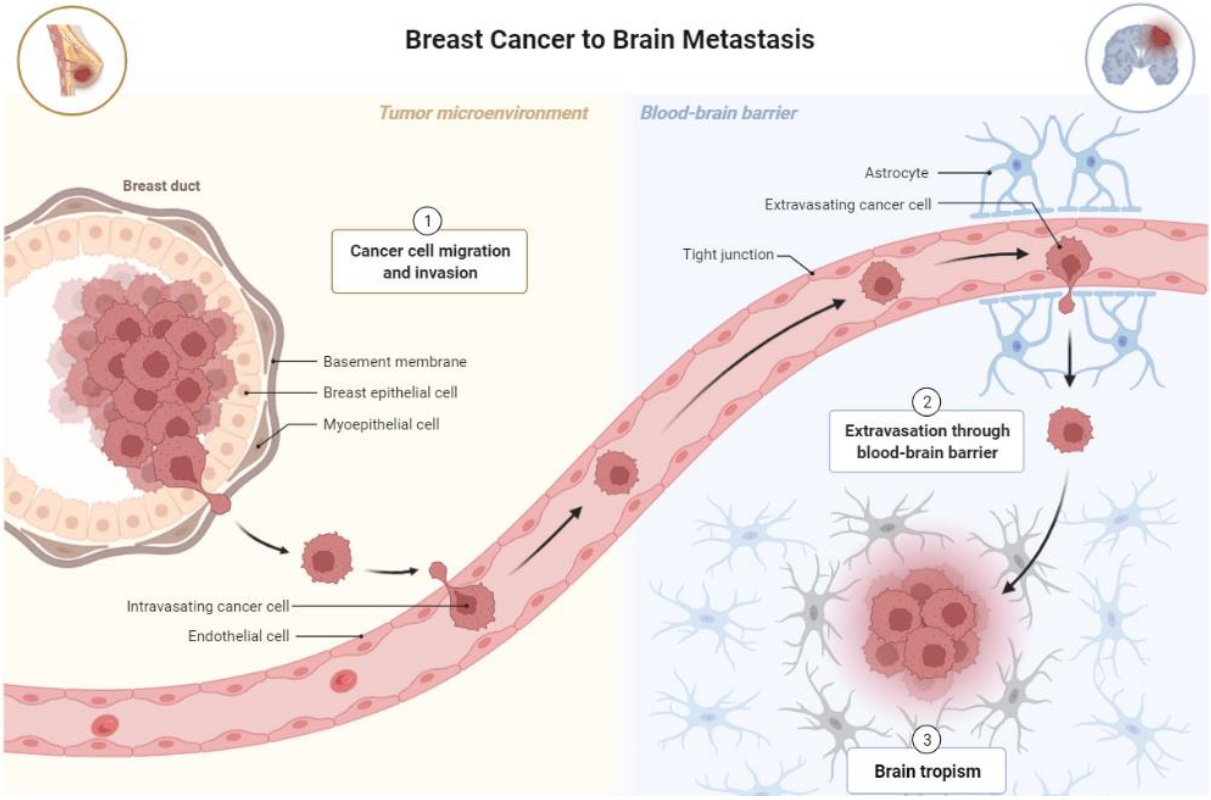

***Figure 2**. Metastatic cancer: the tumor spreads through the body. Example of breast cancer metastases in the brain at advanced-stage breast cancer.*

Created with BioRender.com

Usually, when cancer is metastasized, the chance for the patient to survive becomes very low [28, 29], demonstrating the importance of developing cancer therapeutics able to target cancer metastases [30]. Fortunately, many different techniques are available to detect and treat cancer.

2.3 Tumor microenvironment

The tumor microenvironment (TME) is a corrupted ecosystem, independent of the biology of the body [31]. The composition and the architecture of the TME is unique, different from any health tissues. The TME of a solid tumor is characterized by a low pH, hypoxia, acidosis, and high interstitial pressure [32]. A solid tumor is composed of malignant parenchyma which support the tumor structure and stromal cells that help tumor growth [33]. **Figure 3** shows

the interplay of tumor cells and immune cells in the TME as well as the main physiological conditions in this environment [31]. Different types of cells have been identified in the TME, such as cancer-associated fibroblasts (CAFs) [34], malignant cells, necrotic and hypoxic cells, mesenchymal stem cells, vascular endothelial cells, adipocytes, and pericytes. The TME encompasses multiple types of immune cells: tumor-associated neutrophils (TANs), tumor-associated macrophages (TAMs), dendritic cells (DCs), myeloid-derived suppressor cells (MDSCs), mast cells, granulocytes, T lymphocytes, T-regulatory cells (Tregs), B cells, and natural killer (NK) cells [35]. The TME also contains diverse non-cellular compounds such as extracellular matrix, cytokines and multiple signaling molecules involved in numerous communication pathways between the cells [36]. In addition, the TME presents abnormal vascular structure [37]. In the environment of a solid tumor, the vasculature is different from the vasculature in healthy tissues and highly heterogeneous [38]. The structure of the vasculature surrounding a tumor is specialized for the increased supply to the tumor.

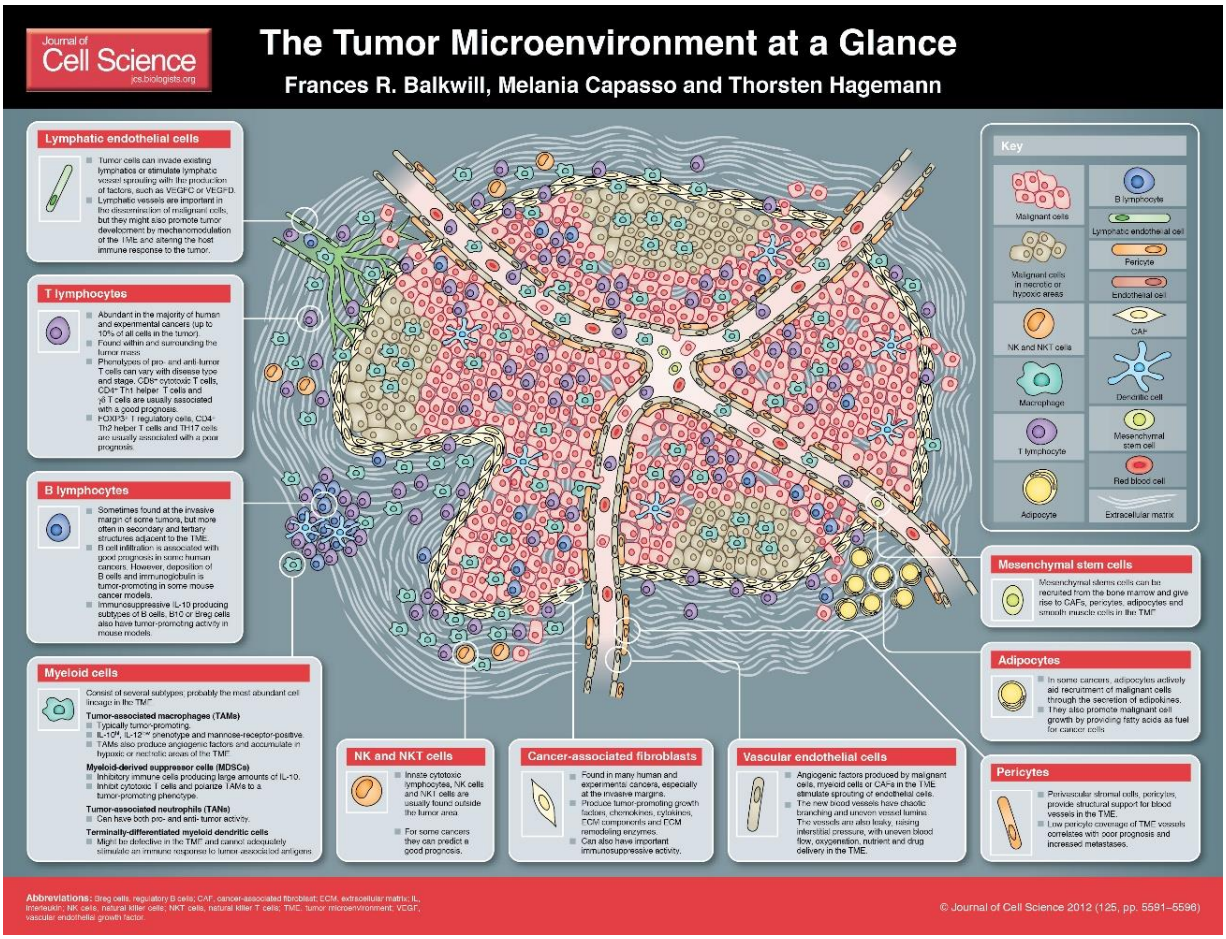

Figure 3. *The tumor microenvironment at a glance* [31].

The composition of a tumor and TME determines how cancer responds to therapies such as radio and/or chemotherapy [39, 40] as well as immunotherapy [41], cellular and acellular components of the TME being able to reprogram tumor initiation, growth, invasion, and metastasis. The TME transforms infiltrating cells to help maintain tumor homeostasis and promote the survival of cancer cells [42]. In response to signals from the tumor, various immune cells are recruited to the tumor site, often having their antitumor functions inhibited and being stimulated to promote tumor growth while anti-tumor effector cells die by apoptosis. As a result, the tumor escapes from the host's immune system [43, 44]. The various components actively interact with one another and interplay in the complexity of the TME. In short, the TME participates in immune evasion, tumor escape, hypoxia, acidosis, metabolic exchange, local invasion of distant locations (metastasis), angiogenesis, and tumor growth.

The suppressive immune microenvironment that helps cancer to avoid immune destruction is closely related to the cancer prognosis [45, 46, 47, 48]. A better understanding of the cellular and molecular pathways involved in the immune escape mechanisms at stake in the TME would allow cancer researchers to better apprehend how to block tumor escape [49]. Thus, novel therapeutic strategies are designed to change the pro-tumor microenvironment to one favoring acute responses and potent anti-tumor activity [50, 35, 51]. Since the composition and morphology of both the tumor and the TME strongly affects the response of tumors to therapy, as many parameters as possible should be included in models that simulate tumor growth and tumor response to cancer treatment modalities. Those data are used to determine the most effective treatment schedule depending on tumor properties, the goal being to improve, personalize, and customize treatment plans on an individual patient basis. Thus, accurate simulations of the tumor and TME are important in exploring and optimizing targeting cancer treatment techniques [52].

2.4 Cancer immunology

Cancer biology is related to the immune system since immunity plays a key role in tumor progression. Cancer immunoediting describes the mechanism by which the immune system responds to cancer and vice versa. The mechanism is divided into four phases, as described in **Figure 4**.

The first phase is called the *initiation* phase, when cancer starts to develop.

The second phase is the *elimination*, which corresponds to immunosurveillance, where the immune system recognizes and attacks tumor cells. Several immune cells are involved in tumor elimination. For instance, NK cells are innate immune cells which can kill tumor cells *via* three ways: NK cells can respond to an activation signal, lack of self-recognition molecules or having the CD16 receptor binds to an antibody bound to the tumor cell. $CD4^+$T cells are adaptive immune cells that can kill tumor cells through two pathways: 1) *Direct* tumor killing in case the $CD4^+$T cell is tumor antigen-specific by binding to MHC II-expressing tumor cells. Helper T cells can directly kill cancer cells by secreting tumor-killing molecules; 2) *Indirect* tumor killing by initiating the activation of tumor-infiltrating macrophages. $CD8^+$T cells, or cytotoxic T cells (CTLs), are adaptive immune cells that can directly kill tumor cells by secreting cytokines, perforins, and granzymes. B cells are adaptive immune cells producing antibodies which specifically bind to the tumor cells. B cells can secrete cytokines and release granzymes to directly kill tumors. But this phenomenon is still not fully understood.

After elimination comes the *equilibrium* phase, when some tumor cells can evade immune recognition, survive, and grow. During the equilibrium phase, immune cells can no longer kill cancer cells. During the equilibrium phase, the more aggressive tumors are selected. Some tumors can indeed overcome immune cells' anti-tumor activities. If tumor cells stop expressing MHC I on their surface, anti-tumor immune cells are no longer able to recognize the tumor cells. Immunosuppressive molecules expressed on the surface of tumor cells can also prevent tumor killing. Furthermore, cytokines can influence the tumor-killing ability of T cells.

Phase four is the *escape* phase: the tumor that escaped the immune system expands in an uncontrolled manner and grows in the surrounding tissues.

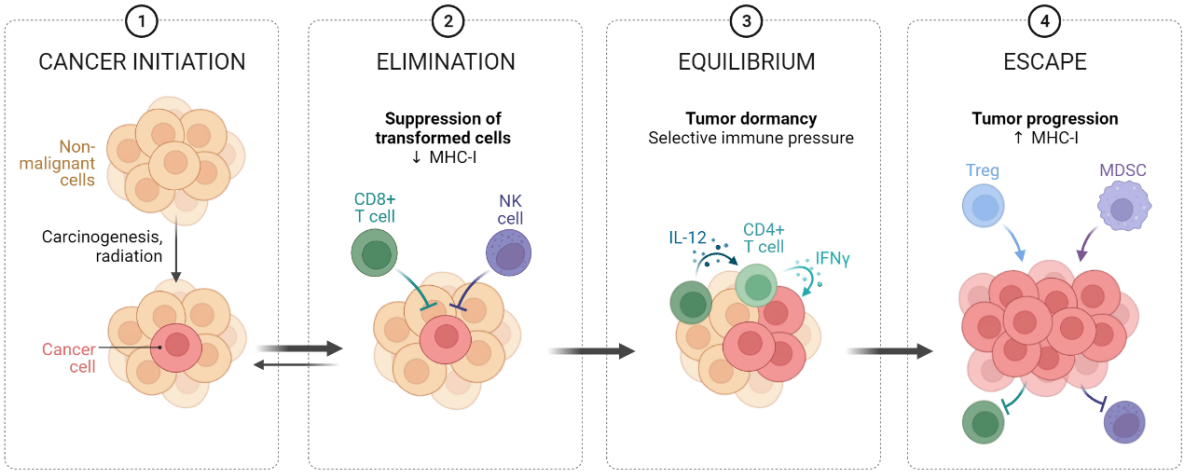

Figure 4. *Cancer immunoediting.*

Created with Biorender.com

The T cell-mediated tumor cell killing activity in the elimination phase is illustrated in **Figure 5**. When some tumor cells start to undergo CTL-mediated apoptosis, tumor-specific antigens are generated by apoptotic cells. Those antigens are internalized and presented at the surface of antigen-presenting cells (APCs), such as macrophages and dendritic cells. Mature APCs migrate to the lymph nodes, where they present the antigens to naïve T cells, leading to the activation of T cells against the specific tumor the antigens come from. Activated T cells next migrate to the tumor site, where their CTL activity causes tumor cell apoptosis, further generating antigens and maintaining the tumor-specific T cell induction and anti-tumor function.

To activate a naïve T cell in the germinal center, the tumor antigen presented by the MHC I of a dendritic cell must be recognized by the T-cell receptor (TCR) of the T cell. In addition to the MHC-I / TCR interaction, CD80 and CD86 receptors of the dendritic cell must successfully interact with CD28 at the surface of the T cell. Thus, the naïve T cell is activated into an effector T cell, proliferates, and migrates to the tumor site. When the TCR and the CD8 of the CTL successfully interact with the MHC I molecule of the target tumor cell, molecules like perforins and granzymes kill the tumor cell through the formation of pores in the membrane of the target cell. The effector T cell also produces cytokines such as interferon gamma (IFN γ) and tumor-necrosis factor alpha (TNF-α) leading to tumor cell apoptosis. When the tumor cell is dying from the damages caused by the $CD8^{+}$T cell, the receptors of the two cells separate from each other and the T-cell is released.

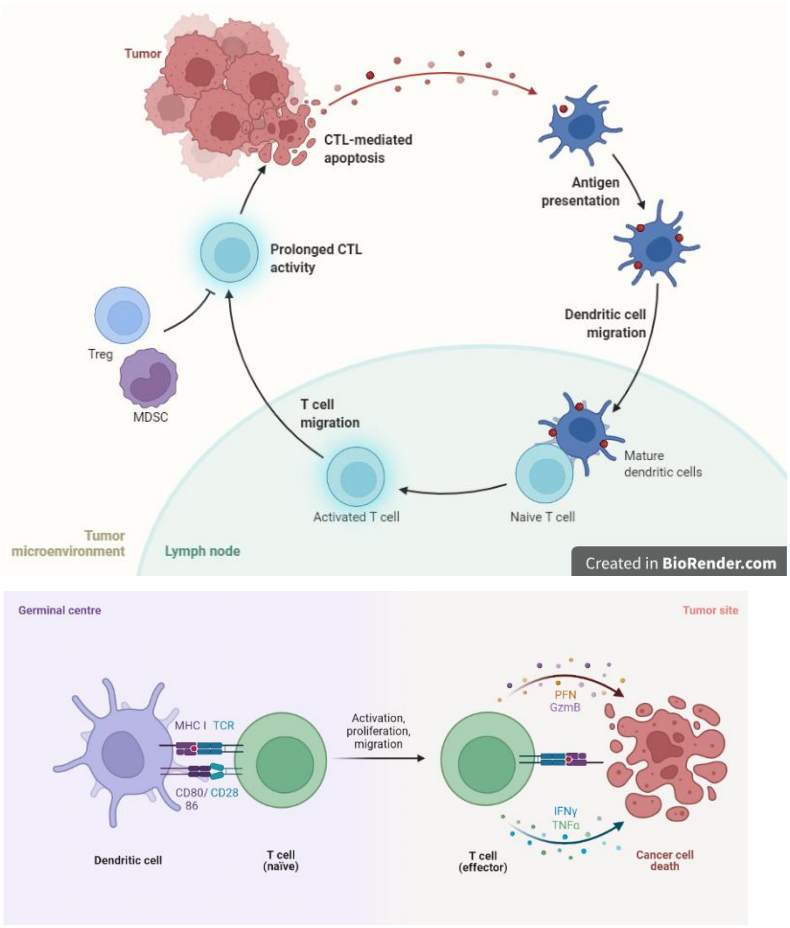

Figure 5. *T cell-mediated tumor cell killing.*

Created with Biorender.com

To sum up, the TME is a very complex ecosystem. Cancer and immunology are complexly interconnected. They adapt and evolve together with tumor progression. The TME is complex and unique to each individual tumor, even in the same patient. This is the reason why multimodal, personalized therapeutic approaches are required to completely unleash the power of the immune system to kill tumor cells.

3 Cancer therapy

Fighting cancer is challenging because the immune system often fails to recognize and fight cancer cells. Cancer therapy has experienced many ups and downs throughout time, mainly because of the limitations and improvable effectiveness of treatments as well as undesirable side effects [13]. Many therapeutics were developed to fight against cancer and to try to cure this highly complex disease. Traditional therapeutics include surgery which is commonly used to remove solid tumors, alongside antitumor drugs and radiation that have been the standard of treatment in some cases. Recently, immunotherapy has become an important cancer treatment modality and is now the first choice for many patients. Nanotechnology has also led to engaging progress for cancer therapy. Nanostructures offer new therapeutic alternatives for controlled drug delivery, combination between imaging and treatment, hyperthermia, and directed target therapy, among others. These therapies can be applied either alone or in combination with other components (antibodies, peptides, folic acid, *etc.*). In addition, gene therapy is also offering promising new options for cancer treatment.

3.1 Surgery, radiation therapy and chemotherapy

Surgery, radiation therapy and chemotherapy are considered standards for cancer treatment.

Surgery is the oldest cancer treatment option. When possible, surgical resection can offer a chance to directly remove solid tumors and resection is often guided by imaging [53]. However, some tumors cannot be surgically operated because of the size, location, and metastasis. The benefit of using cancer surgery is very limited for the patient since cancer is a systemic disease [54]. Surgery can be conducted in some life-threatening situations and be optimized to become as minimally adverse as possible for patients. Combination therapies and minimally invasive cancer therapeutics are preferred to this radical procedure [55]. Thanks to medical advances the objective is now to preserve the patient's quality of life as much as possible while enhancing survival. For tumors that cannot be treated by surgery, the standards of care usually involve radiation therapy and chemotherapy.

Radiation therapy, also called radiotherapy, is a standard of care for cancer treatment and approximately 50% of all cancer patients received radiation therapy during their treatment process [56]. Radiotherapy uses high doses of ionizing radiation that kill tumor cells or cause

mutations leading to cancer cell death and shrinking of the tumor size, especially by decreasing the cell division potential. Radiotherapy can be a localized treatment and can be used on itself for the treatment of a few early-stage cancers. However, it is well known that the side effects of radiation therapy can be adverse for patients [57], because healthy cells and regions located near the treatment area can be damaged, causing nausea, hair loss and fatigue, among others. In addition, cancer cells can develop radioresistance affecting their radiocurability [58]. Research on cancer stem cells is now being conducted to better understand the radioresistance process and the phenotype of resistant cells in order to optimize radiation therapy [59]. In most cases, radiation therapy is used in combination with other cancer treatment modalities [60], such as chemotherapy, especially to control tumor metastases.

Chemotherapy involves drug treatments to kill cancer cells, by using the cytotoxic potential of immune cells to kill tumor cells and by targeting dividing cells. Chemotherapy is usually delivered systematically by an intravenous injection. Therefore, healthy cells can be damaged. Nanotechnology offers the opportunity to co-deliver several drugs having different pharmacokinetics and encapsulated drugs to specific target sites, which is particularly useful for sequential delivery [61]. Drug nanocarriers can be considered as the future of chemotherapy since they allow for advanced targeted therapies [62] and have been extensively studied for breast cancer [63, 64, 65], ovarian cancer [66, 67], and prostate cancer [68, 69], among others.

Radiotherapy and chemotherapy can lead to mild to serious side effects and they focus solely on targeting cancer cells. Furthermore, not all cancers respond to those treatments, hence more advanced cancer therapeutics are needed.

3.2 Phototherapy

Laser irradiation has emerged as a useful cancer treatment option since light can harness the photothermal and photodynamic effects to treat cancer.

Photodynamic therapy (PDT) is a well-established and minimally invasive cancer treatment modality involving the production of reactive oxygen species (ROS), such as singlet oxygen, responsible for cancer cell death by apoptosis. To be effective, PDT requires three elements: 1) visible or near-infrared (NIR) laser light irradiation, between 400 and 700 nm, 2) a molecule called photosensitizer (PS), and 3) an environment containing oxygen. PS usually are aromatic molecules able to absorb light and produce ROS when exited under irradiation at specific wavelength in the presence of oxygen. ROS induce cell death by apoptosis. Thus,

PDT causes tissue damage, cell toxicity and immunogenic cell death (ICD), which subsequently allows for immune stimulation. However, since the TME is a hypoxic environment, the therapeutic efficiency of PDT is limited.

Photothermal therapy (PTT) has drawn increasing attention as an effective and safe treatment method in oncology because of its minimally invasive and selective therapeutic potential [70]. PTT is indeed a well-established and minimally invasive cancer treatment modality involving NIR light and target-located light-absorbing photothermal agents to generate energy and kill cancer cells by heat. PTT can be applied topically or interstitially depending on the depth of the zone to treat. PTT involves the generation of near-infrared light energy by lasers combined with locally placed nanoparticles used for their light-absorbing properties. Nanomaterial-based PTT has especially shown promising results as a viable therapeutics for tumor ablation [71, 72, 73]. The photothermal effects induced by photothermal agents that convert light energy into heat increase the temperature of tumor target tissues and trigger immunogenic cell death (ICD) [74, 75, 76]. PTT-induced ICD activates and directs the host immune system against tumors. Thus, immune cells can be activated and secrete cytokines that properly activate a systemic anti-tumor immune response. PTT can contribute to the treatment of cancer metastasis [77]. Memory immune cells can also be formed, hence allowing for *in situ* cancer vaccination. Furthermore, the laser irradiation source can be external to the target tissues and applied topically or internal tissues can be irradiated by an interstitial fiber. The laser light is precisely directed to the target tissues and light-absorbing agents allow for a specific increase in heat in targeted tumor, hence protecting surrounding healthy nanoparticle-free tissues from a significant temperature change [78]. Laser irradiation with an adjustable dosage allows the selective elimination of various types of cancers and minimizes the damage to the surrounding non-malignant tissues [79, 80].

3.3 Immunotherapy

Metastasis is the major cause of treatment failure for cancer patients because the host immune system cannot detect nor destroy cancer cells, which leads to around 90% of patient deaths. Current cancer treatment modalities show limitations for the treatment of metastases. Local treatments such as surgery and radiation therapy lack systemic effect, leading to tumor recurrence and are unable to prevent the growth of tumors in distant sites. As for chemotherapy, in addition to severe negative side effects, the risk of recurrence is high. Thus,

the potential solution is to target the immunological root causes of cancer by activating, enhancing, and directing the immune system to fight against cancer. It is called cancer immunotherapy. Immunotherapy is a promising solution to metastatic cancers with recent new developments. The principle of immunotherapy relies on the stimulation of the immune system to prevent, control, and eliminate cancer [81]. There are multiple forms of cancer immunotherapy [82], such as targeted antibodies, cancer vaccines, adoptive cell transfer, tumor-infecting viruses, immune checkpoint inhibitors, cytokine therapy, and adjuvants.

When tumor cells die, tumor antigens are released, which have the role of damage-associated molecular patterns (DAMPs). Those tumor-derived DAMPs are critical to the stimulation of robust immune responses against tumors. For instance, tumor-derived DAMPs stimulate the immune response of DCs, which are antigen presenting cells (APCs). When resting DCs encounter tumor antigens, DC maturation is undergone. Mature DCs then present tumor antigens to cytotoxic T cells (CTLs) and CTLs are activated, which is called T cell priming. Activated $CD8^{+}$T cells are tumor-specific and have an antitumor function. In short, one of the strategies of immunotherapy involves the presentation of tumor antigens by DCs, leading to the generation of specific anti-tumor cytotoxic T cells, allowing for cancer vaccination eventually.

Tumors have a multitude of strategies to escape the anti-tumor activity of effector T cells (**Figure 6**). Tumor cells can decrease antigen presentation to T cells, decrease the number of T cell epitopes, induce T regs, inhibit the proliferation and activation of T cells, among others. This is the reason why T cells are key target cells for immunotherapy.

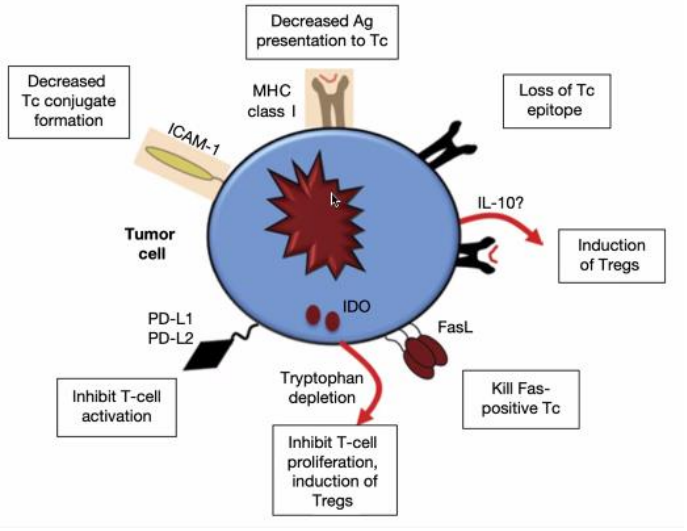

Figure 6*. The multiple immune escape strategies of tumors.*

It has been demonstrated that T cell checkpoint molecules, such as programmed cell death protein 1 (PD-1) and cytotoxic T lymphocyte-associated antigen 4 (CTLA-4) are frequently used by tumor cells to suppress the anti-tumor responses of effector T cells (**Figure 7**). Both tumor cells and immune suppressing cells can express molecules that bind to PD-1 and CTLA-4 on the surface of T cells. PD-1 and CTLA-4 signaling in T cells inhibits effector function and cytokine production, effectively neutralizing their anti-tumor effects.

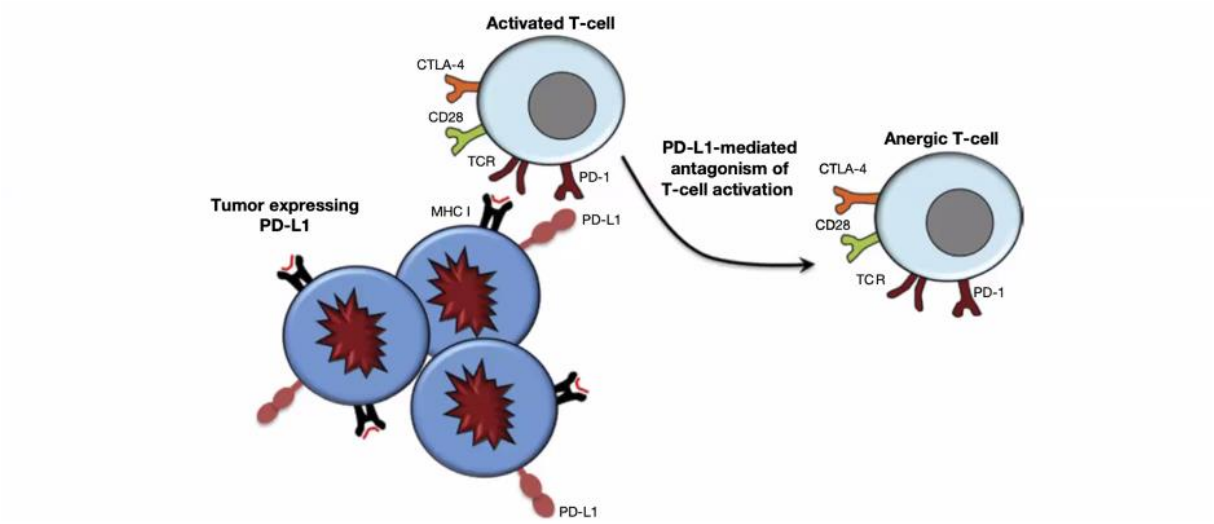

Figure 7*. T cell checkpoint molecules are used by tumors to suppress anti-tumor T cell activity.*

If PD-1 and CTLA-4 signaling in T cells are blocked, it is possible to promote tumor killing (**Figure 8**). If those immune checkpoints are blocked, T cells can recover their effector functions and kill cancer cells. The most common immunotherapeutic drugs used in the clinic to date are anti-PD-1 antibodies, such as pembrolizumab [83, 84] and nivolumab, [85, 86] which bind to PD-1 receptors on T cells. Tremelimumab [87, 88] and ipilimumab [89, 90] are commonly used as anti-CTLA-4 antibodies which bind to CTLA-4 receptors on T cells. Anti-PD-L1 antibodies, such as avelumab [91, 92] and durvalumab, [93, 94] can block PD-L1 interaction between dendritic cells and tumor cells. As a result, T cell proliferation, cytokines, and chemokines production as well as T cell cytotoxicity are augmented. This cancer treatment modality using checkpoint inhibitor drugs is called immune checkpoint therapy (ICT) [95].

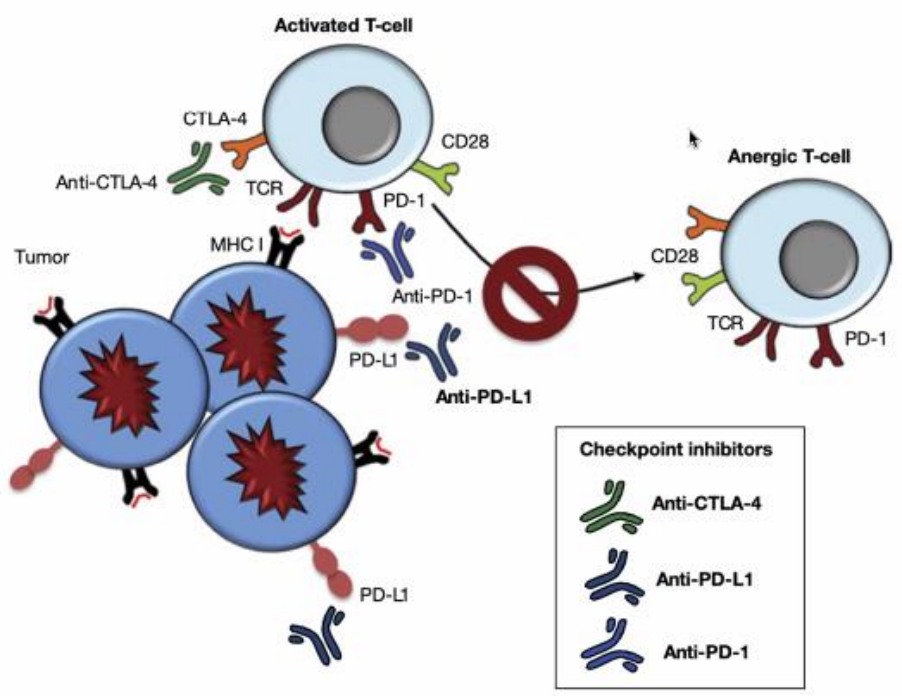

***Figure 8**. Checkpoint blockade immunotherapy.*

Disappointingly, ICT is usually not efficient enough and can be toxic. Failure of ICT can be split into three groups [96]: primary, adaptive, and acquired resistance to cancer immunotherapy. Patients who do not respond to immunotherapeutic strategies because of a lack of a sufficient anti-tumor T cell response present a primary resistance to immunotherapy. In other cases, cells acquire resistance with time (adaptive immune resistance). In that case, cancer is recognized by the immune system but protects itself by adapting to the attacks of the immune cells. It means that the patient's immune cells are activated but cannot kill cancer cells. Even if some patients can initially respond to the treatment, tumors can still progress because of the selection of resistant clones that existed prior to the treatment. If the population of cells resistant to immunotherapy was a small population before treatment, the decrease in the number of cells that are sensitive to immunotherapy allows for the expansion of the resistant cells, leading to a treatment failure eventually. The last group, called acquired resistance, refers to patients who initially responded to the treatment but after a certain period, cancer relapses and progresses due to the selective pressure on tumors to evolve.

The effectiveness of immunotherapy depends on whether the tumor is hot or cold. Hot tumors are immunogenic, *i.e.*, they can be infiltrated with immune cells and have the potential to elicit an immune response to immunotherapy. On the contrary, cold tumors are poorly

immunogenic and very few immune cells are able to infiltrate the tumor. Overall, the colder the tumor is, the poorer the prognosis.

However, generating antitumor immunity is not enough since the immunosuppressive effects of the TME still have to be overcome. The goal is to achieve turning pro-tumor activities into anti-tumor activities by favoring the recruitment of immune cells and enhancing cancer cell immune recognition by directing the metabolic pathways towards a permissive TME. Another strategy that can be combined with promoting anti-tumor activities is to inhibit the pro-tumor metabolisms preventing immune infiltration, survival, and antitumor functions. Combining ICD and ICT is actively investigated to target the immune subversive mechanisms of the TME [97, 98].

To sum up, the TME is a very complex ecosystem that researchers work on to improve the understanding of its nature and function. Multiple hallmarks of cancer are studied (**Figure 9**), so that these challenging aspects of cancer can be overcome for better therapeutic outcomes. Cancer and immune system are complexly interconnected since they adapt and evolve together with tumor progression. The TME is complex and unique to each individual tumor, even in the same patient. This is the reason why multimodal, personalized therapeutic approaches are required to completely unleash the power of the immune system to kill cancer cells. The future of cancer immunotherapeutic is multimodal therapies. The type of combinational therapy must be designed to target a specific tumor type, be patient-tailored and optimized to be able to overcome the immunosuppressive and very complex TME, which is a barrier to the success of anti-tumor immune therapies.

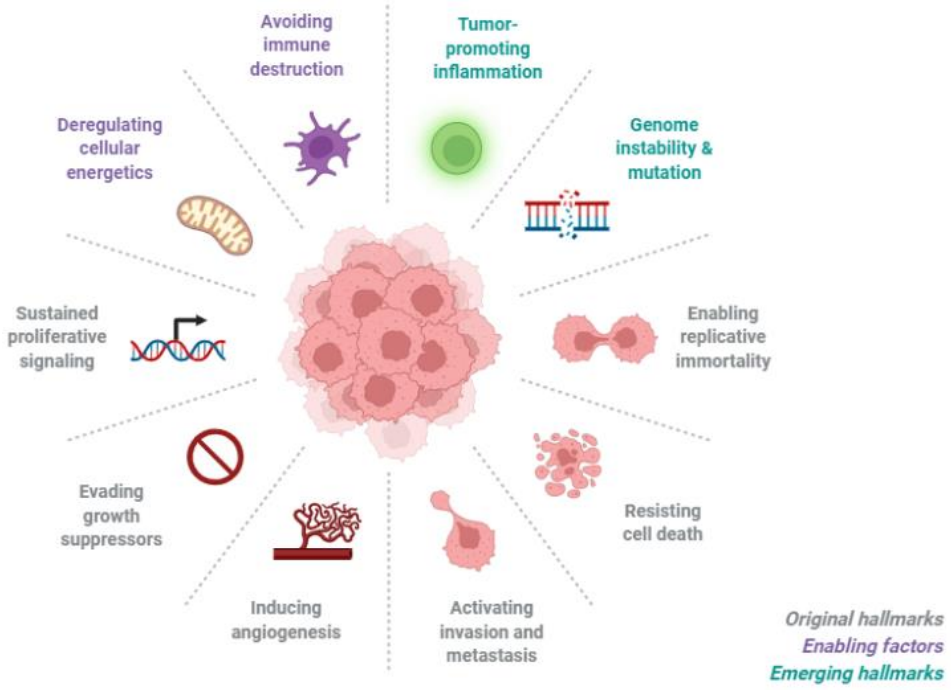

Figure 9. *Hallmarks of cancer.*

Created with Biorender.com

3.4 Laser immunotherapy

When used in combination with immunotherapy, the efficacy of nanomaterial-based PTT can be improved, allowing patients to be vaccinated *in situ* against cancer [99, 100]. In general, ablation-based therapy can utilize different components to enhance the efficacy of the treatment, as shown in **Figure 10**.

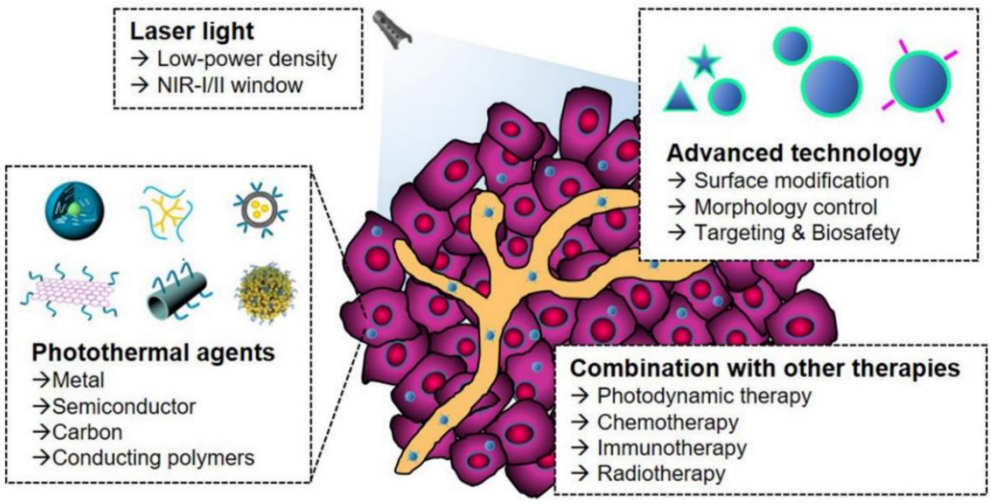

Figure 10*. Components of the nano-ablative photo-immunotherapies for cancer treatments* [70].

Specifically, laser immunotherapy (LIT) is a combinational therapy of targeted therapy and immunotherapy [70]. LIT combines a local intervention that specifically targets and kills the tumor cells with laser irradiation and a local immunological stimulation to induce a systemic, anti-tumor immunity for the treatment of metastatic cancers, as shown in **Figure 11**. *In vivo* results are very promising with significant tumor volume decrease, showing that LIT limits tumor growth. LIT allows for a significant extent of the lifespan of animals and the increase of the mice survival rate. LIT is often combined with other cancer therapies. For instance, nanoparticles are often used to deliver drugs to the tumor and can have NIR light-absorbing properties. The therapeutic efficiency of synergizing nano-ablative immunotherapy has been proved to be safe and effective for cancer treatment [101]. The effects of LIT on different tumor types are actively studied in order to understand the mechanisms of immunotherapy and extend the use of LIT to as many cancer types as possible. The different elements of LIT are also under study with the objective of finding the optimal components and formulating the combinations that are as efficient and safe as possible.

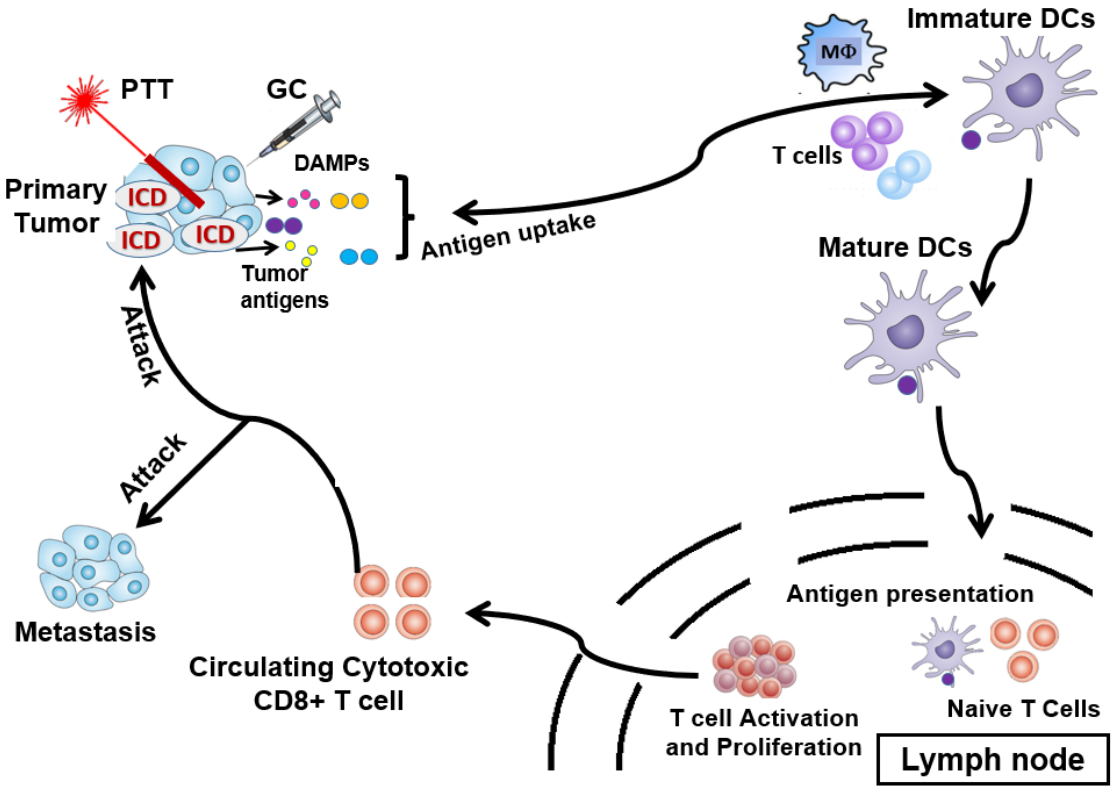

Figure 11. *LIT induces a systemic, anti-tumor immunity for the treatment of metastatic cancers.*

Chitosan (CS) is a nontoxic naturally available polysaccharide converted from chitin[102] and often used for biomedical applications [103]. The chemical structure of the CS molecule is presented in **Figure 12A**. CS is known to have low toxicity [104], good biocompatibility [105, 106], and be well biodegradable [107, 108]. Thus, CS has been broadly used to functionalize nanocarriers to reduce cytotoxicity, improve delivery efficiency and enhance systemic immunological activity [109, 110, 111]. CS is an effective immunostimulant, which can activate immune cells [112]. CS may have the same function as a toll-like receptor 2 (TLR2) ligand, which stimulates a strong immune response [113]. Thus, CS has shown promising results as an immunoadjuvant for cancer immunotherapy and cancer vaccine [114, 115, 116, 117, 118]. However, CS is difficult to dissolve in water, yet immunological experiments require aqueous solutions especially for *in vitro* and *in vivo* tests [119]. Chitosan can be dissolved in acidic solvents, such as 1% acetic acid [120], but even a slightly acidic environment can introduce bias in experiments involving cell responses to stimulation and viability measurements. Therefore, the low solubility of CS is a limitation for stimulating immune responses *in vitro* and *in vivo*.

Modifying the CS structure, by adding galactose molecules to the polysaccharide backbone, allows for a new compound called N-dihydrogalactochitosan, or glycated chitosan (GC) to be water-soluble [102]. The chemical structure of the GC molecule is presented in **Figure 12B**. GC was designed as an effective, safe immunostimulant for immune stimulations in combination with PTT for cancer treatment [121]. LIT, consisting of an intratumoral injection of GC combined with laser irradiation of the tumor, shows synergy of both photothermal and immunological effects. In addition, GC shows low toxicity levels when injected locally, which is an advantage for hosts having metastasized cancer. Previous studies showed that in murine mammary tumor cells (EMT6) treated *in vitro* and *in vivo* by laser irradiation at 980 nm in combination with GC stimulation, GC enters macrophages and stimulates TNF-α secretion. *In vivo* results show immunological effects of GC, particularly in inducing antitumor-specific immune responses. Hence, GC is a strong immunological stimulant for cancer treatment, particularly when combined with laser phototherapies [113, 122]. This cancer treatment modality has shown positive effects for the treatment of metastatic tumors. *In vivo* results indicate that treated primary tumors were ablated, untreated metastases shrunk by abscopal effect, the specific antitumor immune response was triggered,μ and long-term resistance to tumor rechallenge was observed [123]. Thus, GC is a new non-toxic immunological stimulant. LIT using GC is safe and effective to treat metastatic tumors and stimulating the host-specific, systemic, anti-tumor and long-lasting immunity [102].

A common issue that arises when working with nanostructures is congregation, which leads to a non-homogenous solution where compounds are not individually dispersed. Because of the congregation of the NPs, the characterization data and NPs-cell interactions can be biased. Therefore, surfactants are needed to help NPs to be homogeneously dispersed into solution. One of the most common surfactants is polyethylene glycol (PEG). PEG has been extensively studied and used in combination with functional NPs, especially for drug delivery for cancer treatment [124]. For example, PEG was used to coat NPs targeting the tumor microenvironment to overcome multidrug resistance [125]. Polylactic-co-glycolic acid (PLGA) is also commonly used in the field of nanomedicine for cancer therapies [126]. PEG and PLGA were proved to be surfactants for loading on NPs with anti-cancer activities [127, 128]. The chemical modification of bioactive compounds with PEG is known to improve pharmacokinetics and biological properties. However, the molecular weight of the chain and the structural modifications of PEG are of main importance for effective conjugation with other molecules [124]. Therefore, the addition of PEG to the surface of a drug requires meticulous attachment and the effects of the PEGylation process need to be closely examined and characterized [129, 130].

GC is a good surfactant that significantly increases NPs stability and solubility. GC does not require structural modifications to be loaded on drugs - GC being a polymer, it can wrap around NPs and help them stabilize. The surfactant effect of GC has been studied on anti-tumor immunologically modified single-walled carbon nanotubes [131, 132]. On one hand, using GC avoids using other surfactants, and on the other hand, GC is an immune-stimulatory agent. Therefore, GC possesses multiple advantages due to its dual functionality: immune stimulating agent and surfactant. In the following paragraphs, previous studies on therapeutic applications of LIT for the treatment of cancers in animals and patients are described.

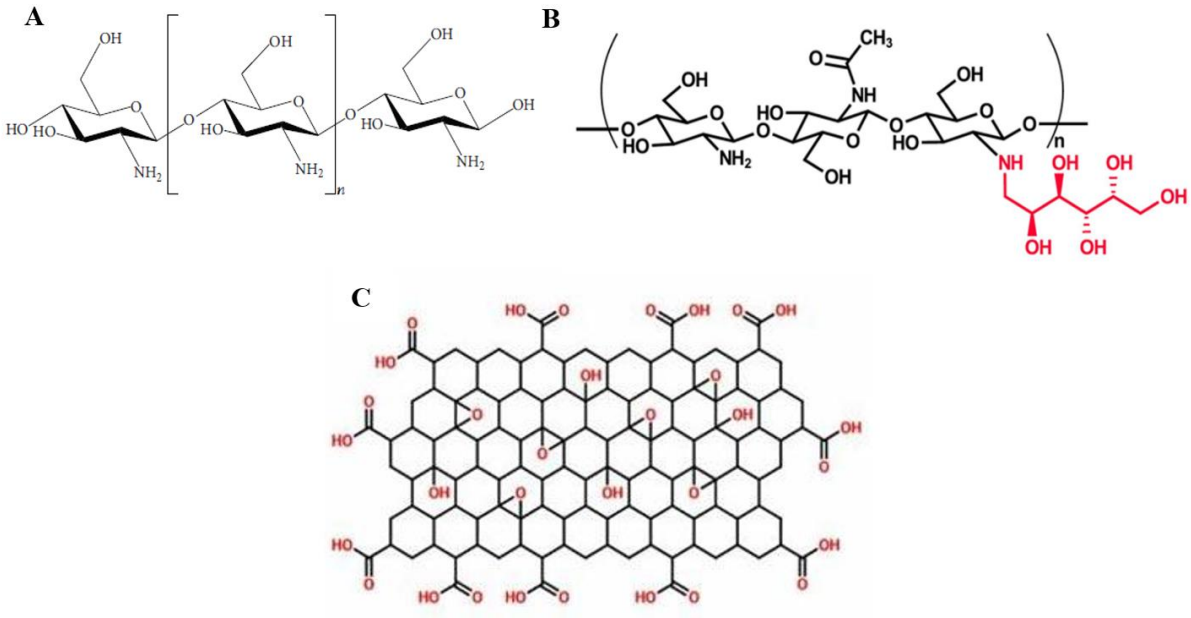

***Figure 12**. Chemical structures of the molecules studied in this thesis work: **(A)** the chitosan molecule [102], **(B)** the N-dihydrogalactochitosan (glycated chitosan) molecule [121], and **(C)** the graphene oxide molecule [133].*

Chen and colleagues studied the effects of the different components of LIT in the treatment of metastatic breast and prostate tumors in rats [123]. The immunostimulant GC and a NIR laser light-absorbing dye called indocyanine green (ICG) were intratumorally injected in order to specifically treat the targeted tumors and to stimulate the immune response. The drug administration was followed by non-invasive laser irradiation. Only the primary tumors were treated with LIT. It was shown that the primary tumor completely regressed and distant metastases decreased in size. This cancer treatment method induced a long-term and tumor-specific immunity. Animals were indeed conferred with a long-term resistance to tumor rechallenge. More precisely, in this work, breast- and prostate-tumor bearing rats were treated with different components of LIT, either individual components or various combinations of the elements of LIT: GC, ICG, and PTT. For breast-tumor bearing rats, treatment groups without GC had poor outcomes whereas GC on itself or in combination with other components of LIT showed a significantly positive effect on the survival of the animals. Nevertheless, the combination of GC+ICG+PTT was the most effective treatment, showing

the highest rate of cured rats. In the case of prostate-tumor bearing rats, the GC+ICG+PTT combination treatment showed a significant shrinkage of primary tumors and regression of metastases, thus positively increasing long-term survival.

In the study conducted by Zhou and colleagues, local PTT was proved to synergize with GC for the treatment of pancreatic cancer through the induction of an immunogenic cancer vaccine in mice [134]. Subcutaneous pancreatic (Panc02) model was injected on the left and right flanks of the animals to study the treatment of distal tumors and the abscopal effect. Mouse tumors were treated 7-10 days after injection of the tumor cells. The survival animals were rechallenged with Panc02 or B16-F10 (melanoma cell line). The treatment consisted in using non-invasive PTT on subcutaneous tumors followed by intratumoral injection of GC. The PTT+GC treatment group showed lower tumor volumes, primary tumor regression, and higher survival rates than the other groups (PTT only and GC only). For the distal tumor study, animals treated with PTT+GC had the lowest secondary tumor volume. PTT induced tumor cell death and the expression of DAMPs, such as HSP70 and HMGB1, was increased in PTT and PTT+GC treatment groups. The levels of secreted IFN γ produced by DCs in PTT+GC groups is significantly higher than in the PTT only and GC only treatment groups, showing that LIT stimulates DCs. The number of CD86+ DC in tumor tissues is much higher in the tumors treated by LIT than the other groups. DC infiltration in LIT-treated tumor tissues is more significant than the DC populations in the tumors treated by PTT only and GC only. T cells from the LIT group tend to upregulate the expression of CD69, proving that LIT activates T cells. To visualize the interaction between GC and DCs, GC was labeled with FITC (a green fluorescence tag) and incubated with DCs before imaging with a confocal microscope. GC-FITC was colocalized with the DCs. Since DCs have a potent phagocytic activity, GC is engulfed by DCs. PTT+GC induces a strong pro-inflammatory response since the levels of TNF-α and IFN-γ are significantly higher than in the other treatment groups. Since only the primary tumors were treated but not the second ones, the shrinkage observed on distant tumors confirms that LIT induces a systemic anti-tumor immune response involving effector CTLs. About 80% of the surviving mice in the PTT+GC group survived more than 100 days after Panc02 tumor rechallenge while none of the cured mice that were rechallenge with B16-F10 survived. This shows that immune memory is tumor-specific.

Overall, LIT is effective against primary tumors and distal metastases. LIT induces tumor cell death, the DAMPs and tumor antigens leading to the activation of DCs. DCs can phagocytose GC, therefore enhancing the anti-tumor immune response. GC+PTT indeed

increases the number of effector T cells (CTLs), enhances the secretion of pro-inflammatory cytokines, and allows for the generation of long-term memory T cells, leading to a protection against future tumor threat.

Cancer photo-immunotherapy attracts interest in cancer research, especially since this technology shows promising results for transitional work from bench to bedside. In a study conducted by Wang and colleagues [135], the therapeutic efficiency of PTT was demonstrated. Single-walled carbon nanotubes (SWNTs) were used as functional nanoplatforms for GC loading and intracellular delivery, leading to an improved CTL response. GC showed the best immunostimulant activity and can be used in synergy with PTT for improved therapeutic outcome. To study the LIT-induced T memory cells production, mice were treated with PTT and GC and later rechallenged. Mice showed lower death rates and survived longer after LIT and rechallenge compared to the other treatment groups. Intravital imaging was conducted on melanoma-bearing mice to visualize the tumor-infiltrating lymphocytes (TILs). The fluorescence of TILs shows a colocalization with cancer cells and is much brighter for cells treated with LIT than for the other treatment groups, proving that LIT enables T cells to effectively infiltrate tumors treated with LIT. The long-term survival and acquired resistance against tumor rechallenge was related to T-cell infiltration in tumors and the creation of memory cells able to protect LIT-treated mice from rechallenge. In addition, LIT was combined with ICB using Ipilimumab, Pembrolizumab, and Nivolumab. Ipilimumab blocks CTLA-4 checkpoint activity and therefore restores the immune response of CTLs. Pembrolizumab and Nivolumab are checkpoint drugs involved in PD-1 pathways. Several studies showed that the combination of LIT with anti-CTLA-4 enhanced systemic anti-tumor response and allowed for longer survival of 4T1 tumor-bearing mice. Other synergistic nanocomposites led to *in situ* vaccination of animals, which developed anti-tumor immune responses, helped by the inhibition of metastases. To further study the promising outcomes of LIT, ten breast cancer patients in stage III and IV with three to six months of life expectancy were treated with PTT+GC. After three years, eight patients were evaluated, four had significant reductions of metastases and one had all lung metastases cured and completely regressed. Eleven patients with a stage III or IV melanoma were treated with LIT and imiquimod (ISPI treatment). Six patients showed a complete response while only two of them partially responded. The 12-month survival rate reached 70%. ISPI could eliminate local tumors and stimulate long-term response.

Nano-ablative immunotherapy

Nanotechnology in medicine and cancer therapy has been extensively studied because it presents many advantages for cancer treatment such as high loading capacity, and controlled release of drugs. The possibilities of different formulations offer multiple therapeutic options. Multiple nanosystems have been used in cancer therapy [75, 73], with different compositions, structures, shapes, and functions, including spherical nanoparticles, nanotubes, nanocages, nanoplatforms, and nanosheets. A broad range of chemical compositions is being explored to evaluate and compare their efficiencies for cancer treatment, and compatibilities to and synergistic effects with other drugs. For instance, iron oxide nanoparticles have been studied for photothermal ablation of tumor cells as well as gold nanoparticles [136], copper-sulfide nanoparticles [137], carbon nanotubes [131], and graphene.

For instance, Zhou and colleagues [138] developed a novel treatment strategy for metastatic breast cancer that triggers host antitumor immunity by synergizing photothermal therapy, chemotherapy, and immunotherapy through a complex nanosystem composed of 1) Reduced graphene oxide (rGO), used for its nanoplatform and immunostimulant properties; 2) Mitoxantrone (MTX), used as the chemo-agent and immunostimulant and 3) SB-431542 (SB) was added to the nanosystem for its function of inhibitor of the transforming growth factor beta (TGF-β) pathway in the TME. The intratumoral injection of the nanosystem rGO/MTX/SB was followed by non-invasive NIR laser irradiation of the 4T1 tumors. The local primary tumors were destroyed by the treatment and did not grow back, and distant metastases were inhibited (**Figure 13**). Approximately 70% of the tumor-bearing mice survived after treatment and were long-term survivors, which demonstrates that those cured mice developed a tumor-type specific immunity. Therefore, rGO/MTX/SB + laser irradiation induced an effective *in situ* cancer vaccination.

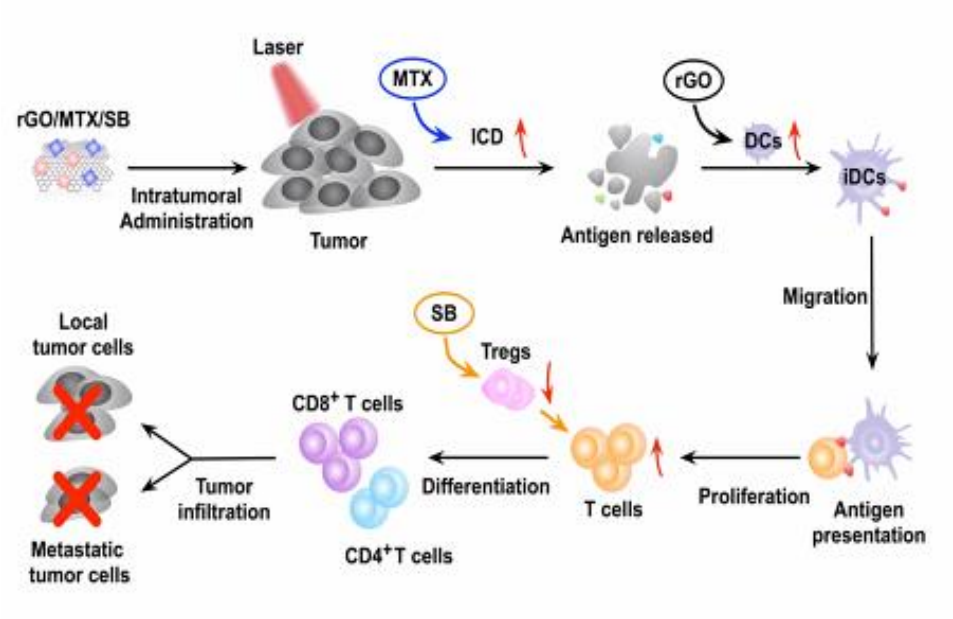

Figure 13*. Nanotechnology-based photoimmunotherapy for cancer treatment.*
F. Zhou et al, Biomaterials, 2020

Graphene oxide (GO) consists of a single layer of carbon atoms arranged in two dimensions that can be used for multiple applications [139]. The chemical structure of the GO molecule is presented in **Figure 12C**. This thin nanomaterial is used as a drug delivery system[140]. It is already known that CS-functionalized GO can be used as a potential immunoadjuvant [141, 142]. In this study, we will investigate if GC-functionalized GO is feasible and compare its properties with those of CS-functionalized GO. Other advantages of surface functionalization of GO are to improve its biocompatibility, thermal stability, and adjuvant activity [143, 111, 142, 144]. In addition, GO has laser light-absorbing properties, which amplifies laser-induced thermal effects, especially in the near-infrared range [144]. Therefore, GO has multiple advantages: good water solubility, large specific surface areas, and surface functionalization ability [143]. GO can also activate immune cells and trigger immune responses involving toll-like receptors [145, 146, 147]. The activation of multiple TLRs would enhance the activity of adjuvants to induce robust immune responses [142, 148]. As CS and GC can activate multiple TLRs, CS-functionalized GO and GC-functionalized GO may trigger an effective and rapid anti-tumor immune response. Plus, GC may prevent GO sheets from aggregating and allow nanoparticles to be stable. In this study, GO is used as a light-absorbing agent to enhance the generation of heat caused by PTT and increase tumor cell killing. GO is also used as a nanocarrier for drug delivery of immune-stimulating molecules.

3.5 Purpose of the work

The long-term goal of the research presented in this master's thesis is to develop a nanomaterial-based ablative photo-immunotherapy for cancer treatment. The nanoparticles presented herein are synergistic nanosystems for photo-activated immunotherapy. The nanomaterial of interest is graphene oxide, combined with anti-cancer drugs, either chitosan or GC for cancer treatment applications. The objective of the study is to evaluate the innovative nanosystem GO/GC as a potentially safe and effective immunoadjuvant for laser-initiated immunotherapy for cancer treatment.

This master's thesis is organized into three main sections. Since GC has never been loaded on GO sheets before, the first step of the work was to study the feasibility of the nanosystem, followed by the characterization of the main parameters of the newly obtained nanomaterial. The next part of the work was to study the photothermal conversion capability of the nanomaterial for PTT treatment applications using 3D phantoms of embedded light-absorbing tumors. Subsequently, the anti-tumor and immune stimulatory properties of the nanomaterials were evaluated *in vitro*, to study the synergy of the combination of GO with GC. In the last section, the results will be discussed, future work and planned improvement will be presented.

4 Study of the photothermal and immunological effects of immunologically modified graphene nanosystems

4.1 Materials and Methods

4.1.1 Materials

Nano graphene oxide (GO) aqueous solution (1 mg/ml) was purchased from Graphene Supermarket (Graphene Laboratories Inc., Ronkonkoma, NY, USA). Chitosan (CS) stock solution (1 wt%, 10 mg/ml) was prepared by dissolving CS powder in 1% (v/v) acetic acid solution. The mixture was stirred overnight to obtain a perfectly homogeneous and transparent CS solution [149]. Extensive sonication was required to fully suspend, and dissolve CS. Medium molecular weight CS powder (190-310 kDa) was purchased from Sigma-Aldrich Inc. (St. Louis, MO, USA). Water-soluble N-dihydrogalactochitosan (GC) stock solution (10 mg/ml)

with a molecular weight of 210-215 kDa was obtained from Immunophotonics Inc. (St. Louis, MO, USA). Agar was bought from Sigma-Aldrich Inc. (St. Louis, MO, USA). Indocyanine green (ICG) solution (0.1 wt%) was prepared by dissolving ICG powder (Sigma-Aldrich Inc.) in water. Cell Counting Kit-8 (CCK-8) was purchased from Sigma-Aldrich Inc. (St. Louis, MO, USA). Colorimetric 3-(4,5-dimethylthiazol-2-yl)-2,5-diphenyl tetrazolium bromide (MTT) kit for cell survival and proliferation assay was purchased from EMD Millipore (Burlington, MA, USA). Mouse IL-6 uncoated ELISA and mouse TNF-alpha uncoated ELISA kits were bought from ThermoFisher scientific (Waltham, MA, USA). All chemicals and reagents were used as received.

4.1.2 Preparation of GO/CS and GO/GC nanoparticles

The graphene oxide (GO) nanoplatform was assembled with chitosan (CS) and glycated chitosan (GC) to form GO/CS and GO/GC nanoparticles (NPs), respectively. CS and GC polymers were chosen with similar molecular weights to study their interactions with GO nanosheets. GO/CS and GO/GC NPs were prepared by self-assembly of both GO and CS and both GO and GC, respectively, in an aqueous solution through electrostatic interactions. In the typical procedure, the GO solution (0.05 mg/ml) was ultrasonicated for 10 min in a water bath sonicator. Three CS solutions and three GC solutions (0.2 mg/ml, 0.5 mg/ml, and 1 mg/ml) were ultrasonicated to have properly dispersed solutions. Then, the GO solution was added drop by drop to the CS or GC solution at equal volume with gentle stirring. The three GO/CS and three GO/GC ratios (1/4, 1/10, 1/20) were synthesized to assess the stability of the NPs and investigate the loading capacity of the graphene sheets. An excess of CS and GC was used for the functionalization of GO to ensure an optimal interaction between the polymers and the carboxylic groups on the GO nanosheets. If needed, the GO/CS and GO/GC mixtures were ultrasonicated. After stirring at room temperature for 2h, GO/CS and GO/GC NPs were collected by centrifugation (16900 g, 30 min). Unreacted CS, CG, and impurities were removed by washing with Milli-Q water. The obtained GO/CS and GO/GC were re-dispersed in PBS for storage and future experiments.

4.1.3 Characterization of GO/CS and GO/GC nanoparticles

The pH of GO, CS and GC solutions was measured using a pH meter (VWR, symphony) at 25°C. Data were averaged over three independent pH measurements. The colloidal size

distribution and surface charge (zeta potential) of the NPs were measured using a dynamic light scattering (DLS) instrument (Malvern ZetaSizer NanoZS, Malvern Panalytical Ltd, Malvern, UK) with a laser wavelength of 632.8 nm. Size and zeta potential were measured at 25°C. Data were averaged over three independent colloidal size distribution and surface charge measurements.

4.1.4 Thermal study on near-infrared irradiated nanoparticle-enhanced tissue-mimicking materials

Agar was used to construct soft phantoms that mimic a dye-enhanced inner tumor surrounded by background healthy tissues. Phantoms of tissue-mimicking materials (TMM) simulating surrounding healthy tissues for thermal therapy studies were fabricated by mixing water, milk (20% v/v), and agar (2% w/v) in a beaker with stirring until the mixture looks homogeneous. The dye (GO, GO/CS, GO/GC, or ICG) was added to the solution to obtain dye-enhanced tumor-mimicking phantoms. The solution was then heated with stirring until the temperature reached 90°C. The mixture cooled down at room temperature before being transferred to a 50 ml tube for background TMMs and a spherical-shaped mold for dye-enhanced phantoms. Gels were placed in the refrigerator (4-8°C) for 24 hours. When solidified, one dye-enhanced spherical gel was placed inside a background TMM. A gel layer was poured on top to cover the spherical gel. Tumor-mimicking phantoms were chosen to be spherical because it best simulates the shape of tumor tissues *in vivo*. Milk was used for laser light scattering purposes. 2% w/v agar-based gels are commonly used for the construction of TMM [150] [151]. The dye absorbs the laser light, which increases the temperature of the tissue-mimicking phantom. Dye-enhanced spherical phantoms of target tumors with different dye concentrations (5%, 10%, 30%, 50%, and 80% v/v) were made to evaluate the effect of the dye concentration on light absorption (5%: 2.5 µg/ml GO or ICG, 10%: 5 µg/ml GO or ICG, 30%: 15 µg/ml GO or ICG, 50%: 25 µg/ml GO or ICG, 80%: 40 µg/ml GO or ICG).

TMMs were irradiated with both 805-nm (Diomed 30 plus, Cambridge, UK) and 980-nm (Angio Dynamics, Queensbury, NY, USA) lasers for 10 min with a power density of 2 W/cm^2. Laser light was transmitted and directed to the samples by an optical fiber (Pioneer Optics Company, Bloomfield, CT, USA) with a cylindrical diffuser distributing the light intensity uniformly over the surface area. Temperature was measured at different heights of the TMM to investigate the temperature gradient in the gels. Laser irradiation was stopped

after 10 min and the in-depth temperature was measured for an additional 10 min to study the temperature decrease. The temperature was measured using a four-channel thermometer (SD-947, REED) connected to type T thermocouples placed at distinct heights of the TMM, including one being placed inside the dye-enhanced spherical gel (**Figure 14A**). Temperature changes inside the dye-enhanced tumor-mimicking material was also measured at three separate locations to further evaluate the photothermal conversion ability of GO and ICG as well as the temperature gradient inside the phantom of the tumor (**Figure 14B**).

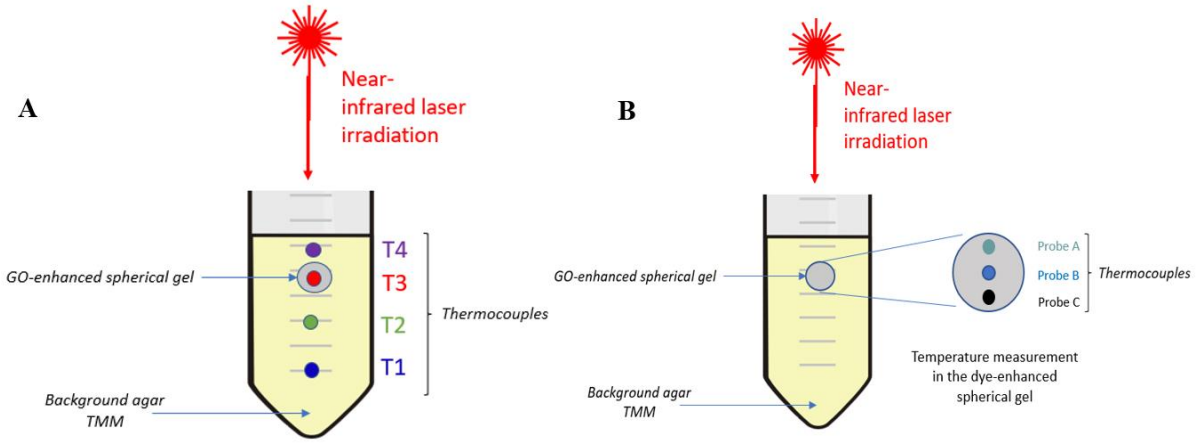

***Figure 14**. Schematic of the phantom set-up for the thermal study. **(A)** Temperature measurement at different depths of the tumor-bearing tissue-mimicking materials. The thermocouple T3 is placed in the center of the GO-enhanced spherical gel. The distance between 2 probes is 0.7 cm. **(B)** Temperature measurement at different depths of the tumor-mimicking spherical phantom. The distance between 2 probes is 0.3 cm.*

The needle temperature probes did not prevent the laser light from reaching the deepest parts of the phantoms. The surface temperature of TMMs was measured by a thermal infrared camera (Teledyne FLIR, Sweden).

Laser beams were circular-shaped with a diameter of 1 cm during experiments. The exact optical powers of lasers were measured by a laser power meter (Ophir Optronics, Inc.) before each irradiation of TMM. All temperature data were averaged over three independent experiments.

4.1.5 Tumor and immune cells culture conditions

Melanoma B16-F10 cells, dendritic cells 2.4, and bone-marrow derived macrophages (BMDMs) were purchased from American Type Culture Collection (ATCC) (Manassas, VA, USA). Pancreatic Panc02-H7 cells were obtained from Dr. Min Li of the University of Oklahoma Health Sciences Center. Every cell culture media was purchased from Gibco BRL (Gaithersburg, MD).

Pancreatic Panc02-H7 tumor cells, melanoma B16-F10 cells and BMDMs were cultured in Dulbecco's Modified Eagle Medium (DMEM) (1X) + Glutamax (1X) culture medium containing 10% heat-inactivated fetal bovine serum (FBS) and 1% penicillin/streptomycin. Dendritic cells (DCs) 2.4 were cultured in RPMI-1640 (1X) + Glutamax (1X) culture medium with 10% FBS and 1% penicillin/streptomycin. Cells were cultured at 37°C under 5% CO_2 and 95% relative humidity conditions. All the cells were cultured following standard protocols.

4.1.6 *In vitro* cytotoxicity assay on treated tumor cells

The effect of CS, GC, GO, GO/CS and GO/GC exposure (2.5 μg/ml GO, 50 μg/ml CS and GC) and *in vitro* PTT on the proliferation of tumor cells was determined by standard Cell Counting Kit-8 (CCK-8) assay (Sigma Inc.) 24 hours after incubation. CCK-8 is a sensitive colorimetric method for the determination of the number of viable cells. CCK-8 assay utilizes the tetrazolium salt WST-8 that produces a yellow-colored formazan dye. The amount of the formazan dye generated by the reduction of WST-8 by dehydrogenases in cells is directly proportional to the number of living cells.

Tumor cells were seeded into 96-well cell culture plates at a density of 10 000 cells/well in 100 μl culture media. Cells were precultured for 24 h at 37°C to allow them to adhere to the bottom of the wells. Cells were then incubated with 2.5 μg/ml GO, 50 μg/ml CS and GC NPs for 24h. PBS-added cells are the positive controls and PBS-added cell culture media are the negative control wells. Practically, the culture media was replaced by 100 μL of fresh media containing free GO, free CS, free GC, GO/CS, or GO/GC. Panc02-H7 cells were irradiated by the 980-nm laser at a power density of 0.7 W/cm^2 for 10 min. B16-F10 were irradiated by the 980-nm laser at a power density of 0.5 W/cm^2 for 10 min. Plates were incubated for 24h at 37°C. The CCK-8 solution was sterilized with a 0.2 μm membrane filter. The wells were washed with 100 μl PBS three times before 10 μl of CCK-8 solution (10% of the total volume

in the well) was added to each well for cell viability measurement. The well plates were gently mixed on an orbital shaker after the addition of the CCK-8 solution to ensure homogeneous repartition of the compounds. The cells were then incubated for another 4 h. The absorbance of each well was measured using a microplate reader (Synergy NEO2, BioTek) at a wavelength of 450 nm. The well plates were gently mixed on an orbital shaker for 10 seconds to ensure homogenous distribution of the color before reading the absorbance. The timeline of the cytotoxicity assays is shown in **Figure 15**. The viability of non-irradiated cells was measured 24 h after incubation with different compounds (**Figure 15A**). The viability of laser-irradiated cells was measured 24 h after PTT treatment (**Figure 15B**). For each sample, the cell viability was calculated as indicated below:

$$Cell\ viability\ (\%) = \frac{At - Ab1}{Ac - Ab2} \times 100$$

At is the absorbance of the experimental well containing the treated cells (cells with test compounds); *Ab1* is the absorbance of the blank well containing medium + GO; *Ac* is the absorbance of the control well with the untreated cells (cells with PBS); *Ab2* is the absorbance of the blank well containing medium only. Indeed, GO has a broad absorption peak and its absorbance is still significant at 450 nm [152]. This is the reason why the background noise of GO is subtracted from the absorbance of the experimental wells in case they contain GO. But for cells incubated with free CS and free GC, *Ab1 = Ab2*. The final cell viability was the average of the cell viability values of six wells in parallel (technical replicates). All relative cell viability data were averaged over three independent experiments.

MTT was also used as a colorimetric assay for proliferation and cytotoxicity assays, following the same principle as CCK-8. MTT is a pale-yellow substrate cleaved by living cells, leading to the formation of dark blue formazan products. This process requires active mitochondria, and even freshly dead cells do not cleave a significant amount of MTT. MTT was used as an indicator of cell viability as determined by its mitochondrial dependent reduction to formazan. In detail, 100 µl of cells were seeded into 96-well plates at a density of 1×10^5 cells/ml. After incubation for 24 h, the culture media were replaced with 100 µl of fresh media containing free GO, free CS, free GC, GO/CS or GO/GC (2.5 µg/ml GO, 50 µg/ml CS and GC) for further 24 h. After the cells were washed with PBS for three times, 10 µl MTT (5 mg/ml in PBS) was added to the wells for 4 h. Then, the supernatant was removed by aspiration, and the formazan crystals were dissolved in DMSO (100 µl per well), followed by shaking for 5 min. The absorbance was read using a microplate reader (Spectra

Plus, TECAN) at a wavelength of 570 nm. The cell viability (%) relative to control cells was calculated with the same formula as above. For each sample, the final absorbance was the average of those measured from six wells in parallel.

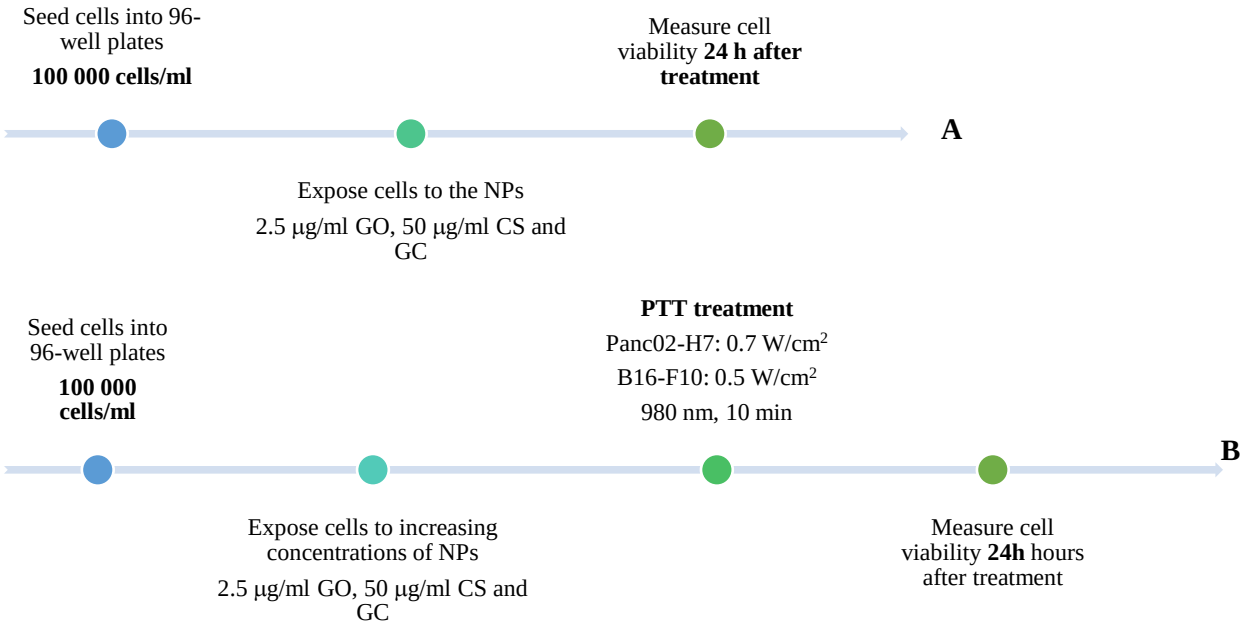

Figure 15. *Timeline of the cell toxicity assay for* ***(A)*** *non-irradiated cells and* ***(B)*** *laser-irradiated cells.*

4.1.7 *In vitro* immune stimulation and measurement of cytokines release via ELISA

The potential of the NPs to stimulate immune cells was evaluated by studying the immunostimulanting activity of the nanomaterial and its capacity to induce an inflammatory immune response. Thus, the production of pro-inflammatory cytokines by DCs 2.4 and BMDMs were measured using enzyme-linked immunosorbent assay (ELISA). ELISA tests were used for the quantitative detection of IL-6 and TNF-α.

To analyze the secretion of cytokines by DCs 2.4 and BMDMs, cells were seeded into 96-well cell culture plates at a density of 1×10^6 cells/ml (200 µl cells/well) and incubated with 10 µl of increasing concentrations of GO (1.5, 2.5, 3.12, 6.25, 12.5, 25, 50, 100 µg/ml) for 24 h at 37°C. Different GO concentrations were screened to titrate the IL-6 and TNF-α responses of DCs 2.4 and BMDMs. PBS-added cells are the positive controls and PBS-added cell culture media are the negative controls. The cell culture supernatant was collected from each

well and the IL-6 and TNF-α levels were measured by ELISA. Extracellular cytokines secreted in cell culture media by treated DCs 2.4 and BMDMs were measured using mouse ELISA kits following the manufacturer's instructions.

4.1.8 *In vitro* immune stimulation and analysis of surface markers by flow cytometry

BMDMs and DC 2.4 (1×10^6 cells/ml, 200 µl cells/well) were incubated with 10 µl of increasing concentrations of GC, CS, GO and GO/CS and GO/GC for 24 h at 37°C to analyze the phenotype of markers expressed on the surface of cells and evaluate the cellular response to the stimulation by those nanomaterials.

Stimulated BMDMs were analyzed by flow cytometry. Cells were stained with the following antibodies: CD86-BV605 (Clone GL-1, Cat# 105037), CD40-Pacific blue (Clone 3/23, Cat# 124626), CD38-PE-Cy7 (Clone 90, Cat# 102717), APC Annexin V (Cat# 640920), all from Biolegend (San Diego, CA, USA). CD11c-FITC (Clone N418, Ref 35-0114-U500), CD11b-APC-Cy7 (Clone M1/70, Ref 25-0112-U100), MHC Class II-redFluor 710 (Clone M5/114.15.2, Ref 80-5321-U025), Viability dye Ghost dye-BV510 (Ref 13-0870-T100), all from Tonbo Biosciences (San Diego, CA).

Stimulated DC 2.4 were analyzed by flow cytometry. Cells were stained with the following antibodies: CD86-BV605 (Clone GL-1, Cat# 105037), CD40-Pacific blue (Clone 3/23, Cat# 124626), CD80-FITC (Clone 16-10A1, Cat# 104705), APC Annexin V (Cat# 640920), all from Biolegend (San Diego, CA, USA). CD11c-PE (Clone HL3, Cat# 553802) from BD Biosciences (San Jose, CA, USA). CD11b-APC-Cy7 (Clone M1/70, Ref 25-0112-U100), MHC Class II-redFluor 710 (Clone M5/114.15.2, Ref 80-5321-U025), Viability dye Ghost dye-BV510 (Ref 13-0870-T100), all from Tonbo Biosciences (San Diego, CA).

UltraComp eBeads (Ref 01-2222-42) from Thermofisher were used as compensation beads for antibody compensation. Cytometer QC beads (Cat# B7-10001) from Cytek were used as QC beads. All the cells were examined using a Cytek Flow Cytometer (Northern Light, Cyteck biosciences). The data were analyzed using FlowJo software (FlowJo, BD).

4.1.9 Statistical analysis

Statistical analysis was performed using GraphPad Prism 7 (GraphPad Software, Inc., La Jolla, CA, USA). The statistical analysis is described in each figure legend. Data are presented as mean values ± standard deviation (SD). Comparisons between groups were performed by ANOVA (multiple comparisons). If $p>0.05$, results are not statistically different. Differences were considered to be statistically significant when $*p<0.05$, $**p<0.01$, $***p<0.001$ and $****p<0.0001$.

4.2 Results

4.2.1 Synthesis and characterization of GO/CS and GO/GC nanoparticles

GO/CS and GO/GC were prepared by self-assembly of GO, CS, and GC in an aqueous solution. Both GO/CS and GO/GC NPs formed through noncovalent electrostatic interactions since GO is negatively charged, and the polymers (CS and GC) are positively charged at physiological pH. Therefore, GO and CS as well as GO and GC assembled by themselves into nanosystems. Three ratios (1/4, 1/10, 1/20) of GO/CS and GO/GC were synthesized to determine the optimal NPs stability with different polymer concentrations and the capability of loading CS and GC on graphene sheets.

The pH of the individual solutions was measured before synthesizing the NPs to evaluate the potential of GO to assemble with CS and GC *via* electrostatic interactions (**Figure 16A**). The pH of the GO solution was between 6-6.5. CS and GC solutions had a pH of 5.7 and 5.8, respectively. The pHs of the three solutions were close, creating a proper slightly acidic environment where GO could assemble with either CS or GC. Indeed, at this pH range, GO remained negatively charged and CS and GC were polycationic. Plus, the pHs of CS and GC were alike, which confirmed that they could assemble with GO similarly.

The expected NPs synthesis was first verified by size measurement (**Figure 16B**). The colloidal size distribution of GO and the solutions of the three ratios of GO/CS and GO/GC in aqueous solutions were characterized using dynamic light scattering (DLS). The free GO size was in the diameter range provided in the product datasheet (90 nm-200 nm). GO/CS and GO/GC had bigger sizes than free GO, showing that CS and GC were successfully loaded on the GO sheets. More GO sheets were conjugated to the polymers when the proportions of CS and GC increased. However, the NPs size was not proportional to the ratio, as 1/20 NPs were not two times bigger than 1/10 NPs, which could suggest a limited number of loading sites on

the GO nanosheets. The 1/4 and 1/10 ratios showed aggregation while the 1/20 GO/CS and 1/20 GO/GC remained stable without forming aggregates. Therefore, 1/20 NPs solutions were more homogeneous than other ratios because the high concentration of the surfactant molecules CS and GC helped to stabilize the nanosystems. It was noticed that GO/GC NPs were more stable and more easily dispersed in water and PBS than GO/CS, showing that GC has better surfactant properties than CS, thus preventing GO NPs to clump.

Zeta potential analysis further validated the successful synthesis of GO/CS and GO/GC NPs (**Figure 16C**). The zeta potential of free GO was -35 mV, which confirmed that free GO is negatively charged at physiological pH. After functionalization with cationic CS and GC, GO/CS and GO/GC NPs were positively charged. The higher the CS and GC concentrations, the higher the surface zeta potential, proving that more polymers were loaded on GO sheets. The zeta potential of 1/4 GO/CS and 1/4 GO/GC was positive, which means that enough CS and GC were loaded on GO even at the lowest tested ratio. The highest zeta potential values were observed for the 1/20 ratios, showing that 1/20 GO/CS and 1/20 GO/GC NPs presented the highest proportion of functionalized GO nanosheets. In short, cationic CS and GC showed strong electrostatic interactions with anionic GO, which led to the successful formation of positively charged GO/CS and GO/GC NPs.

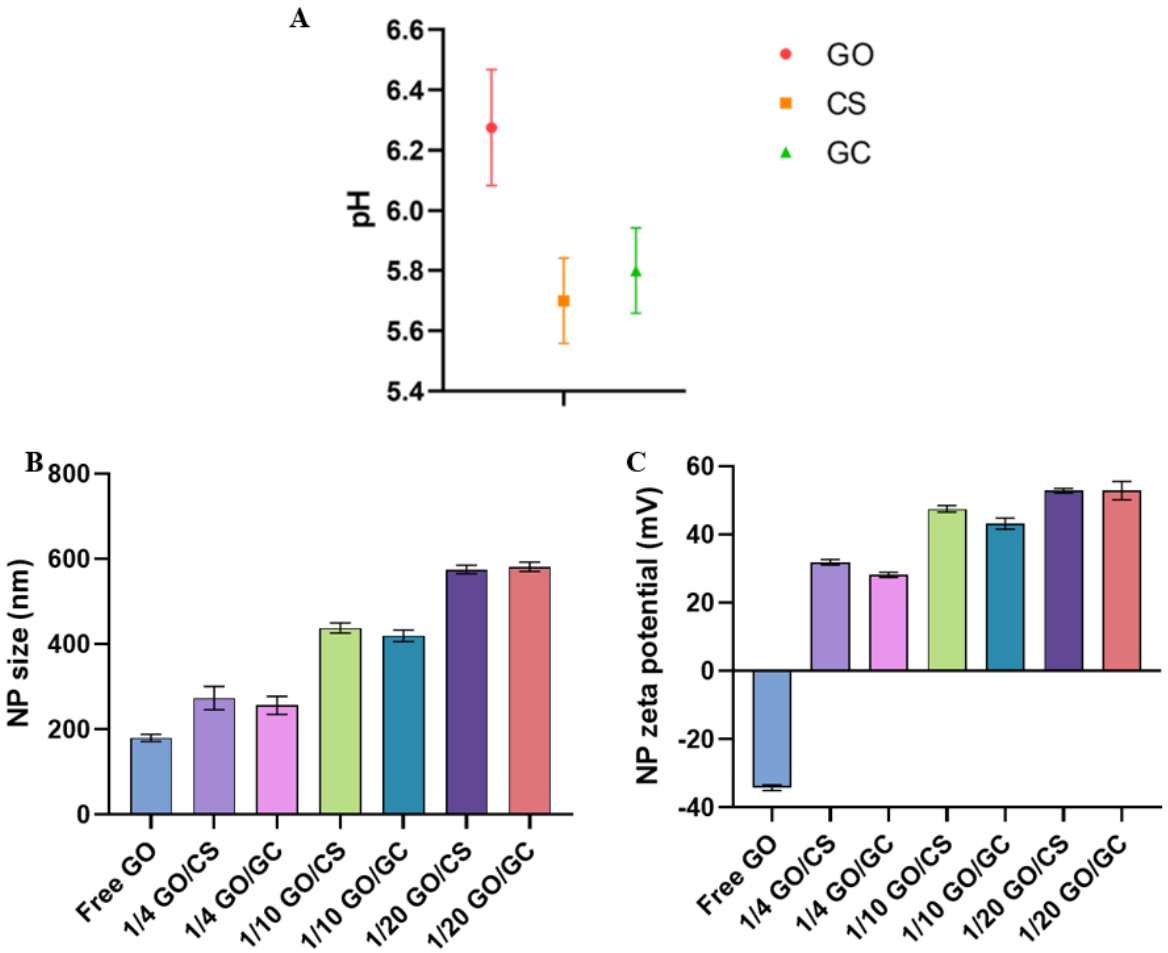

Figure 16. *Characterization of graphene oxide (GO), chitosan (CS), glycated chitosan (GC), CS-functionalized GO (GO/CS) and GC-functionalized GO (GO/GC) nanoparticles (NPs).* ***(A)*** *pH of GO (1 mg/ml), CS (10 mg/ml), and GC (10 mg/ml) solutions;* ***(B)*** *Size measurement (colloidal size distribution) of free GO and 1/4, 1/10, 1/20 ratio of GO/CS, and GO/GC NPs in Milli-Q water;* ***(C)*** *Zeta potentials (surface charge) of free GO and 1/4, 1/10, 1/20 ratio of GO/CS and GO/GC NPs in Milli-Q water. The concentrations of the solutions are the following: 1/4 NPs: 0.05 mg/ml GO, 0.2 mg/ml CS and GC. 1/10 NPs: 0.05 mg/ml GO, 0.5 mg/ml CS and GC. 1/20 NPs: 0.05 mg/ml GO, 1 mg/ml CS and GC. Data are presented as mean ± SD (n=3).*

Overall, with the size and zeta potential results, the successful binding between GO and CS, as well as between GO and GC was confirmed. Compared with free GO, GO/CS and GO/GC had bigger sizes and positive surface charges. Anionic GO and polycationic polymers CS and GC could self-assemble by electrostatic interactions. The 1/20 GO/CS and 1/20

GO/GC were the most stable NPs, but 1/20 GO/GC were the most uniformly dispersed and stable NPs.

Therefore, thermal and cell studies were conducted using exclusively 1/20 GO/CS and 1/20 GO/GC.

4.2.2 Thermal effect of near-infrared irradiated nanoparticle-enhanced phantoms of tumors

Thermal studies were conducted on phantoms of agar-based soft tissue-mimicking materials (TMMs), which mimic healthy tissues. TMMs contained GO-enhanced spherical phantoms to mimic absorption-enhanced target tissues to investigate the thermal effect of GO when irradiated with a near-infrared laser. Temperature changes in GO-enhanced TMMs were compared with the thermal effects of GO/CS, GO/GC, and indocyanine green (ICG). The dye-enhanced gel phantoms were made spherical because this shape mimics tumors growing in *in vivo* tissues. Plus, the goal of the treatment is to inject GO, GO/CS, and GO/GC inside the tumor to combine anti-tumor drug delivery with cancer cells killing *via* ICD induced by photothermal therapy (PTT). Therefore, dye-enhanced gel phantoms were made to mimic the tumor containing GO or GO/GC or GO/CS NPs. TMMs containing dye-enhanced tumor-mimicking gels were irradiated with lasers at wavelengths of 980 nm and 805 nm for 10 min. The temperature of the spherical tumor-mimicking phantoms was measured. Increasing GO and ICG concentrations were tested to study the correlation between the dye concentration and its thermal effect intensity.

Temperature changes were measured at four different depths of the irradiated phantom as depicted on the schematic of the experimental set-up in **Figure 17A** to determine the diffusion of the heat following a vertical thermal gradient. As shown in **Figure 17B**, the temperature of the different spots in the TMM is inversely proportional to the distance to the tip of the laser fiber, the surface of the gel being the hottest measured spot and the bottom of the gel being the coldest area. This confirms the heat diffusion in the irradiated TMM and the thermal effect of NIR laser irradiation on phantoms of tissues.

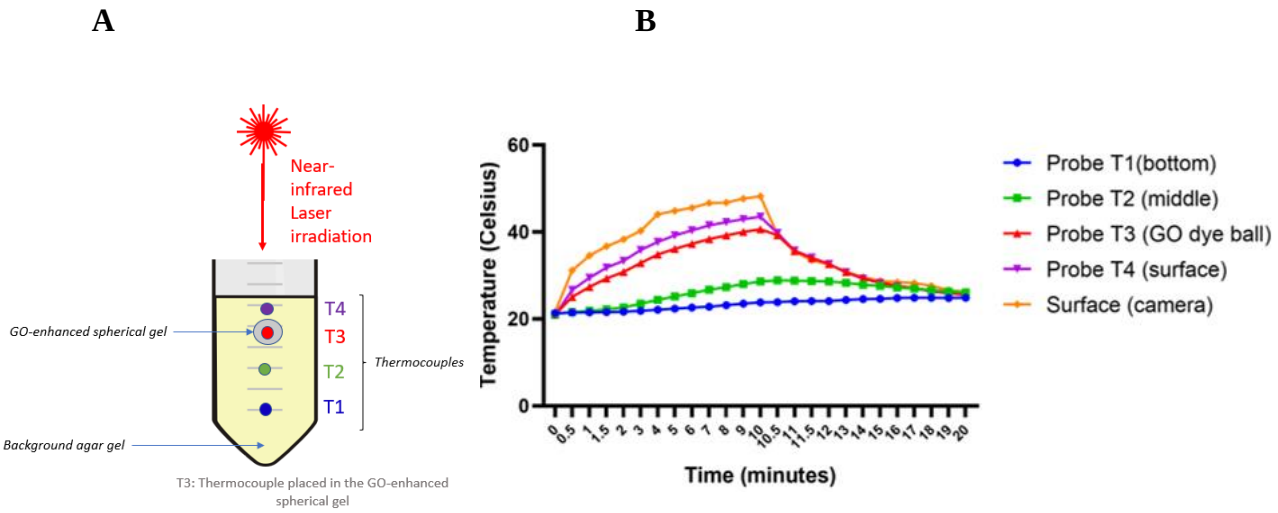

Figure 17. *In -depth temperature measurement of laser irradiated tissue-mimicking materials (TMM).* ***(A)*** *Schematic of the set-up for the measurement of the temperature changes at different depths of the tumor-bearing tissue-mimicking materials. The temperature was measured using a four-channel thermometer connected to four type T thermocouples placed at different heights of the TMM (T1-T4 on the schematic), including one being placed inside the dye-enhanced spherical gel (T3).* ***(B)*** *Temperature changes at different depths of the GO-enhanced TMM that was irradiated at 980 nm for 10 minutes. The thermocouple T3 measures the temperature changes at the center and the middle of the GO-enhanced spherical gel.*

Figure 18 illustrates the temperature changes measured at the center and the middle of the dye-enhanced spherical tumor phantoms. The evolution of the temperature was compared for different dye concentrations to study the effect of the dye percentage in the phantom on the temperature changes. The temperature was higher when GO-enhanced TMMs were irradiated at 980 nm than at 805 nm (**Figure 18A** and **B**). Gel phantoms reached almost 50°C at 980 nm whereas the maximum temperature was only 30°C at 805 nm. Indeed, GO in an aqueous solution was used to prepare the TMMs and pure water has a strong absorption peak at 980 nm [153, 154, 155]. **Figure 18C** shows that GO, GO/CS and GO/GC-enhanced phantoms reached higher temperatures at 980 nm than at 805 nm. It was expected that GO/CS and GO/GC react the same way as free GO when irradiated with a near-infrared laser because GC and CS don't have any absorption peak or thermal property at near-infrared wavelengths [156, 157].

The next part of the thermal study on TMMs was to compare the thermal effects of GO and ICG dyes, ICG being another dye used for tumor treatment by laser immunotherapy. To compare the effectiveness of GO and ICG in terms of laser light absorption capacities, ICG-enhanced spherical tumor phantoms were placed in surrounding agar-based TMMs. Those gels were irradiated at 805 or 980 nm, and the temperature changes of the ICG-enhanced TMMs were measured. The tested ICG concentrations in ICG-enhanced gels were the same as GO-enhanced gels so that GO and ICG thermal effects with the same dye concentrations can be compared. This way, it also showed how the thermal effect of ICG depended on its concentration in TMMs. **Figure 18D** illustrates that GO-enhanced TMMs irradiated at 980 nm reached the highest temperature, followed by the ICG-enhanced gels irradiated at 805 nm.

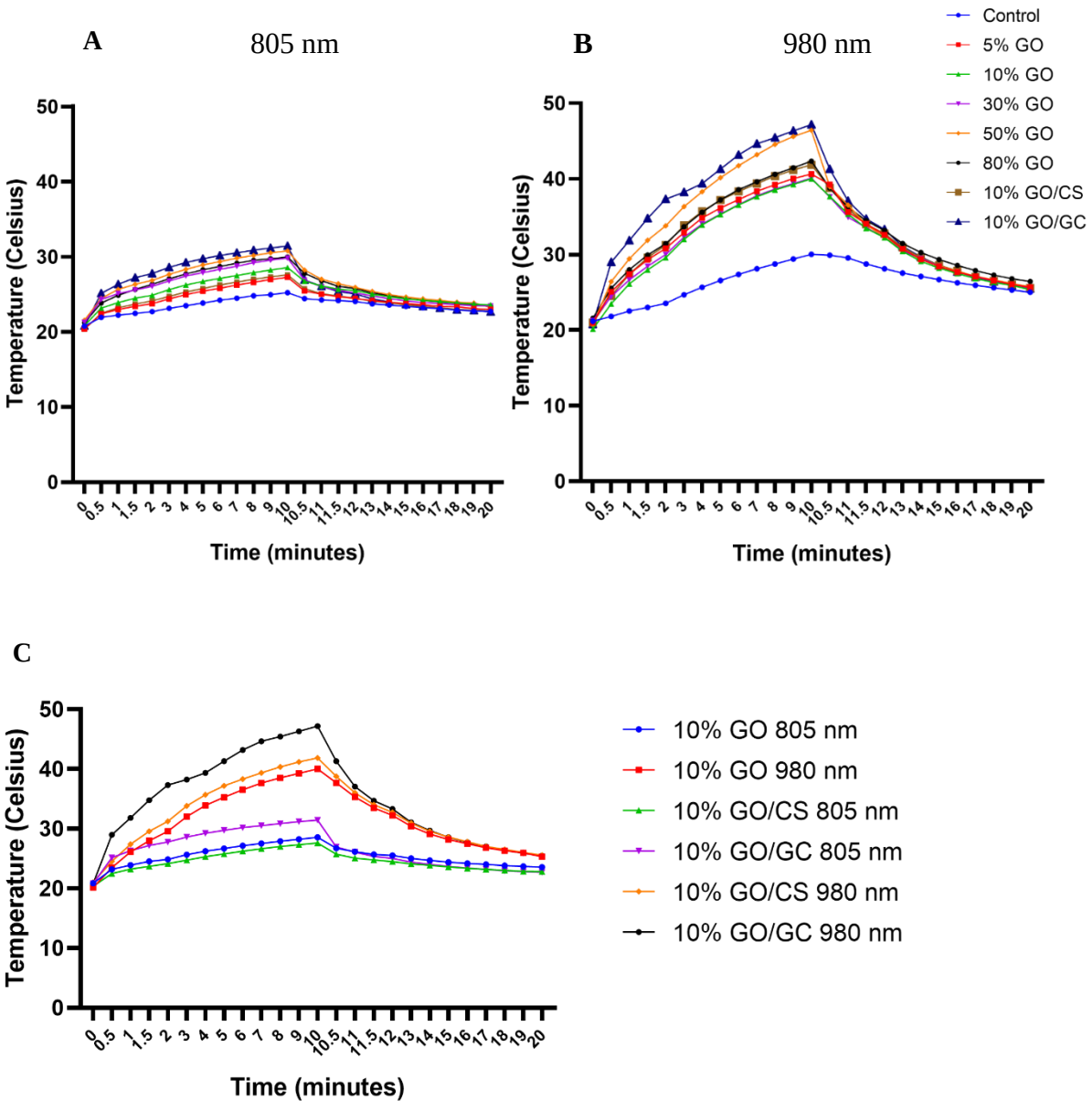

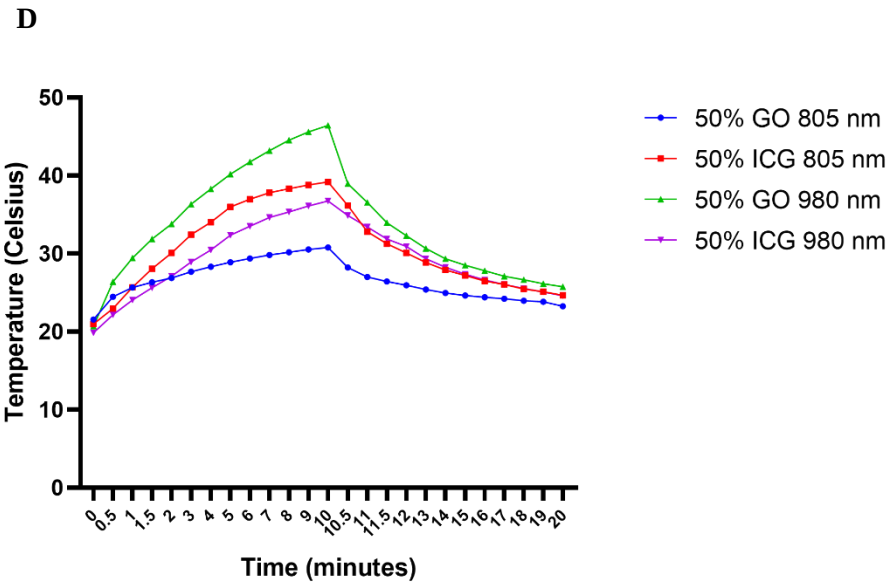

Figure 18. *Thermal study on spherical dye-enhanced tumor phantoms.* ***(A)*** *TMMs with GO-enhanced spherical gels irradiated at 805 nm for 10 min;* ***(B)*** *TMMs with GO-enhanced spherical gels irradiated at 980 nm for 10 min;* ***(C)*** *GO/CS- and GO/GC-enhanced TMMs compared with GO-enhanced TMMs;* ***(D)*** *50% GO- and 50% ICG- enhanced TMMs thermal effects comparison. 5%: 2.5 µg/ml GO, 10%: 5 µg/ml GO, 30%: 15 µg/ml GO, 50%: 25 µg/ml GO, 80%: 40 µg/ml GO, 10% GO/GC and 10% GO/CS: 5 µg/ml GO and 100 µg/ml CS and GC. GO and ICG are at the same concentrations in the phantoms, thus 50% ICG: 25 µg/ml ICG. The power density is 2 W/cm^2 at 805 nm and 980 nm. (n=3).*

Figure 19 depicts the temperature changes at different depths of the GO-enhanced spherical phantom of tumors. The temperature difference between the probes was approximately constant for each dye concentration, showing a proper distribution of the energy generated by the laser irradiation. Those results confirmed the higher thermal conversion potential of GO when irradiated at 980 nm than at 805 nm, since tumor phantoms reached higher temperature at the highest wavelength. Phantoms of tumors containing 50% GO showed the most uniform diffusion of heat along a vertical temperature gradient and reached the highest temperature compared to the other GO-enhanced phantoms of tumors.

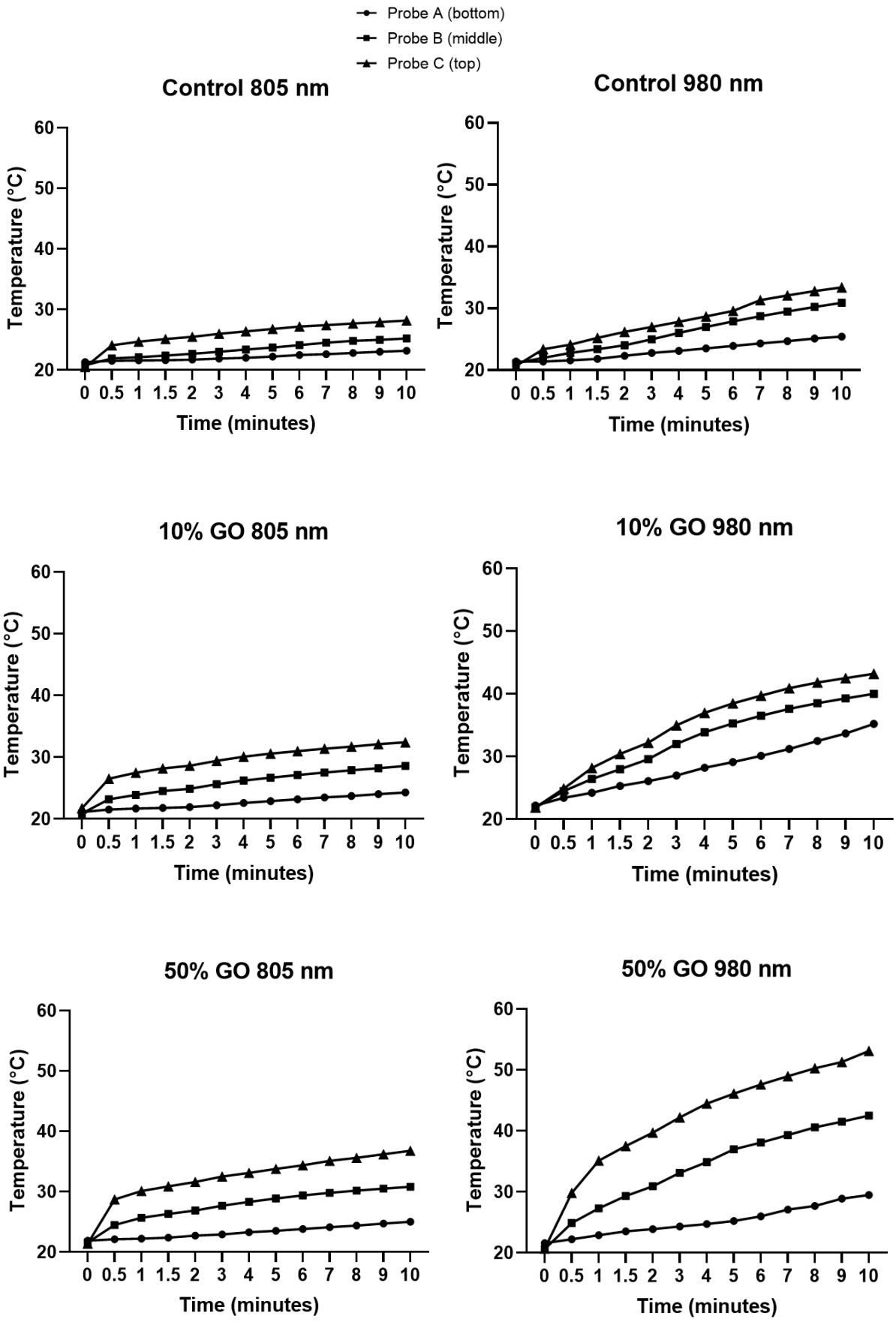
Probe A (bottom)
Probe B (middle)
Probe C (top)
Control 805 nm
Control 980 nm
10% GO 805 nm
10% GO 980 nm
50% GO 805 nm
50% GO 980 nm
Temperature (°C)
Time (minutes)
20
30
40
50
60
0 0.5 1 1.5 2 3 4 5 6 7 8 9 10

***Figure 19**. Temperature changes at different depths of GO-enhanced spherical phantom of tumors irradiated for 10 min with near-infrared lasers. The power density is 2 W/cm^2 at 805 nm and 980 nm. (n=3). The distance between two probes is 0.3 cm., 10%: 5 µg/ml GO, 50%: 25 µg/ml GO.*

Overall, the GO-enhanced phantoms gained 20°C when irradiated. A 20°C increase in temperature *in vivo* is considered efficient to kill tumor cells. Plus, the dye-enhanced spherical gels were 1 cm in diameter and the thermocouple was placed in the middle of the gel. It means that the temperature of the TMMs increased by 20°C on half a centimeter. Therefore, the most promising results were obtained with GO-enhanced gel phantoms irradiated at 980 nm and ICG-enhanced gels at 805 nm. In short, GO-enhanced TMMs showed a promising temperature increase at 980 nm and convincing thermal effect compared to ICG for laser immunotherapy. Plus, a proportion of 10-50% dye in the 3D model of tissue allowed for an efficient temperature increase and heat distribution inside the tumor phantoms.

Subsequent to the study of the thermal effect of near-infrared irradiated GO NPs in 3D tumor phantoms, the effects of GO/CS and GO/GC on tumor cells and immune cells were explored *in vitro*. Cell studies were exclusively conducted with 1/20 GO/CS and 1/20 GO/GC solutions because they are the most stable NPs compared to 1/4 and 1/10 ratios. Those NPs were further evaluated on cells to compare their effect on cancer cells killing and immune stimulation.

4.2.3 *In vitro* tumor cell toxicity induced by nanoparticles-based PTT

To assess the synergistic effects of GO/CS- and GO/GC-based LIT, the potential cytotoxicity of the NPs to the aggressive pancreatic Panc02-H7 cell line was investigated. CCK-8 and MTT kits were used to conduct the cytotoxicity assays. This experiment aimed to evaluate the tumor cells killing effect of NPs + PTT. Cells were incubated with either free GO, free CS, free GC, GO/CS or GO/GC. Cell viability was measured after treatment, either 24h after NPs incubation for non-irradiated cells, or 24h after NPs incubation + PTT for irradiated tumor cells (980 nm, 10 min, 0.7 W/cm^2 for Panc02-H7 and 0.5 W/cm^2 for B16-F10).

As shown on **Figure 20A**, the incubation with free GO led to 30% cell killing when pancreatic tumor cells were not irradiated. The tumor cell killing effect of GO was enhanced by PTT, since 70% of the cells treated with GO + PTT were killed. Cells treated with free GO + PTT had the lowest viability compared to the other treatment groups. Thus, the combination of GO + PTT was the most efficient treatment to kill pancreatic tumor cells by augmentation of temperature. CS and GC without PTT were not toxic to the pancreatic tumor cells since viability was around 100% for those two groups. However, cells incubated with GO/CS and GO/GC exhibited 80% viability without laser irradiation. GO/CS and GO/GC killed 20% of the cells, due to GO cytotoxicity. Nevertheless, GO/CS and GO/GC were less cytotoxic than free GO. Even if CS and GC were not toxic to the cells, groups treated with CS + PTT and GC + PTT showed 80% viability. The 20% cell death was caused by the laser irradiation of the tumor cells. GO/CS + PTT or GO/GC + PTT led to 50% viability only, which suggests that the coating of GO with CS and GC improves the biocompatibility of the nanosheets. Overall, a similar trend was observed for both non-irradiated and irradiated pancreatic tumor cells but the combination of NPs incubation with PTT induced more cell death compared to NPs *in vitro* exposure only. The biocompatibility of GO was improved by the functionalization with CS and GC, GO/CS and GO/GC showing limited cytotoxicity. However, free GO-enhanced laser light absorption caused significant heat-induced Panc02-H7 tumor cell death in the GO+PTT treatment group.

The synergistic effects of GO/CS- and GO/GC-based PTT were also studied on the aggressive melanoma B16-F10 cell line. The aim was to investigate if B16-F10 cells are responsive to the combination treatment in the same way Panc02-H7 were. Cell viability was measured after treatment, either 24h after NPs incubation for non-irradiated cells, or 24h after NPs + PTT (980 nm, 10 min, 0.5 W/cm^2) for irradiated cells. The power density used to irradiate melanoma cells is lower than the one used for PTT on pancreatic tumor cells because melanoma cells are pigmented and naturally absorb more laser light than Panc02-H7 because of their dark color.

Alike pancreatic Panc02-H7, melanoma B16-F10 were first cultured with free GO, free CS, free GC, GO/CS, and GO/GC. As shown in **Figure 20B**, results are really similar to the ones presented in **Figure 20A**, which demonstrates that the cytotoxicity assays were reproducible between different tumors. Therefore, the GO/GC+PTT and GO+PTT treatments were similarly efficient to kill pancreatic and melanoma cells, suggesting that this therapy could be applied for the thermal ablation of multiple tumor types.

A

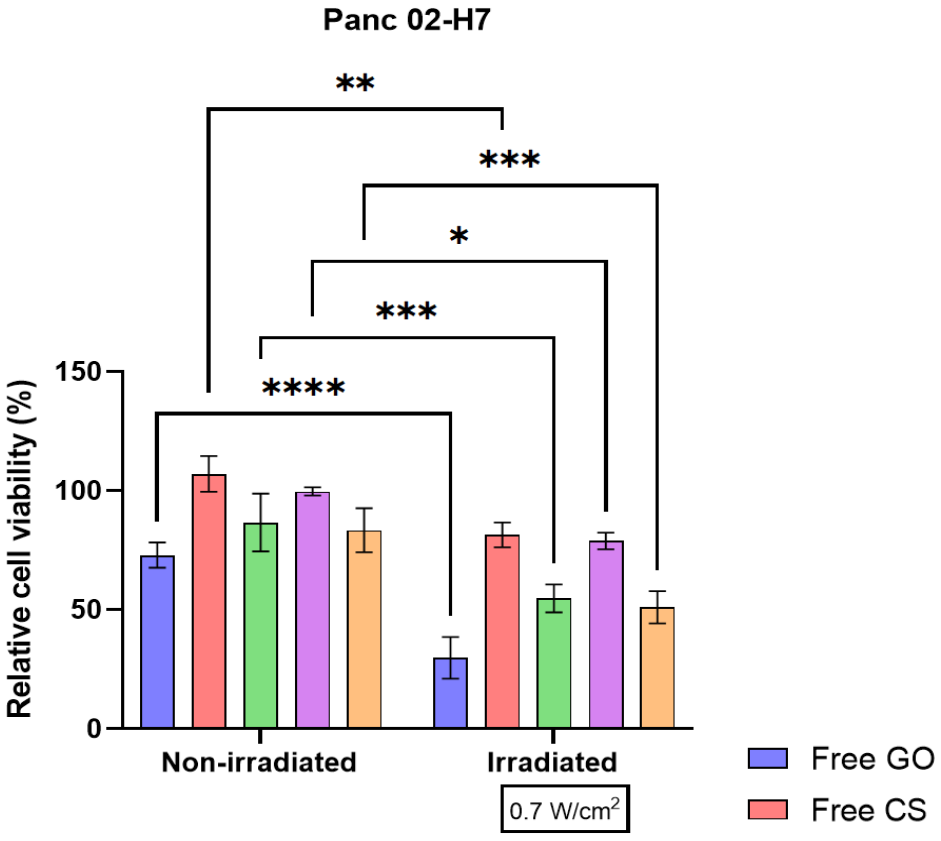
Panc 02-H7
**
***
*
***
****
Relative cell viability (%)
150
100
50
0
Non-irradiated
Irradiated
0.7 W/cm2
Free GO
Free CS
GO/CS
Free GC
GO/GC

B

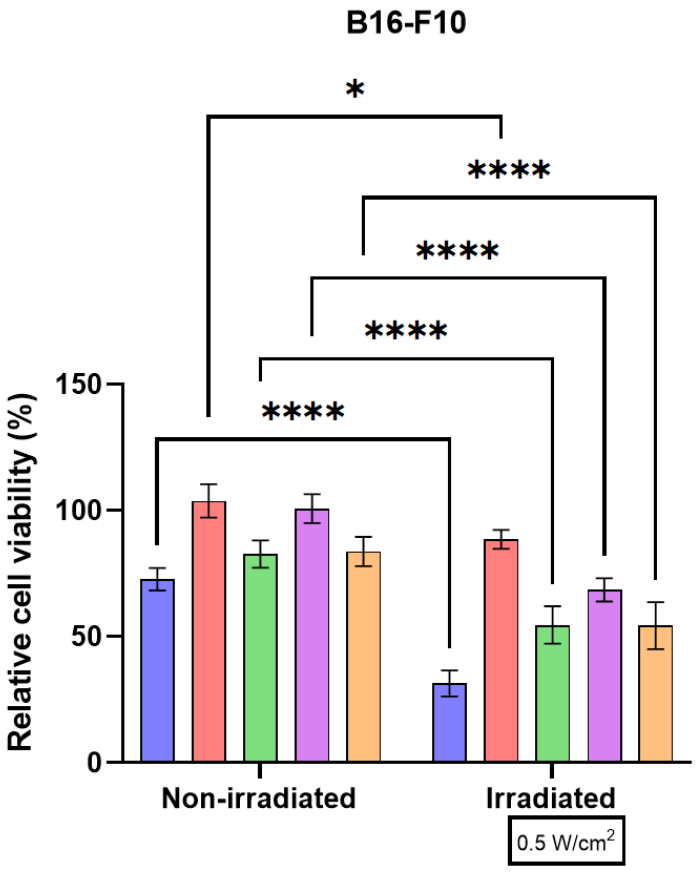
B16-F10
*
****
****
****
****
Relative cell viability (%)
150
100
50
0
Non-irradiated
Irradiated
0.5 W/cm2

Figure 20. *In vitro cytotoxicity assay.* ***(A)*** *Relative cell viability of pancreatic Panc02-H7 cells incubated with free GO, free CS, GO/CS, free GC, and GO/GC (2.5 μg/ml GO and 50 μg/ml CS and GC) for 24h without laser irradiation and with laser irradiation (980 nm, 10 min, 0.7 W/cm^2).* ***(B)*** *Relative cell viability of melanoma B16-F10 cells incubated with free GO, free CS, GO/CS, free GC, and GO/GC (2.5 μg/ml GO and 50 μg/ml CS and GC) for 24h without laser irradiation and with laser irradiation (980 nm, 10 min, 0.5 W/cm^2).*

*Data are presented as mean ± SD (n=6). Relative cell viabilities in all samples were normalized to the control PBS-added samples without laser irradiation (100% viability). Error bars were based on SD of six samples in parallel (technical replicates). Three independent experiments were conducted. P values were calculated by two-way ANOVA (or mixed model): *p < 0.05, **p < 0.01, ***p < 0.001, ****p < 0.0001.*

4.2.4 *In vitro* immune stimulation and nanoparticles potential as immunostimulating agents

Dendritic cells (DCs) and macrophages are antigen-presenting cells (APCs). Therefore, they have important functions in the immune system, such as in the initiation and regulation of immune responses. When stimulated, those APCs produce many cytokines involved in important immune pathways, including cellular immunity activation. Indeed, as APCs, macrophages, and DCs present antigens to cells of the adaptive immune system, such as $CD8^+$ T cells. Once CTLs are activated by APCs, they can kill abnormal self-cells like tumor cells.

To investigate the immune effect of GO, CS, GC GO/CS, and GO/GC, those NPs were incubated with bone marrow-derived macrophages (BMDMs) and DCs. The objectives were to study the immune stimulation of DC 2.4 and BMDMs by those NPs, and to assess whether DC 2.4 and BMDMs are activated in a similar manner and produce the same cytokines when stimulated with different compounds. Thus, DC 2.4 and BMDMs were incubated with different drugs at indicated concentrations, and the levels of secreted cytokines were measured by ELISA. Interleukin 6 (IL-6) and Tumor necrosis factor (TNF)-α are inflammatory cytokines produced by monocytes, macrophages, and dendritic cells in response to stress conditions during acute inflammation. The goals of incubating immune cells with potentially immunostimulatory drugs is to enhance the secretion of those inflammatory cytokines by stimulated immune cells and study the effect of NPs on the inflammatory system biomarkers IL-6 and TNF-α produced by DC 2.4 and BMDMs.

First, BMDMs were incubated with free GO, free CS, GO/CS, free GC, and GO/GC (2.5 µg/ml GO and 50 µg/ml CS and GC) for 24h. The levels of IL-6 and TNF-α secreted by the BMDMs are shown in **Figure 21A** and **B**, respectively. The strongest IL-6 and TNF-α responses were observed for macrophages incubated with 2.5 µg/ml GO. Every other component stimulated the production of those pro-inflammatory cytokines as well but were less effective. To understand the effects of the concentration of GO and GC on the cytokine secretion, BMDMs were incubated with increasing concentrations of those components (see indicated concentrations), as shown in **Figure 21 C-D**. The cytokines levels detected at 2.5 µg/ml GO and 50 µg/ml GC confirmed the results in Figure 21A and B. 25 µg/ml GO seemed to be the optimal concentration to observe a maximal IL-6 secretion (**Figure 21C**), whereas the TNF-α response is proportional to the GO concentration (**Figure 21D**). The levels of IL-6 and TNF-α secreted by BMDMs incubated with increasing concentrations of GC (**Figure 21E-F**) were not concentration-dependent and were much lower than for GO-incubated cells.

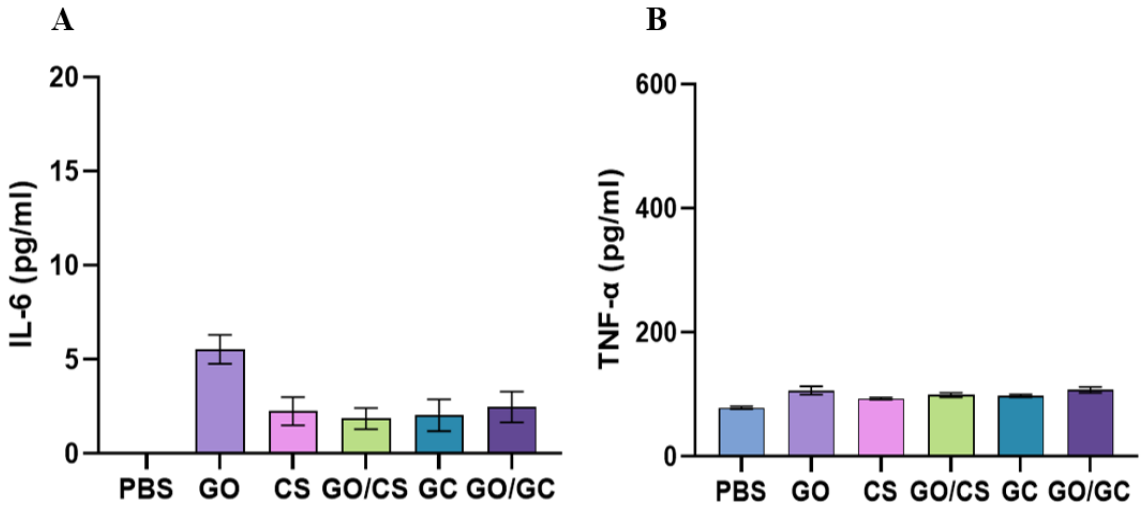

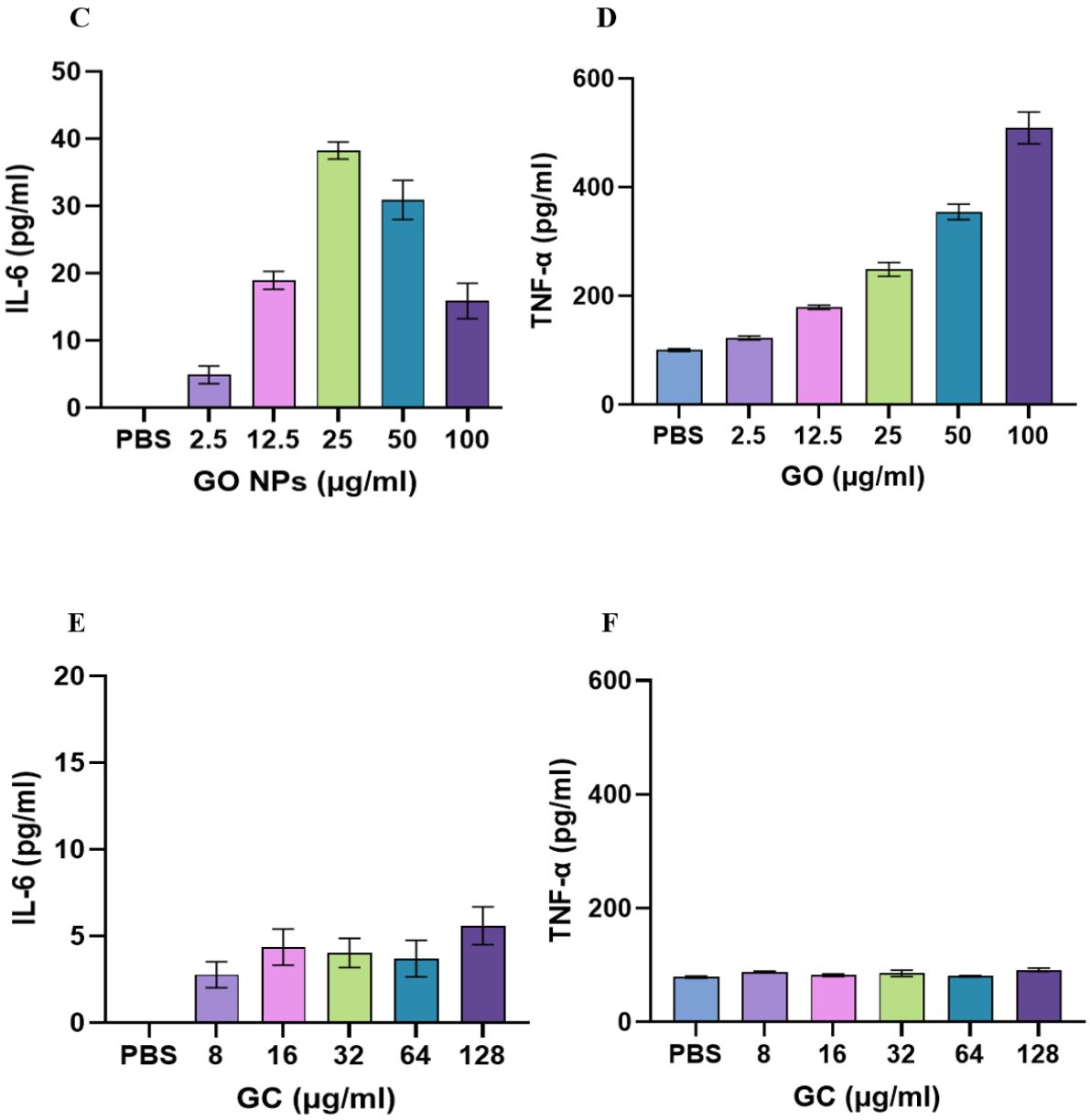

Figure 21. ***(A)*** *Levels of IL-6 secreted by BMDMs incubated with the indicated NPs (2.5 µg/ml GO and 50 µg/ml CS and GC).* ***(B)*** *TNF-alpha secreted by BMDMs incubated with the indicated NPs (2.5 µg/ml GO and 50 µg/ml CS and GC).* ***(C)*** *IL-6 secreted by BMDMs incubated with the indicated concentrations of GO.* ***(D)*** *TNF-alpha secreted by BMDMs incubated with the indicated concentrations of GO.* ***(E)*** *IL-6 secreted by BMDMs incubated with the indicated concentrations of GC.* ***(F)*** *TNF-alpha secreted by BMDMs incubated with indicated concentrations of GC. Data are presented as mean ± SD (n=3).*

Since GO seemed to have the best stimulating effect compared to CS and GC, the response of macrophages to the stimulation by GO was compared to the response of DCs. Thus, GO solutions of different concentrations (100, 50, 25, 12.5, 6.25, 3.12, 1.56 µg/ml) were screened to evaluate the IL-6 and TNF-α responses of DCs 2.4 and BMDMs. The levels of secreted IL-6 in DCs 2.4 and BMDMs samples are shown in **Figure 22A** and **B**. DCs 2.4 and BMDMs produced detectable levels of IL-6 when incubated with GO solutions in a range of 1.5-100 µg/ml. No IL-6 was detected in the negative control, which corresponds to unstimulated cells. DC 2.4 and BMDMs secreted IL-6 even at the lowest GO concentrations. Macrophages seemed more responsive to GO than DC 2.4 since IL-6 levels were higher for GO stimulated BMDMs than GO stimulated DC 2.4. TNF-α concentration in DCs 2.4 and BMDMs samples is illustrated in **Figure 22C** and **D**. DCs 2.4 and BMDMs produced detectable levels of TNF-α when incubated with GO solutions in a range of 1.5-100 µg/ml. Unstimulated DC 2.4 and BMDMs produced TNF-α, this basal level of expression in non-stimulated immune cells being common for those immune cell types [158]. At 2.5 µg/ml GO, DCs 2.4 started to secrete significant levels of TNF-α, whereas BMDMs began to produce significant levels of TNF-α only at 25 µg/ml GO. Overall, GO stimulated dendritic cells and macrophages, as they released pro-inflammatory cytokines.

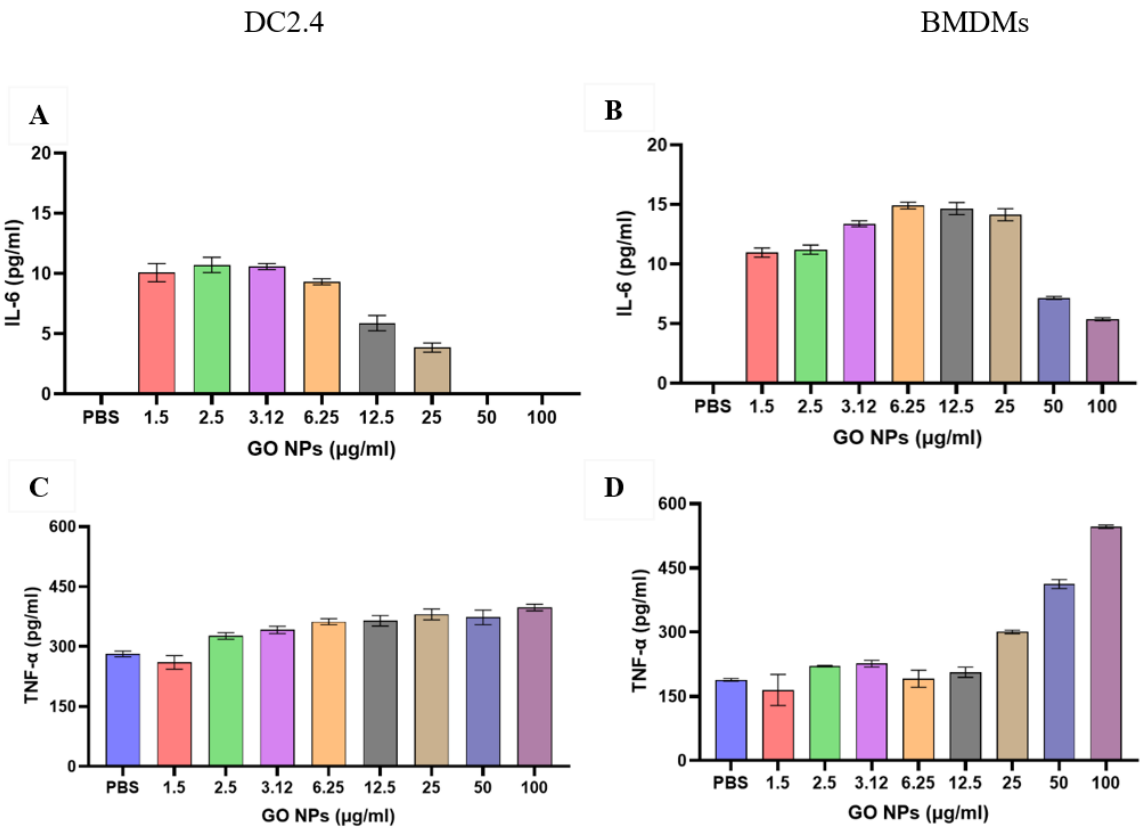

***Figure 22**. Cytokines secretion by dendritic cells 2.4 (DCs 2.4) and bone marrow-derived macrophages (BMDMs) exposed to indicated concentrations of graphene oxide (GO). **(A)** Cytokine IL-6 secreted by DCs 2.4 after 24 h incubation with GO. **(B)** Cytokine IL-6 secreted by BMDMs after 24 h incubation with GO. **(C)** Cytokine TNF-alpha secreted by DCs 2.4 after 24 h incubation with GO. **(D)** Cytokine TNF-alpha secreted by BMDMs after 24 h incubation with GO. Data are presented as mean ± SD (n=4).*

4.2.5 *In vitro* immune stimulation and analysis of surface markers by flow cytometry

To investigate the immunostimulatory effects of the nanomaterials, macrophages incubated with GC were analyzed by flow cytometry to phenotype their surface markers. In this work, we will only focus on the expression of the following phenotype markers: CD38, CD40 and CD86.

The gating strategy that was applied to obtain the results from the raw data collected by the flow cytometer is described in **Figure 23A**. First, the major macrophage population was isolated with an ellipse gate. On those gated events, the live cells were isolated. Then, the frequency of expression of the surface markers expressed by those live cells were analyzed. The live and dead cells groups were populated with the quadrant shown on **Figure 23A**. The quadrant isolated three main populations: live and not stressed (LiveDead- and AnnV-), live and stressed (LiveDead- and AnnV+), dead (LiveDead+ and AnnV+).

To evaluate the effects of GC on the viability of activated DMDMs, the evolution of the live and dead cell population densities was measured (**Figure 23B**). The more the GC concentration increased, the more the population of dead macrophages was big, which means that GC kills macrophages. At the highest GC concentration, almost all macrophages were dead. One can lake the hypothesis that GC induces macrophages death to recruit more immune cells to the tumor site and further activate the anti-tumor immune response.

The next step of the work was to measure the changes in the expression of the markers to evaluate the effects of GC on inflammatory macrophages phenotype modulation, as depicted on **Figure 23C**.

CD11b is a marker for monocytes, macrophages, granulocytes and natural killer cells. The expression of the marker was constant when the GC concentration increased. CD11b is not a marker of cell activation, it was used as a baseline marker, a reference to compare the expression of the other markers.

CD38 was upregulated in inflammatory BMDMs. A baseline expression of CD38 is expected for the usual metabolic functions but a high expression of CD38 is correlated to the enhanced inflammatory cytokine production.

CD40 is a costimulatory molecule for antigen presentation and is expressed by stimulated macrophages. A basal expression of CD40 was measured because macrophages are APCs. However, when cells were incubated with GC, the expression of CD40 was upregulated. GC might enhance the antigen presentation ability of macrophages.

CD86 is expressed on antigen-presenting cells to provide the costimulatory signals necessary for T cell activation. Therefore, GC enhanced the ability of macrophages to stimulate a T cell response against the tumor.

A

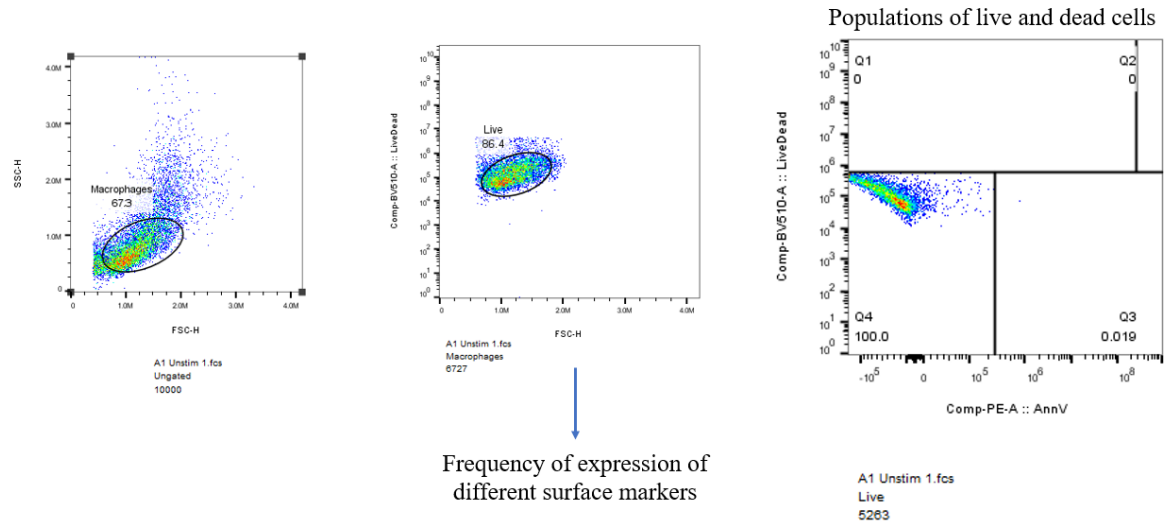

B

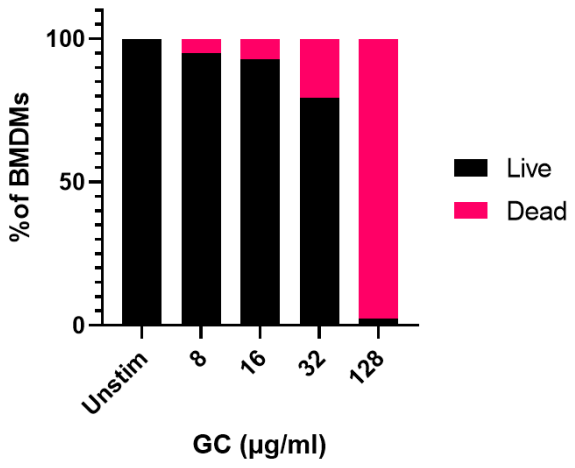

C

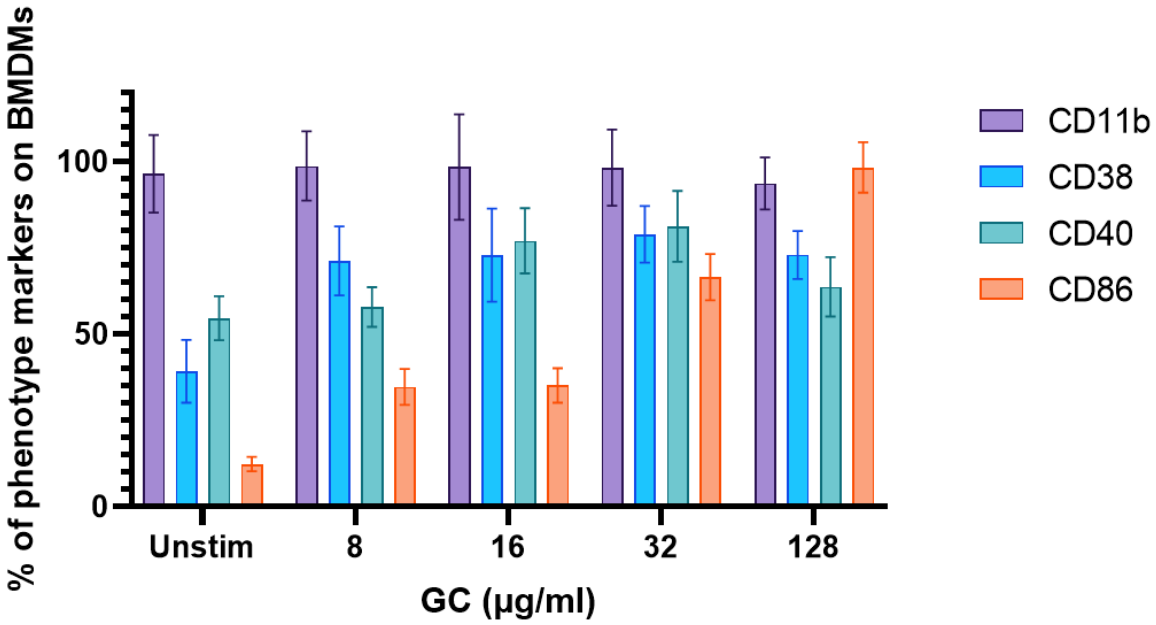

Figure 23. *In vitro immune stimulation and analysis of surface markers by flow cytometry.* ***(A)*** *Gating strategy applied to the flow cytometry data for future analysis.* ***(B)*** *Effects of GC on the viability of activated BMDMs.* ***(C)*** *Expression of the BMDMs activation markers.*

Overall, those results showed that GC induces an activated proinflammatory phenotype in the stimulated BMDMs.

4.3 Discussion

Polycationic CS and GC polymers of similar molecular weight showed strong electrostatic interactions with negatively charged GO nanosheets, which led to the formation of both positively charged GO/CS and GO/GC NPs, as shown on **Figure 16**. Deprotonated carboxylic acids of GO are believed to react with protonated amine groups of CS and GC at pH 7. Cationic and hydrophilic NPs might interact easily with cell membranes that are usually negatively charged. The NPs charge may facilitate cellular uptake and enhance drug delivery efficiency.

Because of the interaction between the hydrophilic CS and GC, which have a p*K*a ≈ 5.5[159], the polymer-grafted GO sheets can be water-soluble with moderate sonication. However, GO can be dissolved in water but congregate in physiological solutions rich in salts or proteins due to electrostatic charges and nonspecific protein binding. Indeed, NPs can be covered by proteins, like FBS, forming a protein corona around the NPs. Due to the protein binding, the size of the NPs increases, and the surface charge can be modified, which disturbs the therapeutic effect of the NPs [111]. Therefore, the surfactant properties of GC are important to obtain a homogenous solution of NPs. The solubility of GO/CS and GO/GC is substantially enhanced by the water-solubility of GC, whereas it is difficult to obtain water-soluble CS. This is the reason why an excess of polymers prevents the NPs to congregate, as demonstrated by the fact that 1/20 GO/CS and 1/20 GO/GC are the most stable NPs compared to the 1/4 and 1/10 NPs, because of the surfactant properties of GC and CS. GC is even more water-soluble than CS, and is a better surfactant than CS, hence 1/20 GO/GC NPs are more stable than 1/20 GO/CS. The hypothesis of the limited number of loading sites on the surface of the GO nanosheets could be explained by the limited availability of the carboxylic groups of GO or by the steric hindrance of the polymers wrapping around the sheets. Overall, 1/20 GO/CS and 1/20 GO/CS were stable samples. The average size of the NPs is enough for our applications.

GO/CS and GO/GC NPs had similar thermal effects as GO (**Figure 18C**). It means that the functionalization of the GO sheets does not prevent GO from absorbing laser light, which is promising for future LIT treatment. Both GO and ICG showed a strong thermal effect but GO had a better photothermal conversion ability than ICG at 980 nm (**Figure 18D**). GO-enhanced phantoms of light-absorbing tumors showed a promising 20°C temperature increase at 980 nm. Both GO and ICG are in aqueous solutions so both GO- and ICG-enhanced TMMs have a strong near-infrared laser light absorption capacity when irradiated at 980 nm. It means that the strongest thermal effect observed for GO-enhanced phantoms compared to ICG at 980 nm is due to GO absorption capacity at 980 nm. Overall, GO had a stronger thermal effect than ICG at 980 nm. *In vivo*, 20°C augmentation in temperature means that tissues heat up from 37°C to 47°C. Even though each tumor and TME are unique, there is a consensus that effective PTT requires the tumor temperature to be comprised between 50 and 60 °C under near-infrared irradiation. This temperature range allows for optimal tumor cell killing and immune stimulation by ICD [160, 161, 162]. Thus, results obtained on TMMs are promising, showing the efficiency of the near-infrared laser light absorption by GO, GO/CS, and GO/GC

NPs when combined with PTT in a 3D model. In an animal model, the temperature reached by tumor tissues containing GO, GO/CS, and GO/GC NPs might be higher when irradiated with laser because of the blood flow and vasculature.

As suggested by the cytotoxicity of the NPs to the pancreatic and melanoma tumor cells (**Figure 20**), it seems that CS and GC protected the cells from the cytotoxicity of the GO + PTT treatment. One may hypothesize that CS and GC wrap around the GO sheets and might decrease the surface of GO exposed to laser light, hence decreasing the light absorption by the graphene sheets, which might prevent an optimal thermal effect. Nevertheless, significant decrease in the tumor cell viability was noticed when cells are treated with the combination therapy GO/CS + PTT and GO/GC + PTT. One can consider that the functionalization of GO by CS and GC allows for PTT monitoring by adjusting the near-infrared laser light absorption of GO and does not prevent the ICD of tumor cells by heat.

GO efficiently stimulated the secretion of IL-6 and TNF-α by BMDMs and DC2.4 (**Figures 21 and 22**). However, the productions of IL-6 and TNF-α due to the CS and GC stimulations were dose-independent. Therefore, the immune response of BMDMs and DC2.4 to GO might involve pathways that are different from the stimulation by CS and GC. In Dr. Chen's lab, Dr. Hoover showed that GC activates the production of type I IFN and IL-1β. Consequently, GO/CS and GO/GC NPs might stimulate the production of different cytokines involving separate pathways: IL-6 and TNF-α induced by GO, and type I IFN and IL-1β induced by GC. The nanosystems might synergize those cytokines, which will be investigated in the future for anti-tumor purposes.

As shown by the flow cytometry results in **Figure 23**, the advantage of GC is its capability to induce an inflammatory cell death that further enhances APC recruitment and activation. Markers of cell activation are upregulated, and the cells can be phenotyped as M1 macrophages. Therefore, GC-stimulated BMDMs are 1) $CD38^+$, showing that they have an enhanced inflammatory activity; 2) $CD40^+$, presenting an enhanced antigen-presentation ability; and 3) $CD86^+$, hence being able to augment the T-cell stimulation. Those M1 macrophages express specific phenotype markers such as those co-stimulatory molecules and are involved in triggering intensive inflammation. M1-phenotype macrophages promote inflammation by secreting pro-inflammatory cytokines such as IL-6 and TNF-alpha and have an anti-tumor function.

5 Conclusion and future work

Overall, the present work focused on the properties of the GO/GC nanomaterial for nano-ablative photo-immunotherapy purposes. Our feasibility study proved that CS and GC could be used to functionalize the GO sheets. GO/CS and GO/GC nanocomposites were successfully synthesized through non-covalent assembly. The resulting GO/GC nanosystem was stable. Since GO, the nanocarrier, is cationic, it was able to form electrostatic complexes with CS and GC. GO/CS and GO/GC NPs had bigger sizes than free GO and presented positive charges. Subsequently, the photothermal conversion ability of the nanomaterial was evaluated under NIR light, by irradiating GO-enhanced tissue-mimicking materials to evaluate the potential of GO for the treatment of tumors by PTT. Irradiation by the 980-nm laser increased the temperature by 20°C in the center of the GO-enhanced phantoms of tumors. This temperature elevation is promising, being in the optimal range for *in vivo* PTT treatment. These results demonstrate the potential of GO for the treatment of tumors by PTT. Furthermore, *in vitro* studies were conducted to study the interactions between GO/CS and GO/GC with dendritic cells (DCs) and tumor cells. The GO/GC+PTT (LIT) treatment efficiently induced the death of pancreatic tumor and melanoma cells, with GO providing a central function in the thermal ablation of tumor cells. In addition, DCs and macrophages were stimulated by the NPs and produced pro-inflammatory cytokines, hence showing the potential of GO/GC for antitumor immune response. Stimulated macrophages were analyzed by flow cytometry to phenotype their surface markers and compare them with the unstimulated state. Stimulated macrophages upregulated the expression of surface markers of activation and present a $CD38^+$ $CD40^+$ $CD86^+$ phenotype. Those M1 macrophages have a specific anti-tumor activity when stimulated by GC, which induces an activated pro-inflammatory phenotype in the BMDMs.

In the future, more *in vitro* studies will be conducted in order to better understand the immune stimulation effect of GO, CS, GC, GO/CS and GO/GC. The upregulation of the markers of cell activation will be correlated with the cytokine production by stimulated immune cells. One of the next steps of this work is to visualize the NP-cell interaction by fluorescence microscopy and analyze the cell lysates to see if the GO/CS and GO/GC NPs can be phagocytosed by DCs and macrophages. This will open the way to an in-depth study of the mechanism of GO/CS and GO/GC in DCs and macrophages, by exploring the endocytosis

pathways and determining the functions of the two nanosystems on different immune cells. The future aims are 1) to evaluate the therapeutic effects of GO/CS and GO/GC combined with PTT using different tumor models in animals; 2) to investigate the systemic antitumor effect of NPs for cancer vaccination; 3) to explore the mechanism of the immune system in response to the stimulation by laser-initiated immunotherapy; and 4) to study the synergistic effect of GO/CS or GC/GC potentiated LIT with immune checkpoint blockade therapy to further improve the treatment efficacy.

6 References

(1) Sung, H.; Ferlay, J.; Siegel, R. L.; Laversanne, M.; Soerjomataram, I.; Jemal, A.; Bray, F. Global Cancer Statistics 2020: GLOBOCAN Estimates of Incidence and Mortality Worldwide for 36 Cancers in 185 Countries. *CA: A Cancer Journal for Clinicians* **2021**, *71* (3), 209–249. https://doi.org/10.3322/caac.21660.

(2) *Global health estimates: Leading causes of death*. https://www.who.int/data/maternal-newborn-child-adolescent-ageing/advisory-groups/gama/gama-related-resources/gho (accessed 2021-12-09).

(3) Bray, F.; Laversanne, M.; Weiderpass, E.; Soerjomataram, I. The Ever-Increasing Importance of Cancer as a Leading Cause of Premature Death Worldwide. *Cancer* **2021**, *127* (16), 3029–3030. https://doi.org/10.1002/cncr.33587.

(4) Omran, A. R. The Epidemiologic Transition. A Theory of the Epidemiology of Population Change. *Milbank Mem Fund Q* **1971**, *49* (4), 509–538.

(5) Arnold, M.; Rutherford, M. J.; Bardot, A.; Ferlay, J.; Andersson, T. M.-L.; Myklebust, T. Å.; Tervonen, H.; Thursfield, V.; Ransom, D.; Shack, L.; Woods, R. R.; Turner, D.; Leonfellner, S.; Ryan, S.; Saint-Jacques, N.; De, P.; McClure, C.; Ramanakumar, A. V.; Stuart-Panko, H.; Engholm, G.; Walsh, P. M.; Jackson, C.; Vernon, S.; Morgan, E.; Gavin, A.; Morrison, D. S.; Huws, D. W.; Porter, G.; Butler, J.; Bryant, H.; Currow, D. C.; Hiom, S.; Parkin, D. M.; Sasieni, P.; Lambert, P. C.; Møller, B.; Soerjomataram, I.; Bray, F. Progress in Cancer Survival, Mortality, and Incidence in Seven High-Income Countries 1995-2014 (ICBP SURVMARK-2): A Population-Based Study. *Lancet Oncol* **2019**, *20* (11), 1493–1505. https://doi.org/10.1016/S1470-2045(19)30456-5.

(6) *Cancer statistics, 2018 - Siegel - 2018 - CA: A Cancer Journal for Clinicians - Wiley Online Library*. https://acsjournals.onlinelibrary.wiley.com/doi/10.3322/caac.21442 (accessed 2021-10-14).

(7) *Common Cancer Types - National Cancer Institute*. https://www.cancer.gov/types/common-cancers (accessed 2021-07-22).

(8) *SEER Cancer Statistics Review, 1975-2018*. SEER. https://seer.cancer.gov/csr/1975_2018/index.html (accessed 2021-07-22).

(9) *USCS Data Visualizations*. https://gis.cdc.gov/grasp/USCS/DataViz.html (accessed 2021-05-19).

(10) CDCBreastCancer. *Cancer Treatments*. Centers for Disease Control and Prevention. https://www.cdc.gov/cancer/survivors/patients/treatments.htm (accessed 2022-02-16).

(11) Seyfried, T. N.; Huysentruyt, L. C. On the Origin of Cancer Metastasis. *Crit Rev Oncog* **2013**, *18* (1–2), 43–73.

(12) Riggio, A. I.; Varley, K. E.; Welm, A. L. The Lingering Mysteries of Metastatic Recurrence in Breast Cancer. *Br J Cancer* **2021**, *124* (1), 13–26. https://doi.org/10.1038/s41416-020-01161-4.

(13) Arruebo, M.; Vilaboa, N.; Sáez-Gutierrez, B.; Lambea, J.; Tres, A.; Valladares, M.; González-Fernández, Á. Assessment of the Evolution of Cancer Treatment Therapies. *Cancers (Basel)* **2011**, *3* (3), 3279–3330. https://doi.org/10.3390/cancers3033279.

(14) ALTUN, İ.; SONKAYA, A. The Most Common Side Effects Experienced by Patients Were Receiving First Cycle of Chemotherapy. *Iran J Public Health* **2018**, *47* (8), 1218–1219.

(15) Coleman, R. L.; Monk, B. J.; Sood, A. K.; Herzog, T. J. Latest Research and Treatment of Advanced-Stage Epithelial Ovarian Cancer. *Nat Rev Clin Oncol* **2013**, *10* (4), 211–224. https://doi.org/10.1038/nrclinonc.2013.5.

(16) Werner, J.; Combs, S. E.; Springfeld, C.; Hartwig, W.; Hackert, T.; Büchler, M. W. Advanced-Stage Pancreatic Cancer: Therapy Options. *Nat Rev Clin Oncol* **2013**, *10* (6), 323–333. https://doi.org/10.1038/nrclinonc.2013.66.

(17) Oates, J.; Davies, S.; Roydhouse, J. K.; Fethney, J.; White, K. The Effect of Cancer Stage and Treatment Modality on Quality of Life in Oropharyngeal Cancer. *The Laryngoscope* **2014**, *124* (1), 151–158. https://doi.org/10.1002/lary.24136.

(18) *Comprehensive Cancer Information - National Cancer Institute*. https://www.cancer.gov/ (accessed 2021-07-02).

(19) *Proliferation Of Healthy Cells And Cancer Cells. Comparison Illustration Of Normal Cell Proliferation And Cancer Cell Proliferation In The Body.* Freepik. https://www.freepik.com/premium-vector/proliferation-healthy-cells-cancer-cells-comparison-illustration-normal-cell-proliferation-cancer-cell-proliferation-body_8227026.htm (accessed 2021-06-22).

(20) *What do doctors look for in biopsy and cytology specimens?*. https://www.cancer.org/treatment/understanding-your-diagnosis/tests/testing-biopsy-and-cytology-specimens-for-cancer/what-doctors-look-for.html (accessed 2022-02-17).

(21) Baba, A. I.; Câtoi, C. *TUMOR CELL MORPHOLOGY*; The Publishing House of the Romanian Academy, 2007.

(22) *What Is Cancer? - National Cancer Institute*. https://www.cancer.gov/about-cancer/understanding/what-is-cancer (accessed 2022-02-17).

(23) *Cancer Grade Vs. Cancer Stage*. MD Anderson Cancer Center. https://www.mdanderson.org/patients-family/diagnosis-treatment/a-new-diagnosis/cancer-grade-vs--cancer-stage.html (accessed 2022-02-17).

(24) Gockley, A.; Melamed, A.; Bregar, A. J.; Clemmer, J. T.; Birrer, M.; Schorge, J. O.; Del Carmen, M. G.; Rauh-Hain, J. A. Outcomes of Women With High-Grade and Low-Grade Advanced-Stage Serous Epithelial Ovarian Cancer. *Obstet Gynecol* **2017**, *129* (3), 439–447. https://doi.org/10.1097/AOG.0000000000001867.

(25) Bansberg, S. F.; Olsen, K. D.; Gaffey, T. A. High-Grade Carcinoma of the Oral Cavity. *Otolaryngol Head Neck Surg* **1989**, *100* (1), 41–48. https://doi.org/10.1177/019459988910000107.

(26) *Metastatic Cancer: When Cancer Spreads - National Cancer Institute*. https://www.cancer.gov/types/metastatic-cancer (accessed 2022-02-17).

(27) *Definition of metastasis - NCI Dictionary of Cancer Terms - National Cancer Institute*. https://www.cancer.gov/publications/dictionaries/cancer-terms/def/metastasis (accessed 2021-06-22).

(28) *What cancer survival rates can (and can't) tell you*. Mayo Clinic. https://www.mayoclinic.org/diseases-conditions/cancer/in-depth/cancer/art-20044517 (accessed 2022-02-17).

(29) Hemminki, K.; Riihimäki, M.; Sundquist, K.; Hemminki, A. Site-Specific Survival Rates for Cancer of Unknown Primary According to Location of Metastases. *Int J Cancer* **2013**, *133* (1), 182–189. https://doi.org/10.1002/ijc.27988.

(30) Zijlstra, A.; Von Lersner, A.; Yu, D.; Borrello, L.; Oudin, M.; Kang, Y.; Sahai, E.; Fingleton, B.; Stein, U.; Cox, T. R.; Price, J. T.; Kato, Y.; Welm, A. L.; Aguirre-Ghiso, J. A.; The Board Members of the Metastasis Research Society. The Importance of Developing Therapies Targeting the Biological Spectrum of Metastatic Disease. *Clin Exp Metastasis* **2019**, *36* (4), 305–309. https://doi.org/10.1007/s10585-019-09972-3.

(31) Balkwill, F. R.; Capasso, M.; Hagemann, T. The Tumor Microenvironment at a Glance. *Journal of Cell Science* **2012**, *125* (23), 5591–5596. https://doi.org/10.1242/jcs.116392.

(32) Fukumura, D.; Jain, R. K. Tumor Microenvironment Abnormalities: Causes, Consequences, and Strategies to Normalize. *Journal of Cellular Biochemistry* **2007**, *101* (4), 937–949. https://doi.org/10.1002/jcb.21187.

(33) Wu, J.; Liang, C.; Chen, M.; Su, W. Association between Tumor-Stroma Ratio and Prognosis in Solid Tumor Patients: A Systematic Review and Meta-Analysis. *Oncotarget* **2016**, *7* (42), 68954–68965. https://doi.org/10.18632/oncotarget.12135.

(34) Ping, Q.; Yan, R.; Cheng, X.; Wang, W.; Zhong, Y.; Hou, Z.; Shi, Y.; Wang, C.; Li, R. Cancer-Associated Fibroblasts: Overview, Progress, Challenges, and Directions. *Cancer Gene Ther* **2021**, *28* (9), 984–999. https://doi.org/10.1038/s41417-021-00318-4.

(35) Jin, M.-Z.; Jin, W.-L. The Updated Landscape of Tumor Microenvironment and Drug Repurposing. *Sig Transduct Target Ther* **2020**, *5* (1), 1–16. https://doi.org/10.1038/s41392-020-00280-x.

(36) Farc, O.; Cristea, V. An Overview of the Tumor Microenvironment, from Cells to Complex Networks (Review). *Experimental and Therapeutic Medicine* **2021**, *21* (1), 1–1. https://doi.org/10.3892/etm.2020.9528.

(37) Sheth, V.; Wang, L.; Bhattacharya, R.; Mukherjee, P.; Wilhelm, S. Strategies for Delivering Nanoparticles across Tumor Blood Vessels. *Advanced Functional Materials* **2021**, *31* (8), 2007363. https://doi.org/10.1002/adfm.202007363.

(38) Forster, J. C.; Harriss-Phillips, W. M.; Douglass, M. J.; Bezak, E. A Review of the Development of Tumor Vasculature and Its Effects on the Tumor Microenvironment. *Hypoxia (Auckl)* **2017**, *5*, 21–32. https://doi.org/10.2147/HP.S133231.

(39) Harting, C.; Peschke, P.; Borkenstein, K.; Karger, C. P. Single-Cell-Based Computer Simulation of the Oxygen-Dependent Tumour Response to Irradiation. *Phys Med Biol* **2007**, *52* (16), 4775–4789. https://doi.org/10.1088/0031-9155/52/16/005.

(40) Borkenstein, K.; Levegrün, S.; Peschke, P. Modeling and Computer Simulations of Tumor Growth and Tumor Response to Radiotherapy. *Radiat Res* **2004**, *162* (1), 71–83. https://doi.org/10.1667/rr3193.

(41) Giraldo, N. A.; Sanchez-Salas, R.; Peske, J. D.; Vano, Y.; Becht, E.; Petitprez, F.; Validire, P.; Ingels, A.; Cathelineau, X.; Fridman, W. H.; Sautès-Fridman, C. The Clinical Role of the TME in Solid Cancer. *Br J Cancer* **2019**, *120* (1), 45–53. https://doi.org/10.1038/s41416-018-0327-z.

(42) Whiteside, T. L. The Tumor Microenvironment and Its Role in Promoting Tumor Growth. *Oncogene* **2008**, *27* (45), 5904–5912. https://doi.org/10.1038/onc.2008.271.

(43) Vinay, D. S.; Ryan, E. P.; Pawelec, G.; Talib, W. H.; Stagg, J.; Elkord, E.; Lichtor, T.; Decker, W. K.; Whelan, R. L.; Kumara, H. M. C. S.; Signori, E.; Honoki, K.; Georgakilas, A. G.; Amin, A.; Helferich, W. G.; Boosani, C. S.; Guha, G.; Ciriolo, M. R.; Chen, S.; Mohammed, S. I.; Azmi, A. S.; Keith, W. N.; Bilsland, A.; Bhakta, D.; Halicka, D.; Fujii, H.; Aquilano, K.; Ashraf, S. S.; Nowsheen, S.; Yang, X.; Choi, B. K.; Kwon, B. S. Immune Evasion in Cancer: Mechanistic Basis and Therapeutic Strategies. *Seminars in Cancer Biology* **2015**, *35*, S185–S198. https://doi.org/10.1016/j.semcancer.2015.03.004.

(44) Messerschmidt, J. L.; Prendergast, G. C.; Messerschmidt, G. L. How Cancers Escape Immune Destruction and Mechanisms of Action for the New Significantly Active Immune Therapies: Helping Nonimmunologists Decipher Recent Advances. *Oncologist* **2016**, *21* (2), 233–243. https://doi.org/10.1634/theoncologist.2015-0282.

(45) Nonomura, N.; Takayama, H.; Nishimura, K.; Oka, D.; Nakai, Y.; Shiba, M.; Tsujimura, A.; Nakayama, M.; Aozasa, K.; Okuyama, A. Decreased Number of Mast Cells Infiltrating into Needle Biopsy Specimens Leads to a Better Prognosis of Prostate Cancer. *Br J Cancer* **2007**, *97* (7), 952–956. https://doi.org/10.1038/sj.bjc.6603962.

(46) Iamaroon, A.; Pongsiriwet, S.; Jittidecharaks, S.; Pattanaporn, K.; Prapayasatok, S.; Wanachantararak, S. Increase of Mast Cells and Tumor Angiogenesis in Oral Squamous Cell Carcinoma. *J Oral Pathol Med* **2003**, *32* (4), 195–199. https://doi.org/10.1034/j.1600-0714.2003.00128.x.

(47) Ribatti, D.; Ennas, M. G.; Vacca, A.; Ferreli, F.; Nico, B.; Orru, S.; Sirigu, P. Tumor Vascularity and Tryptase-Positive Mast Cells Correlate with a Poor Prognosis in Melanoma. *Eur J Clin Invest* **2003**, *33* (5), 420–425. https://doi.org/10.1046/j.1365-2362.2003.01152.x.

(48) Sahai, E.; Astsaturov, I.; Cukierman, E.; DeNardo, D. G.; Egeblad, M.; Evans, R. M.; Fearon, D.; Greten, F. R.; Hingorani, S. R.; Hunter, T.; Hynes, R. O.; Jain, R. K.; Janowitz, T.; Jorgensen, C.; Kimmelman, A. C.; Kolonin, M. G.; Maki, R. G.; Powers, R. S.; Puré, E.; Ramirez, D. C.; Scherz-Shouval, R.; Sherman, M. H.; Stewart, S.; Tlsty, T. D.; Tuveson, D. A.; Watt, F. M.; Weaver, V.; Weeraratna, A. T.; Werb, Z. A Framework for Advancing Our Understanding of Cancer-Associated Fibroblasts. *Nat Rev Cancer* **2020**, *20* (3), 174–186. https://doi.org/10.1038/s41568-019-0238-1.

(49) Beatty, G. L.; Gladney, W. L. Immune Escape Mechanisms as a Guide for Cancer Immunotherapy. *Clinical Cancer Research* **2015**, *21* (4), 687–692. https://doi.org/10.1158/1078-0432.CCR-14-1860.

(50) Spranger, S. Mechanisms of Tumor Escape in the Context of the T-Cell-Inflamed and the Non-T-Cell-Inflamed Tumor Microenvironment. *Int Immunol* **2016**, *28* (8), 383–391. https://doi.org/10.1093/intimm/dxw014.

(51) Baghban, R.; Roshangar, L.; Jahanban-Esfahlan, R.; Seidi, K.; Ebrahimi-Kalan, A.; Jaymand, M.; Kolahian, S.; Javaheri, T.; Zare, P. Tumor Microenvironment Complexity and Therapeutic Implications at a Glance. *Cell Communication and Signaling* **2020**, *18* (1), 59. https://doi.org/10.1186/s12964-020-0530-4.

(52) Zangooei, M. H.; Margolis, R.; Hoyt, K. Multiscale Computational Modeling of Cancer Growth Using Features Derived from MicroCT Images. *Sci Rep* **2021**, *11* (1), 18524. https://doi.org/10.1038/s41598-021-97966-1.

(53) Montagne, F.; Guisier, F.; Venissac, N.; Baste, J.-M. The Role of Surgery in Lung Cancer Treatment: Present Indications and Future Perspectives—State of the Art. *Cancers* **2021**, *13* (15), 3711. https://doi.org/10.3390/cancers13153711.

(54) Benjamin, D. J. The Efficacy of Surgical Treatment of Cancer – 20years Later. *Medical Hypotheses* **2014**, *82* (4), 412–420. https://doi.org/10.1016/j.mehy.2014.01.004.

(55) Wyld, L.; Audisio, R. A.; Poston, G. J. The Evolution of Cancer Surgery and Future Perspectives. *Nat Rev Clin Oncol* **2015**, *12* (2), 115–124. https://doi.org/10.1038/nrclinonc.2014.191.

(56) Baskar, R.; Lee, K. A.; Yeo, R.; Yeoh, K.-W. Cancer and Radiation Therapy: Current Advances and Future Directions. *Int J Med Sci* **2012**, *9* (3), 193–199. https://doi.org/10.7150/ijms.3635.

(57) Majeed, H.; Gupta, V. Adverse Effects Of Radiation Therapy. In *StatPearls*; StatPearls Publishing: Treasure Island (FL), 2022.

(58) Baumann, M.; Krause, M.; Hill, R. Exploring the Role of Cancer Stem Cells in Radioresistance. *Nat Rev Cancer* **2008**, *8* (7), 545–554. https://doi.org/10.1038/nrc2419.

(59) Moncharmont, C.; Levy, A.; Gilormini, M.; Bertrand, G.; Chargari, C.; Alphonse, G.; Ardail, D.; Rodriguez-Lafrasse, C.; Magné, N. Targeting a Cornerstone of Radiation Resistance: Cancer Stem Cell. *Cancer Lett* **2012**, *322* (2), 139–147. https://doi.org/10.1016/j.canlet.2012.03.024.

(60) LaRue, S. M.; Vujaskovic, Z. Combining Radiation Therapy with Other Treatment Modalities. *Semin Vet Med Surg Small Anim* **1995**, *10* (3), 197–204.

(61) Hu, Q.; Sun, W.; Wang, C.; Gu, Z. Recent Advances of Cocktail Chemotherapy by Combination Drug Delivery Systems. *Advanced Drug Delivery Reviews* **2016**, *98*, 19–34. https://doi.org/10.1016/j.addr.2015.10.022.

(62) Pérez-Herrero, E.; Fernández-Medarde, A. Advanced Targeted Therapies in Cancer: Drug Nanocarriers, the Future of Chemotherapy. *Eur J Pharm Biopharm* **2015**, *93*, 52–79. https://doi.org/10.1016/j.ejpb.2015.03.018.

(63) Sun, R.; Liu, Y.; Li, S.-Y.; Shen, S.; Du, X.-J.; Xu, C.-F.; Cao, Z.-T.; Bao, Y.; Zhu, Y.-H.; Li, Y.-P.; Yang, X.-Z.; Wang, J. Co-Delivery of All-Trans-Retinoic Acid and Doxorubicin for Cancer Therapy with Synergistic Inhibition of Cancer Stem Cells. *Biomaterials* **2015**, *37*, 405–414. https://doi.org/10.1016/j.biomaterials.2014.10.018.

(64) Jain, A. K.; Thanki, K.; Jain, S. Co-Encapsulation of Tamoxifen and Quercetin in Polymeric Nanoparticles: Implications on Oral Bioavailability, Antitumor Efficacy, and Drug-Induced Toxicity. *Mol. Pharmaceutics* **2013**, *10* (9), 3459–3474. https://doi.org/10.1021/mp400311j.

(65) Meng, H.; Mai, W. X.; Zhang, H.; Xue, M.; Xia, T.; Lin, S.; Wang, X.; Zhao, Y.; Ji, Z.; Zink, J. I.; Nel, A. E. Codelivery of an Optimal Drug/SiRNA Combination Using Mesoporous Silica Nanoparticles To Overcome Drug Resistance in Breast Cancer in Vitro and in Vivo. *ACS Nano* **2013**, *7* (2), 994–1005. https://doi.org/10.1021/nn3044066.

(66) Lee, S.-M.; O'Halloran, T. V.; Nguyen, S. T. Polymer-Caged Nanobins for Synergistic Cisplatin−Doxorubicin Combination Chemotherapy. *J. Am. Chem. Soc.* **2010**, *132* (48), 17130–17138. https://doi.org/10.1021/ja107333g.

(67) Cai, L.; Xu, G.; Shi, C.; Guo, D.; Wang, X.; Luo, J. Telodendrimer Nanocarrier for Co-Delivery of Paclitaxel and Cisplatin: A Synergistic Combination Nanotherapy for Ovarian Cancer Treatment. *Biomaterials* **2015**, *37*, 456–468. https://doi.org/10.1016/j.biomaterials.2014.10.044.

(68) Zhang, L.; Radovic-Moreno, A. F.; Alexis, F.; Gu, F. X.; Basto, P. A.; Bagalkot, V.; Jon, S.; Langer, R. S.; Farokhzad, O. C. Co-Delivery of Hydrophobic and Hydrophilic Drugs from Nanoparticle–Aptamer Bioconjugates. *ChemMedChem* **2007**, *2* (9), 1268–1271. https://doi.org/10.1002/cmdc.200700121.

(69) Xu, X.; Xie, K.; Zhang, X.-Q.; Pridgen, E. M.; Park, G. Y.; Cui, D. S.; Shi, J.; Wu, J.; Kantoff, P. W.; Lippard, S. J.; Langer, R.; Walker, G. C.; Farokhzad, O. C. Enhancing

Tumor Cell Response to Chemotherapy through Nanoparticle-Mediated Codelivery of SiRNA and Cisplatin Prodrug. *Proceedings of the National Academy of Sciences* **2013**, *110* (46), 18638–18643. https://doi.org/10.1073/pnas.1303958110.

(70) Han, H. S.; Choi, K. Y. Advances in Nanomaterial-Mediated Photothermal Cancer Therapies: Toward Clinical Applications. *Biomedicines* **2021**, *9* (3), 305. https://doi.org/10.3390/biomedicines9030305.

(71) Xu, P.; Liang, F. Nanomaterial-Based Tumor Photothermal Immunotherapy. *Int J Nanomedicine* **2020**, *15*, 9159–9180. https://doi.org/10.2147/IJN.S249252.

(72) Muñoz, N. M.; Dupuis, C.; Williams, M.; Dixon, K.; McWatters, A.; Avritscher, R.; Bouchard, R.; Kaseb, A.; Schachtschneider, K. M.; Rao, A.; Sheth, R. A. Molecularly Targeted Photothermal Ablation Improves Tumor Specificity and Immune Modulation in a Rat Model of Hepatocellular Carcinoma. *Commun Biol* **2020**, *3* (1), 1–10. https://doi.org/10.1038/s42003-020-01522-y.

(73) Doughty, A. C. V.; Hoover, A. R.; Layton, E.; Murray, C. K.; Howard, E. W.; Chen, W. R. Nanomaterial Applications in Photothermal Therapy for Cancer. *Materials (Basel)* **2019**, *12* (5), 779. https://doi.org/10.3390/ma12050779.

(74) Abadeer, N. S.; Murphy, C. J. Recent Progress in Cancer Thermal Therapy Using Gold Nanoparticles. *J. Phys. Chem. C* **2016**, *120* (9), 4691–4716. https://doi.org/10.1021/acs.jpcc.5b11232.

(75) Chen, J.; Ning, C.; Zhou, Z.; Yu, P.; Zhu, Y.; Tan, G.; Mao, C. Nanomaterials as Photothermal Therapeutic Agents. *Progress in Materials Science* **2019**, *99*, 1–26. https://doi.org/10.1016/j.pmatsci.2018.07.005.

(76) Li, Y.; Liu, X.; Pan, W.; Li, N.; Tang, B. Photothermal Therapy-Induced Immunogenic Cell Death Based on Natural Melanin Nanoparticles against Breast Cancer. *Chem. Commun.* **2020**, *56* (9), 1389–1392. https://doi.org/10.1039/C9CC08447A.

(77) Zou, L.; Wang, H.; He, B.; Zeng, L.; Tan, T.; Cao, H.; He, X.; Zhang, Z.; Guo, S.; Li, Y. Current Approaches of Photothermal Therapy in Treating Cancer Metastasis with Nanotherapeutics. *Theranostics* **2016**, *6* (6), 762–772. https://doi.org/10.7150/thno.14988.

(78) Yang, Z.; Sun, Z.; Ren, Y.; Chen, X.; Zhang, W.; Zhu, X.; Mao, Z.; Shen, J.; Nie, S. Advances in Nanomaterials for Use in Photothermal and Photodynamic Therapeutics (Review). *Molecular Medicine Reports* **2019**, *20* (1), 5–15. https://doi.org/10.3892/mmr.2019.10218.

(79) Happonen, E.; Tamarov, K.; Martikainen, M.-V.; Ketola, K.; Roponen, M.; Lehto, V.-P.; Xu, W. Thermal Dose as a Universal Tool to Evaluate Nanoparticle-Induced Photothermal Therapy. *Int J Pharm* **2020**, *587*, 119657. https://doi.org/10.1016/j.ijpharm.2020.119657.

(80) Li, X.; Lovell, J. F.; Yoon, J.; Chen, X. Clinical Development and Potential of Photothermal and Photodynamic Therapies for Cancer. *Nat Rev Clin Oncol* **2020**, *17* (11), 657–674. https://doi.org/10.1038/s41571-020-0410-2.

(81) *What is Immunotherapy?*. Cancer Research Institute. https://www.cancerresearch.org/en-us/immunotherapy/what-is-immunotherapy (accessed 2022-05-18).

(82) Waldman, A. D.; Fritz, J. M.; Lenardo, M. J. A Guide to Cancer Immunotherapy: From T Cell Basic Science to Clinical Practice. *Nat Rev Immunol* **2020**, *20* (11), 651–668. https://doi.org/10.1038/s41577-020-0306-5.

(83) Kwok, G.; Yau, T. C. C.; Chiu, J. W.; Tse, E.; Kwong, Y.-L. Pembrolizumab (Keytruda). *Hum Vaccin Immunother* **2016**, *12* (11), 2777–2789. https://doi.org/10.1080/21645515.2016.1199310.

(84) Colombo, N.; Dubot, C.; Lorusso, D.; Caceres, M. V.; Hasegawa, K.; Shapira-Frommer, R.; Tewari, K. S.; Salman, P.; Hoyos Usta, E.; Yañez, E.; Gümüş, M.; Olivera Hurtado de Mendoza, M.; Samouëlian, V.; Castonguay, V.; Arkhipov, A.; Toker, S.; Li, K.; Keefe, S. M.; Monk, B. J.; KEYNOTE-826 Investigators. Pembrolizumab for Persistent, Recurrent, or Metastatic Cervical Cancer. *N Engl J Med* **2021**, *385* (20), 1856–1867. https://doi.org/10.1056/NEJMoa2112435.

(85) Fulchiero, E.; Jimeno, A. Nivolumab. *Drugs Today (Barc)* **2014**, *50* (12), 791–802. https://doi.org/10.1358/dot.2014.50.12.2235103.

(86) Guo, L.; Zhang, H.; Chen, B. Nivolumab as Programmed Death-1 (PD-1) Inhibitor for Targeted Immunotherapy in Tumor. *J Cancer* **2017**, *8* (3), 410–416. https://doi.org/10.7150/jca.17144.

(87) Tarhini, A. A. Tremelimumab: A Review of Development to Date in Solid Tumors. *Immunotherapy* **2013**, *5* (3), 215–229. https://doi.org/10.2217/imt.13.9.

(88) Ribas, A.; Hanson, D. C.; Noe, D. A.; Millham, R.; Guyot, D. J.; Bernstein, S. H.; Canniff, P. C.; Sharma, A.; Gomez-Navarro, J. Tremelimumab (CP-675,206), a Cytotoxic T Lymphocyte Associated Antigen 4 Blocking Monoclonal Antibody in Clinical Development for Patients with Cancer. *Oncologist* **2007**, *12* (7), 873–883. https://doi.org/10.1634/theoncologist.12-7-873.

(89) Ipilimumab. *Drugs R D* **2010**, *10* (2), 97–110. https://doi.org/10.2165/11584510-000000000-00000.

(90) Graziani, G.; Tentori, L.; Navarra, P. Ipilimumab: A Novel Immunostimulatory Monoclonal Antibody for the Treatment of Cancer. *Pharmacol Res* **2012**, *65* (1), 9–22. https://doi.org/10.1016/j.phrs.2011.09.002.

(91) Collins, J. M.; Gulley, J. L. Product Review: Avelumab, an Anti-PD-L1 Antibody. *Hum Vaccin Immunother* **2018**, *15* (4), 891–908. https://doi.org/10.1080/21645515.2018.1551671.

(92) Powles, T.; Park, S. H.; Voog, E.; Caserta, C.; Valderrama, B. P.; Gurney, H.; Kalofonos, H.; Radulović, S.; Demey, W.; Ullén, A.; Loriot, Y.; Sridhar, S. S.; Tsuchiya, N.; Kopyltsov, E.; Sternberg, C. N.; Bellmunt, J.; Aragon-Ching, J. B.; Petrylak, D. P.; Laliberte, R.; Wang, J.; Huang, B.; Davis, C.; Fowst, C.; Costa, N.; Blake-Haskins, J. A.; di Pietro, A.; Grivas, P. Avelumab Maintenance Therapy for Advanced or Metastatic Urothelial Carcinoma. *N Engl J Med* **2020**, *383* (13), 1218–1230. https://doi.org/10.1056/NEJMoa2002788.

(93) Alvarez-Argote, J.; Dasanu, C. A. Durvalumab in Cancer Medicine: A Comprehensive Review. *Expert Opin Biol Ther* **2019**, *19* (9), 927–935. https://doi.org/10.1080/14712598.2019.1635115.

(94) Mezquita, L.; Planchard, D. Durvalumab for the Treatment of Non-Small Cell Lung Cancer. *Expert Rev Respir Med* **2018**, *12* (8), 627–639. https://doi.org/10.1080/17476348.2018.1494575.

(95) Ribas, A.; Wolchok, J. D. Cancer Immunotherapy Using Checkpoint Blockade. *Science* **2018**, *359* (6382), 1350–1355. https://doi.org/10.1126/science.aar4060.

(96) Sharma, P.; Hu-Lieskovan, S.; Wargo, J. A.; Ribas, A. Primary, Adaptive, and Acquired Resistance to Cancer Immunotherapy. *Cell* **2017**, *168* (4), 707–723. https://doi.org/10.1016/j.cell.2017.01.017.

(97) Lin, R. A.; Lin, J. K.; Lin, S.-Y. Mechanisms of Immunogenic Cell Death and Immune Checkpoint Blockade Therapy. *Kaohsiung J Med Sci* **2021**, *37* (6), 448–458. https://doi.org/10.1002/kjm2.12375.

(98) Marin-Acevedo, J. A.; Dholaria, B.; Soyano, A. E.; Knutson, K. L.; Chumsri, S.; Lou, Y. Next Generation of Immune Checkpoint Therapy in Cancer: New Developments and Challenges. *Journal of Hematology & Oncology* **2018**, *11* (1), 39. https://doi.org/10.1186/s13045-018-0582-8.

(99) Chen, W. R.; Liu, H.; Nordquist, R. E. Mechanism of Laser Immunotherapy: Role of Immunoadjuvant and Selective Photothermal Laser-Tissue Interaction. In *International Workshop on Photonics and Imaging in Biology and Medicine*; SPIE, 2002; Vol. 4536, pp 82–89. https://doi.org/10.1117/12.462529.

(100) Hou, X.; Tao, Y.; Pang, Y.; Li, X.; Jiang, G.; Liu, Y. Nanoparticle-Based Photothermal and Photodynamic Immunotherapy for Tumor Treatment. *Int J Cancer* **2018**, *143* (12), 3050–3060. https://doi.org/10.1002/ijc.31717.

(101) Hoover, A. R.; Liu, K.; Valerio, T. I.; Li, M.; Mukherjee, P.; Chen, W. R. Nano-Ablative Immunotherapy for Cancer Treatment. *Nanophotonics* **2021**, *10* (12), 3247–3266. https://doi.org/10.1515/nanoph-2021-0171.

(102) Li, X.; Min, M.; Du, N.; Gu, Y.; Hode, T.; Naylor, M.; Chen, D.; Nordquist, R. E.; Chen, W. R. Chitin, Chitosan, and Glycated Chitosan Regulate Immune Responses: The Novel Adjuvants for Cancer Vaccine. *Clin Dev Immunol* **2013**, *2013*, 387023. https://doi.org/10.1155/2013/387023.

(103) Cheung, R. C. F.; Ng, T. B.; Wong, J. H.; Chan, W. Y. Chitosan: An Update on Potential Biomedical and Pharmaceutical Applications. *Mar Drugs* **2015**, *13* (8), 5156–5186. https://doi.org/10.3390/md13085156.

(104) Zargar, V.; Asghari, M.; Dashti, A. A Review on Chitin and Chitosan Polymers: Structure, Chemistry, Solubility, Derivatives, and Applications. *ChemBioEng Reviews* **2015**, *2* (3), 204–226. https://doi.org/10.1002/cben.201400025.

(105) Rodrigues, S.; Dionísio, M.; Remuñán López, C.; Grenha, A. Biocompatibility of Chitosan Carriers with Application in Drug Delivery. *J Funct Biomater* **2012**, *3* (3), 615–641. https://doi.org/10.3390/jfb3030615.

(106) Barra, A.; Alves, Z.; Ferreira, N. M.; Martins, M. A.; Oliveira, H.; Ferreira, L. P.; Cruz, M. M.; Carvalho, M. de D.; Neumayer, S. M.; Rodriguez, B. J.; Nunes, C.; Ferreira, P. Biocompatible Chitosan-Based Composites with Properties Suitable for Hyperthermia Therapy. *J. Mater. Chem. B* **2020**, *8* (6), 1256–1265. https://doi.org/10.1039/C9TB02067E.

(107) Islam, N.; Dmour, I.; Taha, M. O. Degradability of Chitosan Micro/Nanoparticles for Pulmonary Drug Delivery. *Heliyon* **2019**, *5* (5), e01684. https://doi.org/10.1016/j.heliyon.2019.e01684.

(108) Landriscina, A.; Rosen, J.; Friedman, A. J. Biodegradable Chitosan Nanoparticles in Drug Delivery for Infectious Disease. *Nanomedicine (Lond)* **2015**, *10* (10), 1609–1619. https://doi.org/10.2217/nnm.15.7.

(109) Zhang, H.; Yan, T.; Xu, S.; Feng, S.; Huang, D.; Fujita, M.; Gao, X.-D. Graphene Oxide-Chitosan Nanocomposites for Intracellular Delivery of Immunostimulatory CpG Oligodeoxynucleotides. *Mater Sci Eng C Mater Biol Appl* **2017**, *73*, 144–151. https://doi.org/10.1016/j.msec.2016.12.072.

(110) Zhang, H.; Chen, S.; Zhi, C.; Yamazaki, T.; Hanagata, N. Chitosan-Coated Boron Nitride Nanospheres Enhance Delivery of CpG Oligodeoxynucleotides and Induction of Cytokines. *Int J Nanomedicine* **2013**, *8*, 1783–1793. https://doi.org/10.2147/IJN.S43251.

(111) Bao, H.; Pan, Y.; Ping, Y.; Sahoo, N. G.; Wu, T.; Li, L.; Li, J.; Gan, L. H. Chitosan-Functionalized Graphene Oxide as a Nanocarrier for Drug and Gene Delivery. *Small* **2011**, *7* (11), 1569–1578. https://doi.org/10.1002/smll.201100191.

(112) Li, X.; Xing, R.; Xu, C.; Liu, S.; Qin, Y.; Li, K.; Yu, H.; Li, P. Immunostimulatory Effect of Chitosan and Quaternary Chitosan: A Review of Potential Vaccine Adjuvants. *Carbohydrate Polymers* **2021**, *264*, 118050. https://doi.org/10.1016/j.carbpol.2021.118050.

(113) Zhou, F.; Song, S.; Chen, W. R.; Xing, D. Immunostimulatory Properties of Glycated Chitosan. *J Xray Sci Technol* **2011**, *19* (2), 285–292. https://doi.org/10.3233/XST-2011-0293.

(114) Babu, A.; Ramesh, R. Multifaceted Applications of Chitosan in Cancer Drug Delivery and Therapy. *Mar Drugs* **2017**, *15* (4), 96. https://doi.org/10.3390/md15040096.

(115) Fu, S.; Xia, J.; Wu, J. Functional Chitosan Nanoparticles in Cancer Treatment. *J Biomed Nanotechnol* **2016**, *12* (8), 1585–1603. https://doi.org/10.1166/jbn.2016.2228.

(116) Han, H. D.; Byeon, Y.; Jang, J.-H.; Jeon, H. N.; Kim, G. H.; Kim, M. G.; Pack, C.-G.; Kang, T. H.; Jung, I. D.; Lim, Y. T.; Lee, Y. J.; Lee, J.-W.; Shin, B. C.; Ahn, H. J.; Sood, A. K.; Park, Y.-M. In Vivo Stepwise Immunomodulation Using Chitosan Nanoparticles as a Platform Nanotechnology for Cancer Immunotherapy. *Sci Rep* **2016**, *6* (1), 38348. https://doi.org/10.1038/srep38348.

(117) Chen, P.-G.; Huang, Z.-H.; Sun, Z.-Y.; Gao, Y.; Liu, Y.-F.; Shi, L.; Chen, Y.-X.; Zhao, Y.-F.; Li, Y.-M. Chitosan Nanoparticles Based Nanovaccines for Cancer Immunotherapy. *Pure and Applied Chemistry* **2017**, *89* (7), 931–939. https://doi.org/10.1515/pac-2016-0913.

(118) Sharifi-Rad, J.; Quispe, C.; Butnariu, M.; Rotariu, L. S.; Sytar, O.; Sestito, S.; Rapposelli, S.; Akram, M.; Iqbal, M.; Krishna, A.; Kumar, N. V. A.; Braga, S. S.; Cardoso, S. M.; Jafernik, K.; Ekiert, H.; Cruz-Martins, N.; Szopa, A.; Villagran, M.;

Mardones, L.; Martorell, M.; Docea, A. O.; Calina, D. Chitosan Nanoparticles as a Promising Tool in Nanomedicine with Particular Emphasis on Oncological Treatment. *Cancer Cell International* **2021**, *21* (1), 318. https://doi.org/10.1186/s12935-021-02025-4.

(119) Chung, Y.-C.; Yeh, J.-Y.; Tsai, C.-F. Antibacterial Characteristics and Activity of Water-Soluble Chitosan Derivatives Prepared by the Maillard Reaction. *Molecules* **2011**, *16* (10), 8504–8514. https://doi.org/10.3390/molecules16108504.

(120) Ahonkhai, E.; Arhewoh, M.; Okhamafe, A. Effect of Solvent Type and Drying Method on Protein Retention in Chitosan-Alginate Microcapsules. *Tropical Journal of Pharmaceutical Research* **2007**, *5*. https://doi.org/10.4314/tjpr.v5i2.14635.

(121) Song, S.; Zhou, F.; Nordquist, R. E.; Carubelli, R.; Liu, H.; Chen, W. R. Glycated Chitosan as a New Non-Toxic Immunological Stimulant. *Immunopharmacol Immunotoxicol* **2009**, *31* (2), 202–208. https://doi.org/10.1080/08923970802629593.

(122) Chen, W. R.; Korbelik, M.; Bartels, K. E.; Liu, H.; Sun, J.; Nordquist, R. E. Enhancement of Laser Cancer Treatment by a Chitosan-Derived Immunoadjuvant. *Photochem Photobiol* **2005**, *81* (1), 190–195. https://doi.org/10.1562/2004-07-20-RA-236.

(123) Chen, W. R.; Liu, H.; Ritchey, J. W.; Bartels, K. E.; Lucroy, M. D.; Nordquist, R. E. Effect of Different Components of Laser Immunotherapy in Treatment of Metastatic Tumors in Rats. *Cancer Res* **2002**, *62* (15), 4295–4299.

(124) Mishra, P.; Nayak, B.; Dey, R. K. PEGylation in Anti-Cancer Therapy: An Overview. *Asian Journal of Pharmaceutical Sciences* **2016**, *11* (3), 337–348. https://doi.org/10.1016/j.ajps.2015.08.011.

(125) Chen, S.; Yang, K.; Tuguntaev, R. G.; Mozhi, A.; Zhang, J.; Wang, P. C.; Liang, X.-J. Targeting Tumor Microenvironment with PEG-Based Amphiphilic Nanoparticles to Overcome Chemoresistance. *Nanomedicine* **2016**, *12* (2), 269–286. https://doi.org/10.1016/j.nano.2015.10.020.

(126) Rezvantalab, S.; Drude, N. I.; Moraveji, M. K.; Güvener, N.; Koons, E. K.; Shi, Y.; Lammers, T.; Kiessling, F. PLGA-Based Nanoparticles in Cancer Treatment. *Frontiers in Pharmacology* **2018**, *9*.

(127) Wadhawan, A.; Singh, J.; Sharma, H.; Handa, S.; Singh, G.; Kumar, R.; Barnwal, R. P.; Pal Kaur, I.; Chatterjee, M. Anticancer Biosurfactant-Loaded PLA–PEG Nanoparticles Induce Apoptosis in Human MDA-MB-231 Breast Cancer Cells. *ACS Omega* **2022**, *7* (6), 5231–5241. https://doi.org/10.1021/acsomega.1c06338.

(128) Jusu, S. M.; Obayemi, J. D.; Salifu, A. A.; Nwazojie, C. C.; Uzonwanne, V.; Odusanya, O. S.; Soboyejo, W. O. Drug-Encapsulated Blend of PLGA-PEG Microspheres: In Vitro and in Vivo Study of the Effects of Localized/Targeted Drug Delivery on the Treatment of Triple-Negative Breast Cancer. *Sci Rep* **2020**, *10* (1), 14188. https://doi.org/10.1038/s41598-020-71129-0.

(129) *Polyethylene Glycol (PEG) Modification - CD Bioparticles*. https://www.cd-bioparticles.com/support/polyethylene-glycol-peg-modification.html (accessed 2022-04-29).

(130) Bailon, P.; Won, C.-Y. PEG-Modified Biopharmaceuticals. *Expert Opin Drug Deliv* **2009**, *6* (1), 1–16. https://doi.org/10.1517/17425240802650568.

(131) Zhou, F.; Wu, S.; Song, S.; Chen, W. R.; Resasco, D. E.; Xing, D. Antitumor Immunologically Modified Carbon Nanotubes for Photothermal Therapy. *Biomaterials* **2012**, *33* (11), 3235–3242. https://doi.org/10.1016/j.biomaterials.2011.12.029.

(132) Saha, L. C.; Nag, O. K.; Doughty, A.; Liu, H.; Chen, W. R. An Immunologically Modified Nanosystem Based on Noncovalent Binding Between Single-Walled Carbon Nanotubes and Glycated Chitosan. *Technol Cancer Res Treat* **2018**, *17*, 1533033818802313. https://doi.org/10.1177/1533033818802313.

(133) *Graphene Oxide Powders and Solutions*. Ossila. https://www.ossila.com/products/graphene-oxide-powders (accessed 2021-11-30).

(134) Zhou, F.; Yang, J.; Zhang, Y.; Liu, M.; Lang, M. L.; Li, M.; Chen, W. R. Local Phototherapy Synergizes with Immunoadjuvant for Treatment of Pancreatic Cancer through Induced Immunogenic Tumor Vaccine. *Clin Cancer Res* **2018**, *24* (21), 5335–5346. https://doi.org/10.1158/1078-0432.CCR-18-1126.

(135) Wang, M.; Rao, J.; Wang, M.; Li, X.; Liu, K.; Naylor, M. F.; Nordquist, R. E.; Chen, W. R.; Zhou, F. Cancer Photo-Immunotherapy: From Bench to Bedside. *Theranostics* **2021**, *11* (5), 2218–2231. https://doi.org/10.7150/thno.53056.

(136) Vines, J. B.; Yoon, J.-H.; Ryu, N.-E.; Lim, D.-J.; Park, H. Gold Nanoparticles for Photothermal Cancer Therapy. *Front Chem* **2019**, *7*, 167. https://doi.org/10.3389/fchem.2019.00167.

(137) Li, Y.; Lu, W.; Huang, Q.; Huang, M.; Li, C.; Chen, W. Copper Sulfide Nanoparticles for Photothermal Ablation of Tumor Cells. *Nanomedicine (Lond)* **2010**, *5* (8), 1161–1171. https://doi.org/10.2217/nnm.10.85.

(138) Zhou, F.; Wang, M.; Luo, T.; Qu, J.; Chen, W. R. Photo-Activated Chemo-Immunotherapy for Metastatic Cancer Using a Synergistic Graphene Nanosystem. *Biomaterials* **2021**, *265*, 120421. https://doi.org/10.1016/j.biomaterials.2020.120421.

(139) Singh, D. P.; Herrera, C. E.; Singh, B.; Singh, S.; Singh, R. K.; Kumar, R. Graphene Oxide: An Efficient Material and Recent Approach for Biotechnological and Biomedical Applications. *Mater Sci Eng C Mater Biol Appl* **2018**, *86*, 173–197. https://doi.org/10.1016/j.msec.2018.01.004.

(140) Daniyal, M.; Liu, B.; Wang, W. Comprehensive Review on Graphene Oxide for Use in Drug Delivery System. *Curr Med Chem* **2020**, *27* (22), 3665–3685. https://doi.org/10.2174/1381612825666190201296290.

(141) Cao, W.; He, L.; Cao, W.; Huang, X.; Jia, K.; Dai, J. Recent Progress of Graphene Oxide as a Potential Vaccine Carrier and Adjuvant. *Acta Biomater* **2020**, *112*, 14–28. https://doi.org/10.1016/j.actbio.2020.06.009.

(142) Xu, L.; Xiang, J.; Liu, Y.; Xu, J.; Luo, Y.; Feng, L.; Liu, Z.; Peng, R. Functionalized Graphene Oxide Serves as a Novel Vaccine Nano-Adjuvant for Robust Stimulation of Cellular Immunity. *Nanoscale* **2016**, *8* (6), 3785–3795. https://doi.org/10.1039/c5nr09208f.

(143) Yan, T.; Zhang, H.; Huang, D.; Feng, S.; Fujita, M.; Gao, X.-D. Chitosan-Functionalized Graphene Oxide as a Potential Immunoadjuvant. *Nanomaterials (Basel)* **2017**, *7* (3), 59. https://doi.org/10.3390/nano7030059.

(144) Li, Y.; Dong, H.; Li, Y.; Shi, D. Graphene-Based Nanovehicles for Photodynamic Medical Therapy. *Int J Nanomedicine* **2015**, *10*, 2451–2459. https://doi.org/10.2147/IJN.S68600.

(145) Chen, G.-Y.; Yang, H.-J.; Lu, C.-H.; Chao, Y.-C.; Hwang, S.-M.; Chen, C.-L.; Lo, K.-W.; Sung, L.-Y.; Luo, W.-Y.; Tuan, H.-Y.; Hu, Y.-C. Simultaneous Induction of Autophagy and Toll-like Receptor Signaling Pathways by Graphene Oxide. *Biomaterials* **2012**, *33* (27), 6559–6569. https://doi.org/10.1016/j.biomaterials.2012.05.064.

(146) Zhou, H.; Zhao, K.; Li, W.; Yang, N.; Liu, Y.; Chen, C.; Wei, T. The Interactions between Pristine Graphene and Macrophages and the Production of Cytokines/Chemokines via TLR- and NF-KB-Related Signaling Pathways. *Biomaterials* **2012**, *33* (29), 6933–6942. https://doi.org/10.1016/j.biomaterials.2012.06.064.

(147) Qu, G.; Liu, S.; Zhang, S.; Wang, L.; Wang, X.; Sun, B.; Yin, N.; Gao, X.; Xia, T.; Chen, J.-J.; Jiang, G.-B. Graphene Oxide Induces Toll-like Receptor 4 (TLR4)-Dependent Necrosis in Macrophages. *ACS Nano* **2013**, *7* (7), 5732–5745. https://doi.org/10.1021/nn402330b.

(148) Kasturi, S. P.; Skountzou, I.; Albrecht, R. A.; Koutsonanos, D.; Hua, T.; Nakaya, H. I.; Ravindran, R.; Stewart, S.; Alam, M.; Kwissa, M.; Villinger, F.; Murthy, N.; Steel, J.; Jacob, J.; Hogan, R. J.; García-Sastre, A.; Compans, R.; Pulendran, B. Programming the Magnitude and Persistence of Antibody Responses with Innate Immunity. *Nature* **2011**, *470* (7335), 543–547. https://doi.org/10.1038/nature09737.

(149) Wang, J. W.; Hon, M. H. Template Mediated Nanofibrous Structure: Novel Chitosan/Polyethylene Glycol Scaffold for Tissue Engineering. In *Recent Advances in Multidisciplinary Applied Physics*; Méndez-Vilas, A., Ed.; Elsevier Science Ltd: Oxford, 2005; pp 331–335. https://doi.org/10.1016/B978-008044648-6.50053-7.

(150) McGarry, C. K.; Grattan, L. J.; Ivory, A. M.; Leek, F.; Liney, G. P.; Liu, Y.; Miloro, P.; Rai, R.; Robinson, A.; Shih, A. J.; Zeqiri, B.; Clark, C. H. Tissue Mimicking Materials for Imaging and Therapy Phantoms: A Review. *Phys. Med. Biol.* **2020**. https://doi.org/10.1088/1361-6560/abbd17.

(151) Menikou, G.; Damianou, C. Acoustic and Thermal Characterization of Agar Based Phantoms Used for Evaluating Focused Ultrasound Exposures. *Journal of Therapeutic Ultrasound* **2017**, *5* (1), 14. https://doi.org/10.1186/s40349-017-0093-z.

(152) *Fig. 5. UV spectra of graphene oxide and graphene.* ResearchGate. https://www.researchgate.net/figure/UV-spectra-of-graphene-oxide-and-graphene_fig5_263509024 (accessed 2021-10-21).

(153) Li, B.; Zhang, Y.; Zou, R.; Wang, Q.; Zhang, B.; An, L.; Yin, F.; Hua, Y.; Hu, J. Self-Assembled WO3−x Hierarchical Nanostructures for Photothermal Therapy with a 915 Nm Laser Rather than the Common 980 Nm Laser. *Dalton Trans.* **2014**, *43* (16), 6244–6250. https://doi.org/10.1039/C3DT53396D.

(154) *Fig. 3 (a) UV-vis absorption spectrum of the pure water. (b)...* ResearchGate. https://www.researchgate.net/figure/a-UV-vis-absorption-spectrum-of-the-pure-water-b-Temperature-elevation-of-the-pure_fig3_312374622 (accessed 2021-10-27).

(155) Johra, F. T.; Lee, J.-W.; Jung, W.-G. Facile and Safe Graphene Preparation on Solution Based Platform. *Journal of Industrial and Engineering Chemistry* **2014**, *20* (5), 2883–2887. https://doi.org/10.1016/j.jiec.2013.11.022.

(156) *UV-vis absorption spectra of (a) pure chitosan and (b) chitosan:...* ResearchGate. https://www.researchgate.net/figure/UV-vis-absorption-spectra-of-a-pure-chitosan-and-b-chitosan-AgCF3SO3-at-ambient_fig3_261397679 (accessed 2021-10-21).

(157) Aziz, S. B.; Abidin, Z. H. Z. Role of Hard-Acid/Hard-Base Interaction on Structural and Dielectric Behavior of Solid Polymer Electrolytes Based on Chitosan-XCF3SO3 (X = Li+, Na+, Ag+). *Journal of Polymers* **2014**, *2014*, e906780. https://doi.org/10.1155/2014/906780.

(158) Parameswaran, N.; Patial, S. Tumor Necrosis Factor-α Signaling in Macrophages. *Crit Rev Eukaryot Gene Expr* **2010**, *20* (2), 87–103.

(159) Mohammed, M. A.; Syeda, J. T. M.; Wasan, K. M.; Wasan, E. K. An Overview of Chitosan Nanoparticles and Its Application in Non-Parenteral Drug Delivery. *Pharmaceutics* **2017**, *9* (4), 53. https://doi.org/10.3390/pharmaceutics9040053.

(160) Zhang, Y.; Zhan, X.; Xiong, J.; Peng, S.; Huang, W.; Joshi, R.; Cai, Y.; Liu, Y.; Li, R.; Yuan, K.; Zhou, N.; Min, W. Temperature-Dependent Cell Death Patterns Induced by Functionalized Gold Nanoparticle Photothermal Therapy in Melanoma Cells. *Sci Rep* **2018**, *8* (1), 8720. https://doi.org/10.1038/s41598-018-26978-1.

(161) Liu, S.; Doughty, A.; West, C.; Tang, Z.; Zhou, F.; Chen, W. R. Determination of Temperature Distribution in Tissue for Interstitial Cancer Photothermal Therapy. *Int J Hyperthermia* **2018**, *34* (6), 756–763. https://doi.org/10.1080/02656736.2017.1370136.

(162) Nomura, S.; Morimoto, Y.; Tsujimoto, H.; Arake, M.; Harada, M.; Saitoh, D.; Hara, I.; Ozeki, E.; Satoh, A.; Takayama, E.; Hase, K.; Kishi, Y.; Ueno, H. Highly Reliable, Targeted Photothermal Cancer Therapy Combined with Thermal Dosimetry Using a near-Infrared Absorbent. *Sci Rep* **2020**, *10* (1), 9765. https://doi.org/10.1038/s41598-020-66646-x.